THESIS FOR THE DEGREE OF DOCTOR OF PHILOSOPHY

Structure Dynamics and Heterogeneity in Soft Materials Determined by FRAP

JOEL HAGMAN

Department of Chemical and Biological Engineering
CHALMERS UNIVERSITY OF TECHNOLOGY

Gothenburg, Sweden 2012

Structure Dynamics and Heterogeneity in Soft Materials Determined by FRAP
JOEL HAGMAN
ISBN 978-91-7385-683-6

Doktorsavhandlingar vid Chalmers tekniska högskola
Ny serie nr. 3364
ISSN 0346-718X
Department of Chemical and Biological Engineering
Chalmers University of Technology
SE-412 96 Gothenburg
Sweden
Telephone: +46 (0)31-772 1000

Cover:
A concept image of a typical FRAP experiment. From top to bottom: (I) The microscope objective during the bleaching phase. (II) A gelatin/maltodextrin multiphase sample, (III) The intensity profile during a FRAP measurement, averaged over the bleached spot, along with the corresponding images taken by the microscope during the measurement.

Chalmers Reproservice
Gothenburg, Sweden 2012

Structure Dynamics and Heterogeneity in Soft Materials Determined by FRAP

JOEL HAGMAN
Department of Chemical and Biological Engineering
Chalmers University of Technology

Abstract

A common interest in industry today is to be able to control the mass transport inside soft (bio) materials in order to tailor both release and uptake of substances. Most of the materials used are heterogeneous, quite often multiphase or compound materials and often undergo dynamic changes; it is therefore important to have control over the local microstructure in order to tailor the macro scale properties. The work in this thesis expands the toolbox of available techniques for studying diffusion in such materials. This has been achieved by enhancing the usability of a technique called fluorescence recovery after photobleaching (FRAP) as well as by performing FRAP measurements in dynamic and heterogeneous materials. FRAP is an optical technique capable of measuring locally at a micrometer scale in a material sample. The results obtained have given an increased understanding of the structure–mass transport relationship. The technique has been improved by improving the accuracy of the mass transport determination, by reducing the required measurement area, by increasing the range of available materials in which FRAP can be used as well as by analysing the impact of probe selection. The materials used in this thesis work have been used as model materials for FRAP development and at the same time been investigated using FRAP. The materials, along with the key interest, can be summarized to the following choices: κ-carrageenan for the structural heterogeneity, gelatin for the dynamic changes during gelation, gelatin/maltodextrin multiphase samples for the possibility to tailor the domain sizes, super absorbing polymers (SAP) for the possibility to alter the mass transport properties depending on the swelling and both β-lactoglobulin and pasta was used as model material for spatial correlation measurements of FRAP data. These results may be used for improved understanding of other materials as well and the FRAP technique is shown to be one promising tool when tailoring new structures.

Keywords: Fluorescence recovery after photobelaching, Confocal microscopy, Structure dynamics, Soft materials, Heterogeneity

To my family

"Chaos is inherent in all compounded things. Strive on with diligence." – Buddha

List of publications

This thesis is based on the work contained in the following papers, referred to by their Roman numerals in the text.

I Pixel-based analysis of FRAP data with a general initial bleaching profile
Jenny Jonasson, Joel Hagman, Niklas Lorén, Diana Bernin, Magnus Nydén and Mats Rudemo
Journal of microscopy 2010, 239, 142–153

II Effect of Gelatin Gelation Kinetics on Probe Diffusion Determined by FRAP and Rheology
Joel Hagman, Niklas Lorén and Anne-Marie Hermansson
Biomacromolecules 2010, 11, 3359–3366

III Straightforward FRAP for quantitative diffusion measurements with a laser scanning microscope
Hendrik Deschout, Joel Hagman, Sophia Fransson, Jenny Jonasson, Mats Rudemo, Niklas Lorén, and Kevin Braeckmans
Optics Express 2010, 18, 22886–22905

IV Probe diffusion in κ-carrageenan gels determined by fluorescence recovery after photobleaching
Joel Hagman, Niklas Lorén and Anne-Marie Hermansson
Food Hydrocolloids 2012, 29, 106–115

Related publications not included in the thesis

V Fluorescence recovery after photobleaching in material and life sciences: putting theory into practice
Niklas Lorén, Joel Hagman, Jenny K. Jonasson, Hendrik Deschout, Diana Bernin, Francesca Cella, Alberto Diaspro, James McNally, Marcel Ameloot, Nick Smisdom, Magnus Nydén, Anne-Marie Hermansson, Mats Rudemo and Kevin Braeckmans
Manuscript

Non-related publications

VI Increased water transport in PDMS silicone films by addition of excipients
Annika Borde, Mikael Larsson, Ylva Odelberg, Joel Hagman, Peter Löwenhielm and Anette Larsson
Acta Biomaterialia 2011, 8, 579–588

Contribution report

I Significant contribution to the interpretation of the results. Part of the manuscript preparation. Active in planning the study. Performed roughly half of the experimental work.

II Main author. Significant contribution to the interpretation of the results. Active in planning the study. Performed the experimental work.

III Significant contribution to the interpretation of the results. Part of the manuscript preparation. Active in planning the study. Performed roughly half of the experimental work.

IV Main author. Significant contribution to the interpretation of the results. Active in planning the study. Performed the experimental work.

List of abbreviations

AOBS	Acousto-optical beam splitter
AOTF	Acousto-optical tunable filter
CLSM	Confocal laser scanning microscope
FITC	Fluorescein isothiocyanate
FRAP	Fluorescence recovery after photobleaching
GFP	Green fluorescent protein
MLE	Maximum likelihood estimation
NA	Numerical aperture
NMR	Nuclear magnetic resonance
PSF	Point spread function
RMS	Root mean square
ROI	Region of interest
SAP	Superabsorbing polymer
TEM	Transmission electron microscope

Contents

1 Introduction

The movement of molecules, the mass transport, in soft materials is of great importance in everyday life and the ability to control it is vital for many applications. Examples of applications are release of drug molecules from a medical pill, where the release rate and location in the body might make a difference in how effective the treatment is. Another example could be a diaper which needs to absorb and retain body liquids while minimizing discomfort and leakage. A third example could be the food industry where a control of the mass transport could lead to longer shelf life while minimizing the use of additives, which in turn might lead to safer products. The (micro) structure of the material in which the mass transport takes place is an important factor when tailoring desired mass transport properties; a simple example would be that a denser structure will hinder the transport more than an open structure. It is therefore important to know how different structures affect the transport in order to control the mass transport via the structure. In addition, in order to be able to tailor a desired material for specific mass transport properties, it will also be essential to understand how dynamic changes of the structure interact with the transported molecules.

The mentioned examples of applications all include soft (bio) materials. An example of a soft material is a gel, which is a material that have a solid-like appearance even though the major component is a liquid phase. Release of drug molecules from a pill can be controlled by gelling layers surrounding it [128]. Diapers gain much of their ability to absorb from the swelling of a super absorbent polymer which becomes a hydrogel when swollen. In the food industry, gels are often used to control texture and rheological properties. Even though gels are common, it is by no means the only soft material structure. Foods, for example, can consist of many different types of materials and microstructures including gels but also emulsions, foams, solutions, cellular structures, fat crystal networks and liquid fat. Due to the range of different structures which interact in order to give the macroscopic properties, it is critical to be able to measure both locally and globally to determine which structure that yields which properties. The local measurements are vital to determine how a specific structure influences the properties whereas a global measurement would loose information as the influence from the different structures will be averaged. On the other hand, the global measurements are vital in order to determine the integrated macro scale properties that are a function of the different microstructures inside the material. The length scale of the microstructures is often on a micrometer scale or less and the mass transport can therefore be due to both flow and diffusion. A versatile technique to measure diffusion locally inside a material is fluorescence recovery after photobleaching (FRAP). The basic idea behind FRAP is to introduce a light sensitive fluorescing probe to the sample, bleach a portion of the probes with a laser and then record the recovery of fluorescence in the bleached region. The recovery is caused by the movement of both the bleached and the unbleached probes. FRAP is a microscopy technique and a benefit of is that the material can therefore be imaged with the microscope at the same time as FRAP is used, which makes it possible to obtrain a good correlation between structure and diffusion.

FRAP was developed during the mid seventies to measure diffusion in cell membranes [3] and has been utilised to a fair extent in cell biology to study various mechanisms in cells since then [58, 75, 106]. The pharmaceutical industry has used FRAP as a non destructive method

to study transport of drug molecules inside various systems such as gels, solutions, biological extracellular matrices and living cells [82]. Up until recently, FRAP have barely been used to study foods and the studies have been focused on time-dependent changes of the properties of foods during storage as well as the effects of different treatments such as freezing. Here are a few examples. In chocolate, fat can migrate from the filling to the surface of the praline, which causes a dull grayish look and FRAP have been used to study this mechanism [41, 125]. In the case of halibut fish, protease diffusion causes the meat to soften and, in the worst case scenario, dissolve [19]. The mechanism to stabilize acidified milk drinks have been studied using FRAP a method for evaluating he mobility of the proteins in the drinks [59].

Much of the time-dependant changes which have been studied by FRAP so far have been on a much longer time scale than the time it takes to perform a single FRAP measurement. Structural changes which occur on a time scale near that of a single FRAP experiment is an area which have been neglected. This is to a large extent due to the difficulties in controlling the dynamic changes in the samples while performing the measurements. Another area that warrants further study is the development of evaluation models for FRAP. There have been ongoing developments during the past decade, which have resulted in evaluation models with increasing precision. Despite the development of newer evaluation models, it is still possible to find recent litterature in which unreliable evaluation models have been used. This is likely due to the fact that they have been simple to use and have not required heavy calculations. The problem with many of the previous evaluation models is that they neglect important factors, such as the energy distribution of the laser or the point spread function of the microscope, and therefore risk yielding large errors. The lack of FRAP models that can estimate the local diffusion coefficient with high precision in very small bleaching areas hamper the ability to determine local diffusion in highly heterogeneous materials such as multiphase samples. Consequently, it has until now been a great challenge to use FRAP in dynamic systems and in highly heterogeneous materials.

These challenges are addressed in this thesis work. New high-precision FRAP models that efficiently utilise all available temporal and spatial information in the FRAP data have been developed. These models can estimate the local diffusion coefficient in small areas which makes it possible to use FRAP in highly heterogeneous materials. The new models have been applied to heterogeneous multiphase systems. Time series of consecutive FRAP measurements have been used to follow the time-dependent changes of the diffusion coefficient during swelling, aggregation and gelation. The trends in diffusion have been compared with rheological measurements to reveal the effects of dynamical changes of the structure. This requires the possibility to quickly determine the local diffusion coefficient with high precision.

This thesis has been a part of the VINN Excellence Centre SuMo Biomaterials (Supermolecular Biomaterials – Structure dynamics and properties), which is a joint effort between academia and industry partners. Structure–mass transport relationship is of high interest for the SuMo Biomaterials centre. By improving the FRAP technique, this thesis work has expanded the toolbox for the SuMo partners and everyone that has an interest in determining local diffusion properties in heterogeneous materials or materials undergoing dynamic changes.

2 Objectives

The main objectives of this thesis were to further develop the FRAP methodology and expand it into new areas where FRAP is applicable. These new areas include determination of local diffusion during structure dynamics and estimation of local diffusion in highly heterogeneous materials. Detailed tasks can be formulated as follows:

- Develop evaluation models for FRAP that utilize all available information in the acquired data in order to increase the precision of how well a local diffusion coefficient can be determined.
- Decrease the lower size limit of FRAP to enable measurements inside smaller regions in a heterogeneous material structure.
- Make FRAP able to handle arbitrary bleach shapes and profiles.
- Enable the possibility to use FRAP during dynamic conditions as well as record FRAP data during dynamic transitions.
- Make use of FRAP to different diffusion properties in a multiphase system.
- Relate diffusional properties, determined by FRAP, to rheological properties.
- Improve the understanding of probe behaviour and properties in FRAP methods.

3 Background

This chapter gives an basic background on the FRAP technique and some underlying mechanisms.

3.1 Diffusion

There are two mechanisms for mass transport inside a material structure: diffusion and flow, and which of these become the dominant contributor to the mass transport largely depends on length scale of pores and voids in the structure. Diffusion always takes place but is, at larger scales, shaded by the presence of a flow. Flow, on the other hand, needs an external force to exist. Figure 3.1 illustrates the importance of flow and diffusion at different length scales. The total mass transport inside a material with a given pore size is the combination of the flow and diffusion. There is no flow inside a material if the pore size of the structure drops down to or below ∼100 nm [51, 54], since the pressure drop would become too large and the structure would rupture [131]; instead the main mechanism of transport inside denser areas is due to diffusion. For a material pore size range of roughly 100–200 nm, both flow and diffusion are be relatively equal contributors while at longer length scales, flow usually dominates.

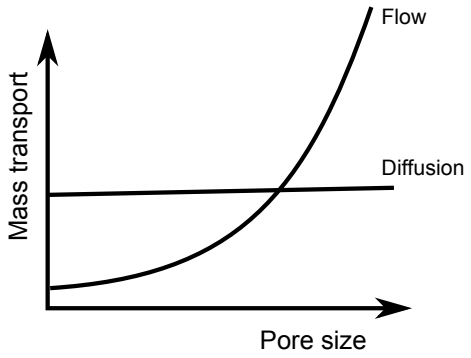

Figure 3.1: A concept image showing the relationship between flow and diffusion in relation to the pore size of the media in which mass transport takes place.

The difference between flow and diffusion is that flow is a directed transport of particles in a gas or a liquid while diffusion is the random movement of particles in any medium, either gas, liquid or solid. Brown [14] was the first to observe this random motion by studying pollen debris and the theory behind the process was explained by Einstein [37] and Smoluchowski [116]. Stated simply, it can be described as the spread of particles through random motion from regions of higher concentration to regions of lower concentration; however this is not entirely true. Diffusion will take place regardless of concentration gradients as it is driven by the internal heat of each molecule (k_BT) [38]; that is, all molecules moves constantly and are displaced through collisions with other molecules and with boundaries within the media. The process is entirely stochastic and if the diffusion is unhindered, all directions are equally likely to be the direction in which the molecule moves. Since all directions are equally probable, defining a velocity for the molecules

becomes difficult as the mean displacement is zero. Figure 3.2A shows the trajectory for a molecule and the final displacement of the molecule depends on for how long the molecule is monitored. Since the motion is entirely random, it can be seen in the example that the molecule (gray circle) does not move far away from the original start location (dotted circle). Figure 3.2B shows the probability of the displacement for the diffusing molecule, which is normal distributed with mean zero. Since the mean displacement is zero, a way to characterize the diffusion is to use the mean *square* displacement. This can be expressed as $\langle r(t)^2 \rangle = 2nDt$, where r is the time dependant displacement [m], n is the number of dimensions, D is the diffusion constant [m^2/s] and t is the time [s].

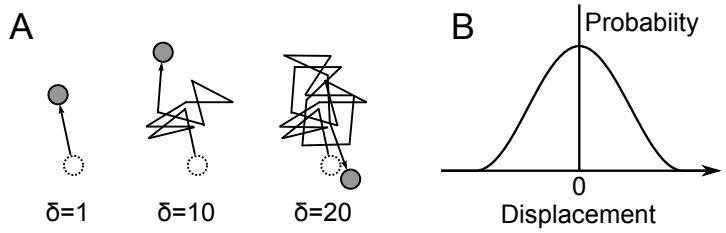

Figure 3.2: A concept image of molecular displacement. (A) The trajectory monitored for three different time scales with a uniform step size (δ), starting at the dotted circle and ending at the gray circle. (B) The probability for a specific displacement from the start location.

When following an ensemble of molecules, each individual molecule still diffuses around randomly, but considering the ensemble at large in the presence of a concentration gradient, the diffusion will appear to have a net direction. The net movement is seen simply because it is statistically more likely that the molecules move from an area with high concentration to an area with low concentration. In a continuum, the diffusion process can be described by a partial differential equation [39]. The diffusion equation is

$$\frac{\partial C(r,t)}{\partial t} = \nabla \cdot \left(D(C,r) \nabla C(r,t) \right), \tag{3.1}$$

where $C(r,t)$ is the concentration of molecules depending on location, r, and time, t, and D is the combined diffusion coefficient which depends on the concentration at each location. If the diffusion coefficient is constant, then Equation 3.1 is simplified to

$$\frac{\partial C(r,t)}{\partial t} = D \nabla^2 C(r,t). \tag{3.2}$$

For the special case of probe diffusion in an infinitely diluted solution, the diffusion coefficient can be described with the Stoke-Einstein relation

$$D = \frac{k_B T}{6\pi\eta r_H}, \tag{3.3}$$

in which k_B is the Boltzmann's konstant, T is the absolute temperature, η is the solution viscosity and r_H is the hydrodynamic radius of the probe. This relation can be useful to either describe a theoretical diffusion constant for a probe or to estimate the probe size.

In the cases in which the diffusion is not linear with regard to time, the diffusion is called anomalous and described as $\langle r(t)^2 \rangle = 2nDt^\alpha$ [110]. For $\alpha = 1$ the expression is the normal mean square displacement. For $\alpha > 1$ it is a "super-diffusion" which is aided, for example, by cellular transport; for $\alpha < 1$ the diffusion is hindered in some way, such as from binding to the material or by diffusion through a porous material in which the molecule not only has to travel along the larger voids of the material but also can diffuse into closed cavities [10].

3.2 Diffusion in gels

Inside gels, the diffusion of (probe) molecules is not entirely free since there are gel strands present which hinder the diffusion and the molecules might interact with the gel strands. Furthermore, the gel strands can self diffuse ("breathe") which might create locally denser areas that retard the molecules or which open up the structure to allow large molecules to pass. There are a few different models which attempt to describe diffusion in gels [80], although not all of them take the heterogeneity of the material or the probesize into account [1]. The free volume theory describes the probe retardation as a reduction of the average free volume available to diffuse through [78]. The obstruction theory considers the gel strands as rigid obstacles which make the gel network act like a sieve [2, 60, 90]. The hydrodynamic theory adds an friction interaction between the molecules and the gel strands [25, 99]. There are also models which combine different aspects of the other theories [23, 61].

3.3 FRAP

Fluorescence recovery after photobleaching (FRAP) is an optical technique that measures local diffusion in soft (bio) materials. A soft material means, in this work, that the material has some fraction of liquid phase in which the probe can be dissolved and transported. It might be possible to have a completely dry material, although it is not practical as solid phase diffusion will take too long to monitor. The general procedure for taking a FRAP measurement is to introduce a fluorescent probe in the sample, locally bleach a volume and then study the recovery of fluorescence. As FRAP is currently performed with a confocal laser scanning microscope (CLSM), the precision of the technique depend greatly on the performance of the microscope; the minimum resolution depend on the optical resolution and limits in the diffusion rate depend on the image acquisition rate as well as the stabillity of the microscope and sample. On a modern CLSM, a bleached spot is usually a few micrometers or larger, more commonly around 30 µm in material science [11, 62]. The diffusion coefficients possible to capture lie in the range of 0.1 to 300 $\mu m^2/s$; slower diffusion coefficients are possible to obtain but tedious to measure as the measurement takes a very long time and requires very stable conditions while faster diffusion coefficients will only be limited by the image acquisition rate of the CLSM and the signal-to-noise level of the images.

The concept of FRAP can be seen in Figure 3.3, where Figure 3.3A shows an illustration of a typical FRAP experiment. The stained sample is first analyzed with a low intensity laser beam in order to locate an area of interest in the sample. When a suitable area is found, the FRAP starts with a prebleaching step (t<0). During this step a couple of frames are recorded, still with

a low intensity laser, to make sure that the laser intensity is low enough so that the fluorescent probes are stable during the recovery phase. A region of interest (ROI) for bleaching is marked in the image and at t=0, the laser intensity is significantly increased while the laser beam is inside the bleach ROI. Outside the ROI, the laser intensity is kept low. This is regulated by an acousto-optical tunable filter (AOTF). Directly after the bleaching step, the laser intensity is reduced and the entire area is then monitored with a low intensity laser beam during the recovery phase (t>0). The recovery comes from fresh probe molecules which diffuse into the bleached volume at the same time as the bleached probe molecules diffuse out from the bleached volume. The rate of diffusion is directly correlated to the recovery rate of the bleached volume. In order to quantify the recovery, the pixel intensity is assumed to be linearly dependent on the concentration of probe molecules, which is true as long as the probe concentration is low.

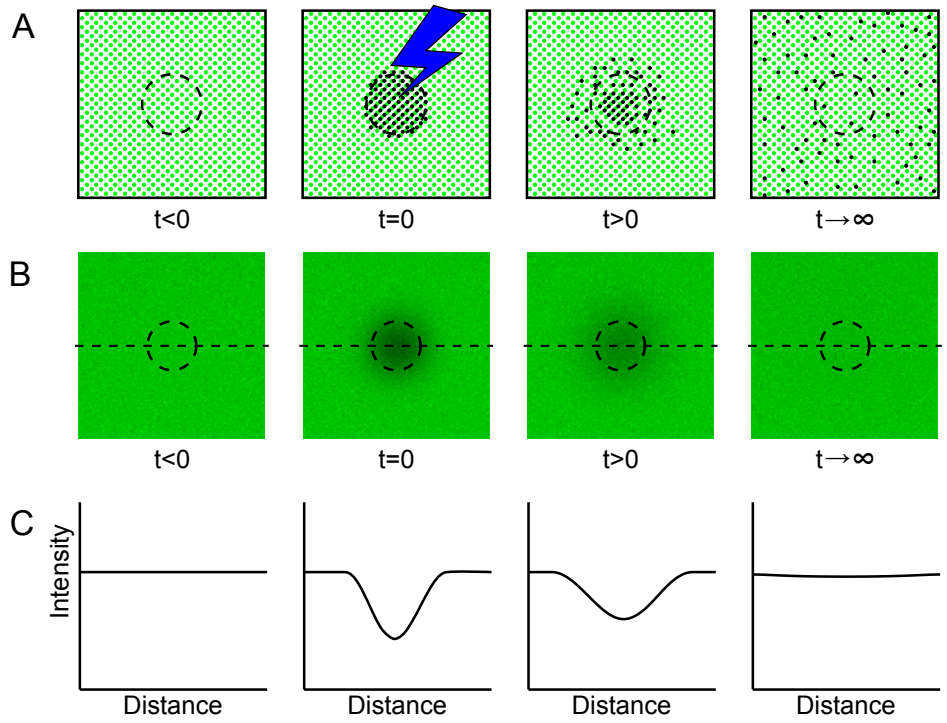

Figure 3.3: A typical FRAP experiment. The dashed circle represents the selected bleach ROI. (A) A conceptual image with the fluorescing molecules heavily exaggerated. (B) A real example of fluorescein in a 5% gelatin gel with 15% sugar added. (C) The bleach intensity measured along the dashed line going through the middle of the bleach ROI in (B).

Figure 3.3B shows a real FRAP experiment performed in a gelatin gel with 15% suger added using Na_2-fluorescein as diffusionprobe. At t<0, the probe is homogeneously distributed in the solution and there are no gradients present. The dashed circle represent the bleach ROI and t=0 show the first image after the bleaching step (the actual bleach image is recorded by the CLSM but show no relevant information as it is saturated by the laser). As the bleached probe molecules diffuse out from the bleached area while fresh probe molecules diffuse in, the bleached area recovers (t>0); eventually the area fully recovers and there are no longer any trace of the

bleaching as the average intensity is back to the initial intensity ($t \to \infty$). Figure 3.3C displays how the intensity profile, measured along the dashed line in Figure 3.3B, varies with time in the image. At $t<0$, no bleaching has occurred yet and the intensity profile show the background intensity of a fresh sample. In the first image after the bleaching step ($t=0$), the intensity profile assumes a Gaussian like shape due to a relatively quick diffusion. As the sample recovers, the intensity profile will even out as a diffusing Gaussian profile ($t>0$) and when the recovery is complete, the intensity profile will again be linear. It should be noted that there are occations when the intensity will not fully recover. If the amount of bleached probe is negligible in comparison to the amount of fresh probe present in the material then recovery will bring the background intensity to the same level as the initial intensity. If there is too little fresh probe, or if the probe attaches to the material, then there will not be a full recovery and the final intensity in the ROI will be lower than the initial intensity.

3.3.1 A brief history of FRAP

A look at the development of FRAP throughout the past 40 years reveals a somewhat broken history. In the mid 1970s, the first evaluation models for FRAP data was proposed by by Peters et al. [96] and Axelrod et al. [3]. The interest then was to measure lateral diffusion in membranes by tagging lipids with fluorescent groups. The bleaching and analysis were performed using a modified fluorescence microscope with a non-scanning laser as light source and a photo-multiplier tube as a detector. Smith and McConnell [115] (1978) introduced fringe pattern FRAP in which the bleached area is not a uniform spot but instead a raster caused by putting a grid in front of the laser. The idea behind this was to increase the accuracy, to follow the diffusion over longer distances and also to differentiate probes with different diffusion coefficients. Davoust et al. [27] (1982) made some improvements to the fringe pattern model by changing the mechanical grid into a grid caused by interference between two modulated laser beams. This change increased the signal to noise as all noise not related to the laser beam modulation could be suppressed. However, the fringe pattern method have not been used as much as spot bleaching and one explanation could be that the that it later on became difficult to implement in commercial microscopes. Early on, most groups performing FRAP experiments had been specialized labs but after Soumpasis [119] (1983) made theoretical improvements to the evaluation model proposed by Axelrod et al. [3], which made it much easier to use, more groups started to use the technique. Despite this, no significant improvement of the FRAP technique could be noted up until the 1990s.

Blonk et al. [8] (1993) published a paper in which they incorporated the FRAP technique into confocal laser scanning microscopy (CLSM). They used a stationary beam for bleaching and a scanning beam for analysing the sample. This led to much better imaging of the sample, better control of the laser and was the start of a new era of development of the FRAP technique. Kubitscheck et al. [69] (1994) published a new evaluation model which had higher accuracy than previous models, however it had some drawbacks as it required larger areas to be bleached because it did not take the point spread function of the microscope into account. Wedekind et al. [130] (1994) introduced the acousto-optical modulator, which allowed higher control of the laser as it was possible to change the intensity on a pixel basis and therefore possible to bleach regions with arbitrary size and shape with a scanning laser instead of a stationary beam. This technique was then taken up by the different producers of confocal microscopes and later developed into

the modern acousto-optical tunable filter (AOTF). To address the limitations in previous models, Braeckmans et al. [11] (2003) introduced the uniform disc model. This model took many overlooked aspects such as the bleaching phase and scanning into account but was limited in how small the bleach areas were that it allowed. As a way to decrease the lower limit of the bleached disc size, Braeckmans et al. [12] (2007) introduced line FRAP in which a thin line was bleached. The problem with line FRAP, however, was that it required calibration of the effective bleaching resolution before doing any FRAP experiment, which was a too tedious task to make it popular. Jonasson et al. [62] (2008) upgraded the accuracy of uniform disc model by taking the information from every pixel in every image into account but the model could not accurately account for slow diffusion since it assumed Gaussian shaped starting profile. The evaluation models proposed in Paper I and Paper III take this into account and a benefit of the model in Paper III is that it allows for any size and aspect ratio of the bleached area.

There are a number of other FRAP models which try to address different aspects not mentioned in the brief history. There are such aspects as multi-photon FRAP to bleach a 3D volume [13, 81], to take binding reactions into account [65, 120] and a numerical evaluation model which addresses heterogeneity in tissue [117], to mention a few. There are also two transform models: Fourier transform FRAP [126] and Hankel transform FRAP [64] in which the diffusion equations are solved in transform space, which means that they do not need any initial estimates of probe distribution and therefore are independent of the size and shape of the bleach ROI as well as diffusion during bleaching. However, neither of them takes the imaging point spread function into account.

3.3.2 Other techniques to measure diffusion

FRAP is an optical technique that measures local diffusion at micrometer scale. A few other techniques to measure diffusion are:

- Dynamic light scattering (DLS) is a technique to measure movement and size distribution of particles in solutions. A laser beam illuminates the sample and as the particles diffuse through the beam, they will scatter the light. The fluctuations of the intensity of the scattered light can then be correlated to the diffusion [7]. For the technique to work, the solutions need to be transparent and highly diluted.

- Single particle tracking (SPT) is an optical technique through which individual particle trajectories inside a solution or material structure can be observed. It can be used to measure diffusion (and flow) locally down to 10 nm scale in the sample [74, 109, 124]. The samples should be relatively thin to prevent the particles to leave the focal plane, else it can become difficult to track longer trajectories. Usually a CCD camera is required in order to capture images quickly enough for tracking.

- Fluorescence correlation spectroscopy (FCS) is a technique which measures local diffusion in a very small observed volume ($\sim 10^{-15}$ l). The diffusion is obtained from the intensity changes caused by probe diffusion in and out of the observed volume [6, 105]. This means that the sample is not imaged at the same time as the measurement is performed. A

sensitive photon counting detector is required in order to capture the intensity fluctuations accurately enough to correlate it to the probe diffusion.

- Image correlation spectroscopy (ICS) is an extension of FCS that utilizes an entire microscope image and therefore performs FCS in parallel in several spots. This is useful for slower processes when a single spot would take too long time to yield useful information. [97, 121]. Since ICS correlates intensity fluctuations between image frames, the image acquisition rate limits the technique to relatively slow diffusion.

- Raster image correlation spectroscopy (RICS) is an alternate version of ICS which uses a time stack of images taken with a confocal laser scanning microscope. This makes RICS slightly similar to FRAP but with the major differences that FRAP requires a bleaching step. Instead of the bleaching step, RICS works as ICS but utilizes the time lag in the raster scanning of the laser beam to obtain both temporal and spatial information [31, 32]. A drawback is that it requires careful calibration of the detector to work.

- Nuclear magnetic resonance diffusometry (NMRd) is a non-labelled and noninvasive method for measuring translational motion. It measures global diffusion inside a material by applying a magnetic gradient and then analysing the relaxation of the affected molecules and can be used on most materials [18, 104, 113]. Diffusion of molecules are monitored on a time scale of miliseconds to seconds and the technique is therefore limited to relatively fast diffusion.

- Thin sectioning of a sample can be used to measure how deep a diffusant has penetrated. The concentration of the probe can be measured for each slice using different spectroscopical methods, which will depend on the sample and probe used. The accuracy of this method is highly dependent on the thin sectioning equipment. It can can take very long time to create the samples if the diffusion of the probe is slow.

3.4 FRAP Models

The development of new evaluation models for FRAP data have slowly gone forward since the intial development in the 1970s. The slow development has been due, at least in part, to the need of more powerful computers to solve the equations on a feasible time scale. As the computational power has increased, so has the accuracy of the models. More and more experimental issues have been taken into account in the models and the complexity of them has increased. In general, while the mathematical details may differ to some extent, most FRAP models rely on three basic modeling steps: photobleaching, diffusion and imaging.

The purpose of modeling the diffusion is, in essence, to solve the diffusion equation (Equation 3.2) while at the same time taking surrounding aspects into consideration. The surrounding aspects depend on the material in which the diffusion takes place, such as whether there are reactions between the probe and the material or whether there is anomalous diffusion or a flow present. A reaction between the probe and material could, for example, be when the probe binds to the material structure for a period of time before releasing and diffusing on as if free [65, 120].

Anomalous diffusion could, for example, be directed movement inside cells. An aspect which complicates the modelling of the diffusion can be if the probes, such as GFP variants, exhibit reversible photobleaching. This would mean that the intensity increment over time is not solely caused by diffusion of the molecules but also a reactivation of bleached probes [114].

In order to be able to solve the diffusion equation, there is a need to know how the initial concentration of fluorophores after bleaching is distributed as well as the boundary conditions. This can either be estimated from the first image after bleaching (Paper I) or by means of modelling the bleching step. An alternate way would be to use a model which does not equire the knowledge of the initial distribution of the fluorophores [64, 126]. Another aspect of the bleaching step is the energy distribution of the laser beam as well as the amount of bleaching introduced. Quite often the beam energy distribution (BID) is approximated as a Gaussian function limited to the first diffraction maxima, however Braeckmans et al. [11] showed that a bleached spot quite often is influenced by both the second and third diffraction maxima. Due to this, the shape and size of a bleached area needs to be calculated using an apparent BID which takes the extra maxima into account, else the diffusion calculations will depend on erroneously estimated geometry.

The imaging step is highly influenced by the point spread function (PSF) of the microscope [63]. The PSF describes how a point in a sample will be imaged.A spherical point will take a "butterfly" shape and this distortion needs to be corrected for, especially when bleaching small regions. The original image can be obtained through deconvolution if the PSF is known. The PSF depends on the laser wavelength, objective and immersion media and can be estimated with the aid of immobilized fluorescing spherical beads (quantum dots) with subresolution size. If the PSF is not known, it needs to be estimated in the FRAP model. When estimating the PSF, the shape is often assumed to be 3D Gaussian.

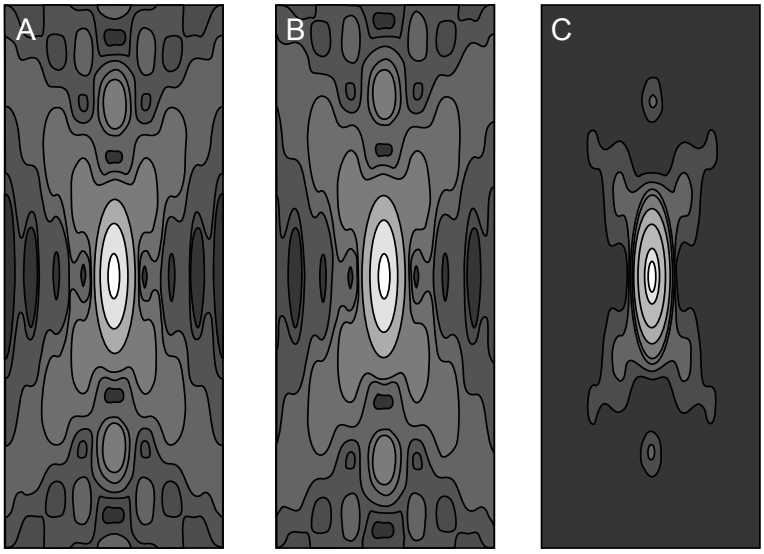

Figure 3.4: The product of an illumination PSF (A) and the detection PSF (B) of a CLSM will produce the confocal fluorescence PSF (C). This is a description of how a point object will be interpreted by the microscope. Image adapted from Jonkman and Stelzer [63].

3.4.1 Averaged bleaching region models

When completing a FRAP experiment, it is common to plot the average intensity of the bleached spot over time to see that the experiment proceeded as intended, in order to see that the probes did not bleach during the pre and post bleach phase and to see that the recovery looks reasonable. Most modern CLSM have software included to do this automatically at the end of an experiment and also often include the function to make a curve fit of the plotted data in order to analyse the characteristic recovery time of the sample. Figure 3.5 shows a typical recovery curve and it can be seen that the shape of the recovery curve closely resembles an exponential function. The curve can be described as

$$\frac{F(t)}{F(0)} = 1 - be^{-t/\tau}, \tag{3.4}$$

where $F(t)$ is the fluorescence intensity at time t, $F(0)$ is the initial fluorescence intensity, b is the fraction of bleached fluorophores, and τ is the characteristic recovery time, $t_{1/2} = \tau \ln 2$. The half recovery time, $t_{1/2}$ is the time it takes for the intensity to reach halfway to the maximum intensity. The half recovery time can be related to the diffusion coefficient as

$$D = \gamma \left(\frac{\omega^2}{4t_{1/2}} \right), \tag{3.5}$$

which was suggested by Axelrod et al. [3]. The relation was derived for a stationary laser beam bleaching a small spot with radius ω. The γ term is a correction function which will have a constant value of 0.88 for a uniform circular spot but will, however, become a function which varies between 1.1 to 3 depending on the bleaching introduced into the sample if the sample is bleached by a laser with Gaussian energy distribution.

Since this model is mainly derived from empirical data, it does not take bleaching processes into account and, if the size of the bleached spot is not well determined, the accuracy of the resulting diffusion constant is highly questionable. Instead, it is useful as an initial estimate of the magnitude of D and it can be used as an starting guess when estimating the diffusion coefficient using a more comprehensive model.

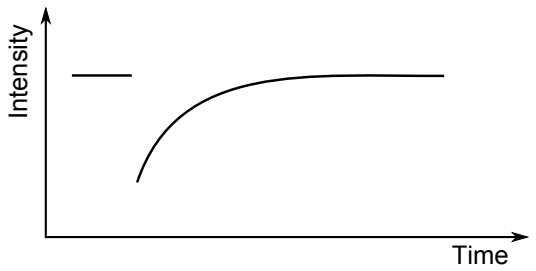

Figure 3.5: A typical recovery curve showing the averaged intensity from the bleached ROI over time.

As the early FRAP models were derived for use with a stationary laser, the implementation of FRAP with CLSM which was done by Blonk et al. [8] changed the process. Braeckmans et al. [11] suggested a new model, the uniform disc model, which would take the scanning of the laser beam into account in the evaluation. Their goal was to make a robust model with an analytical

solution to make it "easy to implement" and therefore more accessible. The model averages the intensity in the bleached ROI, which yields a higher signal-to-noise ratio but therefore also loses information from individual pixels.

3.4.2 Pixel based models

The model which Braeckmans et al. [11] derived offers a beautiful analytical expression to describe the recovery of a FRAP experiment with high accuracy, although there is still a limitation in it as it uses the average intensity in the bleached disc. The benefit with the averaging is that the analytical expression can be quickly calculated by fitting the FRAP model to the time dependent recovery curve. However, the limitations that follow mean that the fluorophore distribution after bleaching need to be known exactly, which in turn means that either effective photobleaching should be known or large discs needs to be bleached. Another drawback with the averaged models is that a large portion of the available information is removed when averaging. Some early models adress this by taking the pixel based information into account [67, 111].

A limitation of the early pixel based models was the lack of incorporation of the noise in the model. A solution to improve this was suggested by Jonasson et al. [62], where the noise in each pixel was estimated as independent and Gaussian distributed. The initial fluorophore concentration after photobleaching is approximated as a Gaussian distribution and the parameter estimation is done with maximum likelihood statistics, which have the benefit of giving an error estimate of each parameter.

A drawback with the Gaussian model described by Jonasson et al. [62] is that the starting profile is assumed to be Gaussian shaped. This is not true for very slow diffusion, where instead the initial starting profile will have a shape that more closely resembles an inverse hat function. One way to circumvent this would be simply to remove all images in the start recovery series until the intensity distribution have taken on a Gaussian shaped profile, although this would lead to a decrease in accuracy due to a loss of initial data.

3.4.3 Maximum likelihood

Maximum likelihood is a method to estimate parameters in a statistical model. In contrast to probability, which determines the chance of a specific outcome given a set of parameters, likelihood determines the most likely parameter values given a specific outcome [94].

The basic principle behind maximum likelihood estimation (MLE) is to consider a set of n independent observations $(x_1, x_2, \ldots, x_n)$ of a sample with parameters θ, which has an unknown probability density function. The true values of the parameters θ_0 are unknown and are sought after.

If the observations are independent and evenly distributed, then the joint density function of all observations is defined as

$$f(x_1, x_2, \ldots, x_n \mid \theta) = f(x_1 \mid \theta) \cdot f(x_2 \mid \theta) \cdot \ \ldots \ \cdot f(x_n \mid \theta) = \prod_{i=1}^{n} f(x_i \mid \theta) \tag{3.6}$$

The product is called the likelihood and the log likelihood is then defined as

$$\begin{aligned} L(\theta \mid x_1, x_2, \ldots, x_n) &= \prod_{i=1}^{n} f(x_i \mid \theta) \\ \log L(\theta \mid x_1, x_2, \ldots, x_n) &= \log \prod_{i=1}^{n} f(x_i \mid \theta) = \sum_{i=1}^{n} \log f(x_i \mid \theta) \end{aligned} \tag{3.7}$$

By considering the observed variables (x_i) as fixed and by letting the unknown parameters (θ) be varied freely, the parameters which are most likely correct are those which maximise the log likelihood function.

3.4.4 Spatial analysis

Spatial autocorrelation is of interest in the analysis of material structures. Spatial statistics are used to analyse any data with topological or geometrical properties and, combined with autocorrelation, can be used to analyse the correlation of properties as a function of length scale(s) in a material structure. By measuring the degree of correlation of geographical points in the material, periodicity and heterogenity can be detected [46].

Correlating the diffusion coefficients in the case of material science means that measurements done inside the same type of structure should yield the same (or similar) diffusion coefficients since the probe would experience the same type of hindrance. As the different structures have a limited physical length, it means that the diffusion at spot X would be correlated to the diffusion in spot X+δ, as long as both spots are in a similar type of structure.

If the spatial data is obtained along only one dimension, then the correlation between the data at position x and the data at position $x + \delta$ can be calculated as [20]

$$r(\delta) = \frac{\frac{1}{N-\delta} \sum_{x=1}^{N-\delta} \left(\left(Y_x - \bar{Y} \right) \left(Y_{x+\delta} - \bar{Y} \right) \right)}{\frac{1}{N} \sum_{x=1}^{N} \left(\left(Y_x - \bar{Y} \right)^2 \right)}, \tag{3.8}$$

where δ is the step size, Y_x is the data value at position x, $\bar{Y}$ is the mean of Y, N is the number of data points and $r(\delta)$ is the correlation coefficient for data points separated with a step size of δ. A discrete autocorrelation function is obtained by varying the step size (δ) and calculating r for each δ.

A method of analysing the autocorrelation in 2 (or 3) dimensions is by computing Moran's I [83]; which is a quantification method weighted for distance. Moran's I is sensitive to the global autocorrelation and is calculated as

$$I = \frac{N}{\sum_i \sum_j \omega_{ij}} \frac{\sum_i \sum_j \omega_{ij} \left(X_i - \bar{X} \right) \left(X_j - \bar{X} \right)}{\sum_i \left(X_i - \bar{X} \right)}, \tag{3.9}$$

in which i and j is the spatial index, N is the number of points, X is the variable of interest, $\bar{X}$ is the mean of X and ω_{ij} is the weights, often defined as the inverse distance between the points. Moran's I varies between -1 to 1, where a negative value indicates negative correlation and vice versa.

4 Materials

This chapter offers a brief overview of the materials used within this thesis. There is a close relationship between the materials and the development of the fluorescence recovery after photobleaching (FRAP) technique as FRAP has been used to study the properties of the materials while, at the same time, the materials have been used as model materials to develop FRAP. The different types of materials involve gels, phase separated gels and pasta.

By changing the ionic conditions, biopolymer concentration and end temperature, different microstructures and aggregation kinetics in the κ-carrageenan gels were evaluated. The effects of free volume and heterogeneity on probe diffusion in κ-carrageenan gels were determined by a combination of FRAP, transmission electron microscopy and rheology. Gelatin offers nice possibilities to tailor the gelation rate and the gel strength by adjusting the gelatine concentration and the end quench temperature. Formation of transient structures were determined in gelatin gels using a combination of FRAP and rheology. Pasta and β-lactoglobulin gels was used to probe structural heterogeneity and correlation between heterogeneity and the diffusion behaviour. Local diffusion coefficients were determined in phase separated biopolymer mixtures of gelatine and maltodextrin with very heterogeneous microstructures. A FRAP model was developed to be able to measure local diffusion in such heterogeneous systems. The effect of swelling on probe diffusion in super absorbent polymers (SAP) was evaluated using FRAP. A FRAP model that can handle arbitrary initial bleaching concentration profiles and thereby cover a large span of diffusion coefficients was developed.

4.1 κ-carrageenan

κ-carrageenan is one of many carrageenan types, where carrageenan is a polysaccharide extracted from seaweed. It is commonly used as an additive in foods due to its ability to form structures ranging from viscoelastic liquids to hard gels and for its non animal origin. Different types of carrageenan gels are also widely used in different pharmaceutical formulations because of their stabilizing, thickening and gelling properties [45].

The gelling mechanism of κ-carrageenan and similar biopolymers functions by going from individual polymer chains in a random coil formation to a state in which the random coils form a helix. The helices will then form the gel network by branching either on the helical level or the super helical level [127]. To initiate gelation, the aggregation is usually promoted by lowering the temperature and adding ions. The building up of a percolating network influences both the mechanical and diffusion properties of the carrageenan gels. κ-carrageenan gels are thermo reversible and the gel temperature differs depending on carrageenan type, carrageenan concentration and the ion type and concentration used [43, 50, 89]. It is believed that the gel matrix that is formed during the instantaneous gelling is not completely locked; it instead rearranges after the gelling and continues to aggregate and forms transient networks [52]. Depending on which salt is used, the different ions will interact differently with the carrageenan [84]. For example, potassium ions will bind strongly on specific sites and give a gel network that can vary from a finer type with small voids to coarse strands separated by larger voids, depending on the amount of potassium used [77, 129].

4.2 Gelatin

Gelatin is one of the most commonly used industrial gels and is therefore one of the most widely investigated gels. Gelatin is a protein based material which is derived from the collagen found in the skin and bones of animals.

The gelation of gelatin involves a formation of triple helices, where the individual gelatin strands are stabilized by hydrogen bonds in a right-handed helix [34]. The gelation of gelatin follows the percolation theory, where the gelatin triple helices form aggregates in the solution. The aggregates then grow, interconnect and form larger and larger domains until the whole volume is percolated and the gel point is reached [28, 33]. The gelation is sensitive to temperature and gelatin concentration such that lower temperatures and higher concentrations lead to faster gel formation and stronger gels [34].

Transient networks are believed to rapidly form locally in the system, which will rearrange and eventually disappear. The lifetime of these networks increases when the system moves towards gelation and, at the gelation point, the transient networks percolate throughout the whole system. Exactly what happens in the gelatin before percolation is not fully known but extensively investigated [9, 28, 33, 42, 100].

4.3 β-lactoglobulin

β-lactoglobulin is the dominating protein in the whey fraction of bovine milk [108]. It is a heat setting gel which forms an aggregated gel near the isoelectric point as long as the concentration is high enough.

The size of the individual protein globules are around 2 nm and the gel formation is complex with different structures forming depending on the ionic conditions, pH and temperature ramp during heating [70]. Below the denaturation temperature and at a pH around 5.4 (near the pI) there will be particle formation and aggregation [122]. These aggregates are around 1 µm and will then cluster together into a network with domains which ranges between ∼10–50 µm depending on ionic conditions and temperature ramp [70]. Depending on the pH the aggregation process can take two different paths. At low pH, the β-lactoglobulin forms branched strings of monomers where the branching depends on the ionic condtions. At a pH of around 7, the aggregation will follow a two step process where the β-lactoglobulin monomers first cluster together to form primary aggregates (∼100 monomers), and these primary aggregates then associate into larger clusters which will form the gel [103]. The temperature ramp drives the rate of aggregation, but the structure does not depend on temperature [73].

An interesting feature of β-lactoglobulin is the different length scales on which it aggregates. Going from the ∼2 nm large monomer up to a gel with domains in the size range of ∼10–50 µm, several aggregations emerge that form self-similar structures [4, 70, 71, 93]. This means that it can be possible to tailor the material for domains of very different sizes on several length scales, which is an interesting feature to utilize when using FRAP as a tool for correlation measurements.

4.4 Maltodextrin

Maltodextrins are partially hydrolysed starch products, consisting mainly of D-glucose, maltose, oligosaccharides and polysaccharides with broad molecular weight distributions [22]. The starch sources are commonly maize, oats, rice, tapioca, potato, sorghum or sago palm. The maltodextrins have various interesting properties such as being watersoluble, fermentable, having low hygroscopicity and can be used to increase viscosity of a solution or to create a gel. These properties make them useful as texture providers, film formers, freeze-control agents, spray-drying aids and bulk agents [79]. Hydrolysed starch products are commonly characterised by their degree of hydrolysis, expressed as dextrose equivalence (DE). The DE is the percentage of reducing sugars present and it is calculated on a dry-weight basis relative dextrose [79]. It takes several hours for maltodextrin to form a gel and the gel strength increases with maltodextrin concentration. There is also a minimum concentration needed to form a gel, ranging between ∼10–20% depending on the type of maltodextrin [22].

4.5 Phase separated gels

Phase separated gels can be created from a mixture of two or more (bio) polymers in solution. The phase separation will be either through a segregative process, in which the polymers enriches into separate phases, or associative process, in which the polymers are enriched in the same phase; the final mixture becomes a water-in-water emulsion [88]. The driving force towards phase separation is an enthalpy gain as the entropy is lowered by a lowered temperature and if the polymers are slightly incompatible, then they will prefere solitude prior to the mixing. The entalpy gain is described by the Flory-Huggins interaction parameter [76, 88]. The stability of biopolymer mixtures is commonly described by the phase diagrams of specific mixtures and the border between a stable mixed system and meta-stable systems is called the binodal. While in the meta-stable region of a mixture, phase separation will occur through nucleation with a subsequent growth of domains. The border between the meta-stable and the unstable region is called the spinodal. When a mixture is in the unstable region, it phase separates through spinodal decomposition. Spinodal decomposition is caused by concentration fluctuation with a characteristic wavelength and will give rise to a self-similiar mottled pattern which, unlike nucleation, grows simultaneously in the whole sample. The structures formed can be both bicontinuous or discontinuous depending on the phase volume of the biopolymers. If the phase separation is allowed to continue for a very long time, the domains will coarsen and finally the system will bulk phase separate with the phase with the highest density at the bottom. If the gravitational pull is removed or can be neglected, then the phase with the highest affinity for the surface of the beaker enclose the other instead of being ordered by density [56]. When/if one or more of the phases gels, then the phase separation will cease and the structure will become kinetically trapped; from this, desired structures can be tailored through means of the interaction between phase separation and gelation. In this work, biopolymer mixtures made of gelatin and maltodextrin were used to create kinetically trapped phase separated gels with heterogeneous microstructures.

4.6 Pasta

Pasta is a staple food which is made from hydrated wheat flour that has been kneaded into a dough, cut and then dried. Eggs can be used in fresh pasta, but dried pasta is generally only flour and water.

Normally, pasta is made from durum wheat which consists of 74–76% starch and 12–15% proteins (dry basis). The starch granules exists as two types in pasta: type A which have a disc like shape and average size of 30 µm while type B is more spherical and an average size of 2–3 µm [16]. When the durum wheat pasta is boiled, the structure of the pasta changes significantly [26], where the main changes are caused by protein coagulation and starch swelling [98].

The starch contains amylose and amylopectin. The most important structural change to a cooked starch-based product is the granule swelling and the subsequent leakage of amylose and amylopectin [53] Amylopectin and amylose is present in the granules where amylopectin is ordered crystals and amylose is in a non ordered state. Upon heating in water, the amylose is solubilized and will gel upon cooling whereas the amylopectin forms a viscous solution. During the swelling of a starch system, the swollen granules are enriched with amylopectin while the amylose leaks out and forms a continous gel phase around the granules.

4.7 SAP

Super absorbing polymers (SAP) is a cross-linked polymer network with a high molecular weight, which can retain extreme amounts of water. The SAP network is highly stable and absorbed water will be retained even if the network is heavily compressed. This makes it a good absorbent for hygiene products, such as diapers and sanitary pads, as the user can sit down without discomfort from leakage. SAP is also used as absorbent for medical waste disposal, spill control and as water conservation material in agriculture [15].

There are several different polymers used to create SAP, such as polyacrylamide, polyethylene oxide, polyvinyl alcohol and polyacrylic acid; the common denominator is that the polymers are water soluble with a high ionic load. Even though there are several different polymers which can be used to create SAP, only SAP made from polyacrylic acid have been used throughout this project. The cross-linking of the polymer chains plays an important role as it makes the network itself non soluble and the driving force behind super absorbance comes from the osmotic pressure caused by the ionic groups on the polymer chains [15]. The resulting network can absorb up to ∼1000 g/g of deionised water; however, if salt is present in the absorbed water it lowers the osmotic pressure and the SAP therefore absorbs significantly less salt solution than deionised water. Nonetheless SAP is still able to absorb more salt water than traditional absorbent materials such as a fibre network [15]. The amount of cross-links also influences the hardness of the gel. Even though it is not possible to expel water by compressing the gel, a stiffer gel can withstand higher external pressure before breaking down. A problem with cross-linking the SAP too much is that becomes difficult to control exactly where on the polymers the crosslinker reagent react. A high amount of cross-links will therefore decrease the absorption properties as they will hinder the swelling of the gel and the need for mechanical stability will have to be weighed against the absorption.

5 Methods

The methods and calculation models used in this project will be described in this chapter.

5.1 CLSM

5.1.1 Basic principles of CLSM

A confocal laser scanning microscope (CLSM) is an advanced, high resolution fluorescent light microscope with the ability to record images in which the information comes from a thin optical section in the sample. The CLSM differs from a wide-field light microscope (LM) in a few key ways: the light source of a CLSM is a laser instead of a light bulb, images are formed by scanning a focused laser beam instead of recording the whole image simultaneously, there are two pinholes to remove out of focus light and the signal-to-noise ratio is much higher in a CLSM. The laser light has a number of unique properties such as small divergence, a high degree of monochromaticity and spatial and temporal coherence, plane-polarized emission, high brightness, and a Gaussian beam profile that makes it an almost ideal light source for use in a CLSM [44].

The Basic principle of a CLSM [95] is shown in Figure 5.1. Since different fluorophores require different excitation wavelengths, an array of lasers is required in order to cover the most essential wavelengths for multiple staining of samples. The transmitted laser intensity is controlled by an acousto-optical tunable filter (AOTF), which adjusts the proportion of light coming from each laser in the array and thereafter transmits it to the specimen almost instantaneously. Thus the light intensity of each single laser line can be adjusted from pixel to pixel at a high scan rate using real-time electronics. The AOTF will only let desired wavelengths pass through while other wavelengths of the laser will bend away from the beam path and be removed. In an epi-fluorescent CLSM, the laser that passes through the first pinhole will then hit a beam splitter which will direct the incoming laser light towards the specimen and the re-emitted fluorescent light towards the detector. The beam splitter is either made of a filter that consists of wavelength-discriminating mirrors or an acousto-optic beam splitter (AOBS). Wavelength-discriminating mirrors are dicroic or tricroic mirrors, which reflect light with certain wavelengths and allow light with other wavelengths to pass. The AOBS is an acousto-optical crystal which can be tuned with high precision to let certain wavelengths to pass straight through the crystal while bending the path of other wavelengths. Since the the width of the laser beam is much smaller than the area visualized in the sample, the beam will be moved in order to illuminate a large section. The beam is moved in x and y direction with the aid of scanning mirrors which vibrate in a sinusoidal shaped manner with a frequency of up to 8000 Hz [123]. The width of the linear part of the sinusoidal mirror movement and the on and off positions of the laser light determine the size of the scanned area. After the scanning mirrors, the laser light passes the objective and the immersion medium and then goes into the sample and becomes absorbed by the fluorophores. The fluorescence from the fluorophore will then go back to through the whole system up to the pinhole and the detector. The fluorescent light which does not originate from the focal plane will be removed by the second pinhole in front of the detector and, as a result, the sample can be imaged into thin optical sections. The sample resides on a stage with high precision control

of the movement in x-, y- and z direction. This allows the CLSM to move the focal plane and, by combining a stack of images along the z-direction, creates a 3D structure of the sample.

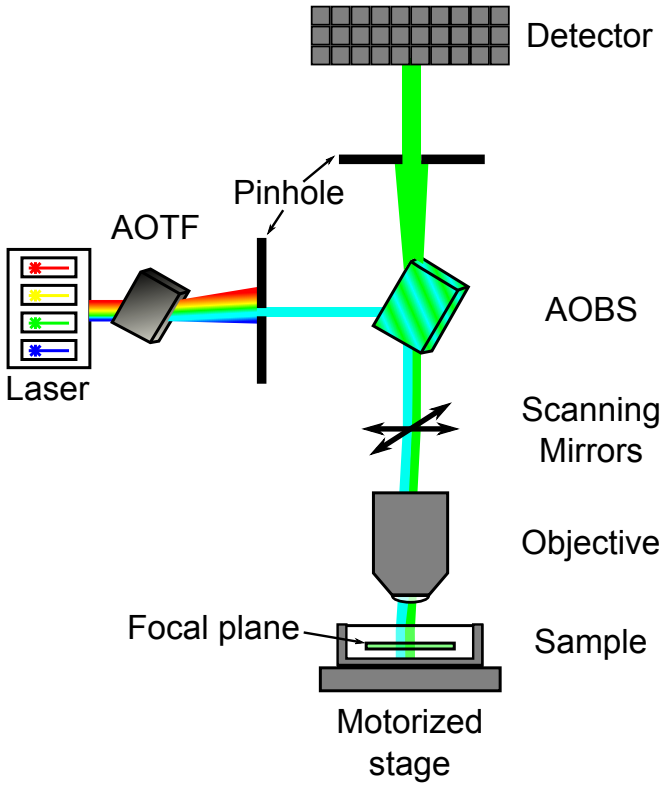

Figure 5.1: The basic principle of a confocal laser scanning microscope. In some systems the acousto-optical beam splitter (AOBS) is replaced by semi transparent mirrors to direct the light.

5.1.2 Fluorescence

Fluorescence works such that illuminated probes absorb photons if they contain enough energy to push the electrons in the sample to a higher energy state. When the electrons relax back to the ground state, they emit light but at a longer wavelength as some of the energy is disposed of as movement (usually seen as heat emitted in the infrared spectrum) [55] or because of interaction with the environment [49]. This process is called Stokes shift. Figure 5.2 shows a simplified energy diagram of the fluorescence process. The absorbed light contains exactly the right amount of energy ($h\nu$) required to raise an electron from the ground state (S) to a valid energy state just above the excited singlet stage (S*). The excited electron falls down to S* relatively quickly by emitting heat or by interaction with the solvent, and the time limiting step in the fluorescence process is the electron fallback to the ground state. All together, the fluorescence process is over in much less than a second, and a single molecule used for imaging a sample can usually be excited several thousand times before undesired bleaching occurs.

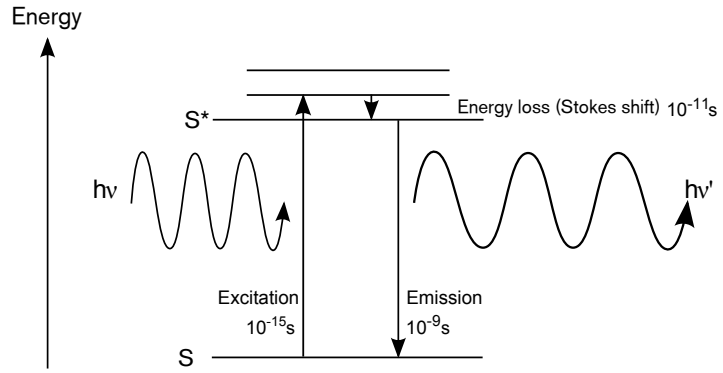

Figure 5.2: A simplified energy diagram illustrating the excitation-emission process which gives rise to fluorescence. S is the ground state and S* is the excited singlet state.

5.1.3 Microscope objectives and resolution

The microscope objective determines much of the information content of an image [66] and the role of the objective is to focus the laser beam and to ensure constructive interference at the focal point. The three-dimensional spatial light intensity distribution of the light around the focal point is described mathematically by the point-spread function (PSF). The PSF is closely linked to the spatial resolution of the CLSM, and a more localised PSF will always produce an image with higher resolution [36]. The resolved details in the specimen, the contrast at which these details are presented, the depth through the specimen from which useful information can be obtained and the diameter of the useful scanned region are all limited by the performance of the objective. This means that, in practice, the most important parameters that a CLSM user must consider are the magnification, the working distance of the objective and the numerical aperture (NA). Objectives exist with magnifications ranging from around two times up to hundred times, with numerical apertures ranging from approximately 0.05 up to 1.45. The numerical aperture basically determines how much of the re-emitted fluorescent light is collected by the objective and it normally increases with the magnification of the objective. Refractive index matching is also essential for the performance of the CLSM because bad refractive index matching will result in a lot of scattering and loss of signal as well as geometrical aberrations. It is therefore important to chose an objective and immersion medium that matches the optical properties of the sample [48]. The working distance is affected by the numerical aperture and it normally decreases as the numerical aperture increases due to the increase in the opening angle, α, of the objective lens. Spatial resolution is defined as the minimum spatial separation required between two point objects to distinguish them as two separate objects. The Rayleigh criterion corresponds to the spatial separation at which a 26.4% contrast separation is achieved [47] (see Figure 5.3). The confocal lateral and axial resolution could be estimated as [63]:

$$R_{lateral} \approx \frac{0.4\lambda_{emission}}{NA} \tag{5.1}$$

$$R_{axial} \approx \frac{1.4n\lambda_{emission}}{NA^2} \tag{5.2}$$

where $\lambda_{emission}$ is the wavelength of the detected light, NA $= n \sin \alpha$, and n is the refraction index of the mount medium. This means, for example, that for an oil objective with NA = 1.4 and $n = 1.518$ and $\lambda_{emission} = 510$ nm, $R_{lateral}$ and R_{axial} will be approximately 150 nm and 550 nm, respectively.

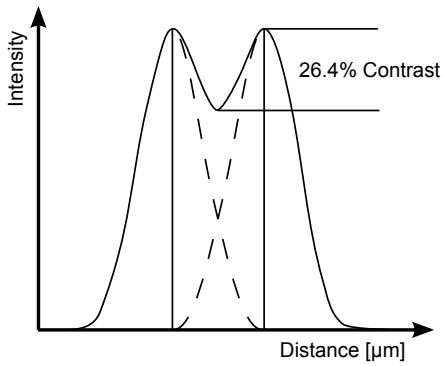

Figure 5.3: The resolution is determined as the distance where there is a 26.4% contrast between two objects.

5.1.4 Requirements for FRAP

There are a few prerequisites for FRAP that need to be taken into account. Most of the prerequisites depend on the FRAP model used for evaluation.

- The probe used must be distributed homogeneously in the sample, otherwise the diffusion will be affected by the concentration gradient.
- Another probe requirement is that there are enough probes present in the sample so that the fraction of bleached probes is negligible.
- The bleaching phase needs to be short enough to not allow any diffusion during the bleaching. Meyvis et al. [82] recommends the bleaching phase to be 15 times shorter than the characteristic recovery time.
- The only transport mechanism that contributes to the recovery is free diffusion; flow can be present only if the model used for calculations can handle flow.
- The medium in which the diffusion occur is assumed to be infinite in comparison to the bleached area; the diffusion should not be affected by phase or sample boundaries.
- The material needs to be transparent enough so that the laser light can penetrate deep enough into the material to fulfil the requirements of the evaluation model used
- The material must be able to withstand the strong laser light during bleaching without being destroyed

5.1.5 Linear relationship

The data from a FRAP experiment comes as a series of images taken by the microscope, in which the recovery will take the appearance of a dissolving disc. The diffusion coefficient is then calculated by solving Fick's second law using pixel intensity changes to correlate the probe concentration changes. This means that the pixel intensity needs to be directly correlated to the probe concentration, i.e. the probe concentration needs to be within the linear regime of fluorescence. Herman [49] gives the relation between fluorescence intensity and absorbance as

$$F = QI_0(1 - e^{-A}), \tag{5.3}$$

in which F is the fluorescence intensity, Q is the quantum yield of fluorophores, I_0 is the light intensity before the sample and A is the absorbed amount. This relation gives an asymptotic growing curve that approaches QI_0 as the absorbed amount goes toward infinity (this effect is called "saturation of the detector"). The solid line in Figure 5.4 indicates this behaviour. This is unwanted as it makes it impossible to relate the concentration of fluorescent probes to the fluorescence intensity, since a high concentration means that there will be a high absorbance and F will be equal to QI_0. At lower concentrations, however, there is a linear relation (shown as a dashed line in Figure 5.4). At low absorbance, $\left(1 - e^{-A}\right)$ approaches A and Equation 5.3 can be approximated as

$$F = kCQI_0, \tag{5.4}$$

where kC, in which C is the concentration and k is a constant, is subsituted for A. It is therefore important to check the intensity dependence of the probe concentration for each FRAP probe in order to use appropriate concentration. Note that an excessively low probe concentration results in a lot of noise in the FRAP experiment which is also unwanted. Another effect which also disturbs the correlation between the concentration and the intensity is inner filtering [49]. Inner filtering is a "crowding" effect caused by an overlap in emission and excitation wavelengths for the probe molecules. What happens is that nearby probe molecules absorb the emitted light from the probes in the focal plane and prevent the light from reaching the detector and the effect is increased for higher concentrations as well as increased depth into the sample. Even though the molecules which absorbed the light eventually will emit it again, they are often outside of the focal plane and the light emitted from those probes will be removed by the detector pinhole.

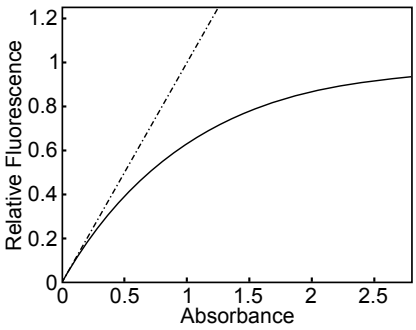

Figure 5.4: The relationship between absorbed light and fluorescence. The solid line represents the actual relationship. The dashed line represents a linear relationship between absorbance and fluorescence.

5.1.6 Bleach profile

Even though the CLSM only shows a thin optical slice of the sample, the penetration of the laser will affect the volume both above and below the focal plane. This means that during the bleaching step, the laser will bleach the sample all the way from the surface, through the focal plane and as deep down as the laser can penetrate. For a circular bleach ROI, the actual bleaching of the sample will take on a cylinder-like volume. How close to a true cylinder the bleaching will result in depends on the numerical aperture (NA) of the microscope objective. A high NA is desired in CLSM imaging as it increases the resolution, whereas a lower NA will give a more cylindrical shaped bleach volume which is desired for FRAP [8]. Figure 5.5 show how the NA will affect the bleach volume. The reason why a cylindrical shape is desired for FRAP is that as long as the width of the bleached ROI is much smaller than the height of the bleached cylinder, the diffusion along the z-axis can be neglected in calculations. There will still be diffusion along the z-axis, but since there will be no fresh probe molecules entering the focal plane along the z-axis during the course of the measurement, the influence of the z-diffusion can be neglected and Fick's law can be simplified to two dimensions.

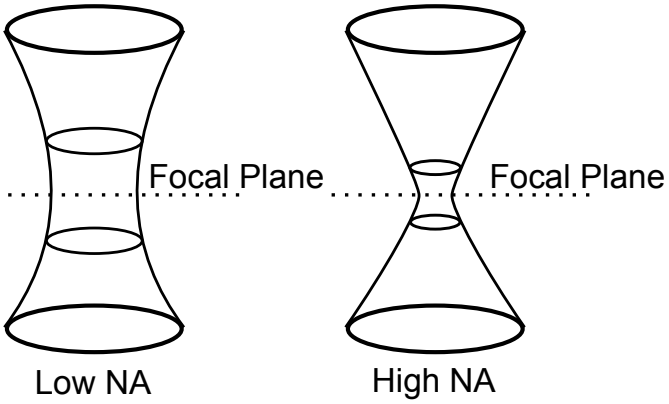

Figure 5.5: The resulting bleach volumes from a microscope objective with a low respectively high numerical aperture (NA).

For a multiphase sample, the 3D structure needs to be taken into account to make sure that the z-axis diffusion can be neglected. Figure 5.6 show a concept image in which the bleached phase in the focal plane does not follow the beam path. Since the two different phases may allow different diffusion rates, the phase in which the bleaching is intended to take place must be continuous along the z-axis for a long enough distance to allow the bleached ROI to only recover by means of 2D diffusion. This is shown as the distance Δ in Figure 5.6, which should be much longer than the width of the bleached area. The volume of the bleached phase must also be large enough to hold enough of the fresh probe to make the bleached portion negligible.

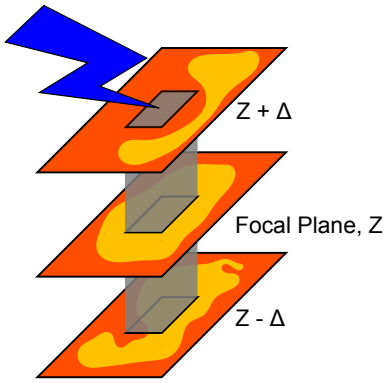

Figure 5.6: The 3D structure of the sample is important to take into account. The phase bleached in the focal plane twists and does not follow the laser path. To ensure a correct recovery, the phase bleached must be continuous in z-direction on a length scale (Δ) longer than the width of the bleached ROI.

5.1.7 FRAP probes

As many samples studied with a CLSM are not auto fluorescent, there is a need to add a fluorescent dye to allow the different structures in a sample to be detected. The dyes normally used for CLSM need to be photo stable in order to not bleach. The probes should also have a high quantum yield to allow as much of the absorbed light to be re-emitted and they should either have high affinity for different areas in the sample or be covalently bound to a specific substance in the sample. There is a large number of probes with these properties which have different absorbance/emission spectra, allowing them to tag different areas in the sample and to be differentiated simultaneously. This means that, for imaging, there is the possibility of, for example, staining fat with one dye, proteins with another and starch with a third dye, allowing the microscopist to see different aspects of the sample at the same time.

Probes used for FRAP are based on the dyes used for imaging, but they have slightly different requirements: A FRAP probe needs to be bleachable during the bleaching stage of a FRAP experiment, they should not be able to regain their ability to fluoresce after being bleached, they shall not bleach at low laser intensity and the bleach process should be preferably of first order kinetics. As most dyes used for imaging are made so that they will not be bleached, there are only a handful of available probes for FRAP. The most commonly used FRAP probes are fluorescein, fluorescein derivates (FITC) and green fluorescent protein (GFP).

Figure 5.7 shows the typical pathways for an average photobleachable fluorophore in a simplified Jablonski diagram. In order for the molecule to be bleached, an electron must be excited from its ground state (S) and reach either the excited singlet stage (S*) or the excited triplet state (T*) and from there reach the photobleached state. Exactly how the photobleaching occurs is different for different molecules, but possible routes are the reaction between two excited molecules or the reaction between an excited molecule and an oxygen molecule; these reactions may either be complete or produce semi-oxidized or reduced compounds[118]. The excitation is done by illumination of the fluorophore; when the light is absorbed, an electron becomes excited. Normal absorption is performed at rate k_a (usually fast) and the excited electron that has

reached S* can then fall back into the ground state via fluorescence (k_f), via internal conversion without radiation (k_{ic}) or cross over to an excited triplet stage (T*) via intersystem crossing (k_{isc}). The k_{ph} transition is a spin forbidden process which take the electron from the excited triplet state through phosphorescence. It is a slow process since since the the electron must change its spin direction. Photobleaching may occur from both S* and T* but, in the case of fluorescein, Song et al. [118] showed that it is almost exclusively the T* state that gives rise to photobleaching. Song et al. [118] also showed that the photobleaching reaction for fluorescein is far enough from a first-order irreversible bleaching reaction to recommend the use of other probes or for it to be necessary for this parameter to be taken into account. Even though fluorescein is not a perfect probe, there are currently not enough probes available to always make it possible to change to a better one.

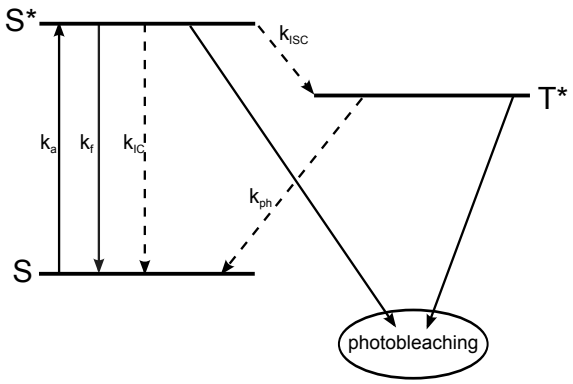

Figure 5.7: A simplified Jablonski diagram of the different processes that take place during photobleaching of fluorescein.

5.2 Rheology

Rheology is the study of deformation and the flow of liquids and semi solids [5]. A perfect Newtonian fluid, such as water, can be described with a temperature dependent viscosity term. The viscosity of the fluid will not change if the stress or strain rate of the fluid is altered. However, the properties of a non Newtonian fluid, such as a polymer melt, will change as a stress or strain is applied. The underlying reason is due to interactions within the material, where cross linking and/or polymer chain entanglement will give a resistance to deformation. At a high deformation rate, the material will appear elastic and rubber-like and will return back to its original state when the deformation is removed; for a low deformation rate the internal structure will change and the material will start to flow; this behaviour is called viscoelasticity.

When using a rheometer, a known deformation (or stress) is applied to the sample and the response from the sample is measured. Figure 5.8 shows a typical experiment using a bob and cup system as an example. The deformation is applied in a sinusoidal manner and the measured response is therefore also sinusodial for sufficiently small deformations, but will have a different amplitude and will lag behind depending on the viscoelasticity of the sample. Two parameters which usually are obtained from a measurement is the complex modulus (G*), which

corresponds to the amplitude of the deformation, and the phase angle (δ), which corresponds to the angular delay of the response. For an elastic material, the phase angle would be 0°as the applied deformation would be transferred immediately through the sample, whereas for a viscous material, the phase angle would be 90°. By varying the frequency and the amount of deformation, different aspects of the sample can be analysed.

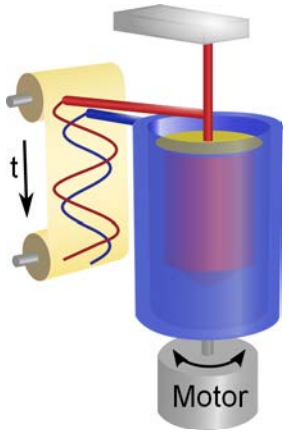

Figure 5.8: A conceptual image of a rheometer using bob and cup. The cup, which applies deformation from the motor, will only be in contact with the bob through means of the sample and the sample response to the deformation can therefore be measured. Image is ©Mats Stading.

The complex modulus is described as $G^* = G' + iG''$, in which $i^2 = -1$. G' is the storage modulus which describes the elasticity of the sample and G'' is the loss modulus which describes the viscous part of the sample. The phase angle is described as $\tan \delta = G''/G'$.

A typical curve for a material which goes from a solution to a gel will be seen as a cross over where the loss modulus is dominant in the solution and the storage modulus is dominant in the gel. If the G'-G'' cross-over is frequency independent, then it will coincide with the gel point of the sample and can be used to indicate the gel point [132].

6 Results and discussion

As the basic idea behind this PhD project has been to try to correlate mass transport to the material structure using FRAP, important questions have been "what can be measured with FRAP?" and "what is required in order to measure the desired properties?". What this chapter will show is that FRAP is a versatile tool, especially when combined with the results from other techniques, as it can then report so much more than just a diffusion coefficient. A good example of this is the combination of FRAP and rheology; dynamic FRAP measurements can show a change of the diffusion coefficient over time and, combined with rheology data, be correlated to the structural changes in the sample.

6.1 Dynamic transition

A dynamic system is defined here as a system that changes its properties and microstructure as a function of time. It can for example be a system that gels, swells, phase separates or crystallises as a function of time. When it comes to measuring mass transport with FRAP in dynamic systems, it is important to realize that the time scale and geometries must match each other to some extent. A FRAP experiment takes roughly 30 seconds to a few minutes to perform depending on the recovery rate, excluding the time it takes for selecting a suitable area and preparing the CLSM. In order to be able to probe the changes in material properties, the dynamics must therefore either be slow enough so that the material properties can be assumed constant during each consecutive FRAP experiment. If that is not possible, then the sample should be locked in a series of pseudo-steady states.

6.1.1 Gelation and transient structures in gelatine gels

(Paper II)

Gelatin gels are formed through percolation and will form a system-wide network with junctions that consist of triple-helices which increase in modulus with ageing as the polymer strands reinforces themselves [33]. An hypothesis for the gel formation is that, as the percolation is about to start in gelatin, there could be locally forming networks that do not percolate the entire structure. These locally formed networks is thought to be transient and will form and collapse. The lifetime of these locally forming networks will increase as the system moves towards percolation. Upon reaching the gel point, the local network would then percolate and become stable. This could, in theory, be shown with a rheometer provided that the strain used can be low enough to not disturb the system. In general, the strain needs to be tested for each sample so that there is a linear relationship [5], however so far rheometers have not been sensitive enough and no articles have been found where rheological data have verified existence of transient networks forming in gelatin prior to percolation. There have been indications that there are transient networks forming in gelatin [107] and the formation of transient networks have been proved in other systems, such as carrageenan [52]. The carrageenan network is highly dynamic and will rearrange itself with time. The gelation of gelatin is quite slow in comparison to the gelation of carrageenan, which happens almost instantly after reaching the gel point. By changing the

gelatin concentration and the end temperature, it is possible to tailor the gel strength and the time it takes for the gelatin to gel. This makes gelatin an ideal model material when testing the possibilities to use FRAP for dynamic studies; the tailoring allows for a way to increase the "window" of time in which FRAP could be used to detect changes in the microstructure prior to percolation. In order to be able to determine when the solution gels, the FRAP measurement was therefore compared with the results from rheological measurements on the same sample.

The experimental design used for determining the diffusion properties during gelatin gelation is shown in Figure 6.1. Two different gelatin concentrations, three different probe sizes and three different end temperatures were used, as shown in Figure 6.1. The study started with the quenching of the solution and then went on for two weeks; FRAP measurements were carried out every 5 minutes during the first 75 minutes, then again at 24 hours, 7 days and 14 days. The samples were kept locked between cover glass slides with the aid of secure-seal spacers; this was to allow them to stay as fresh as possible during the 14 days storage. The rheological measurements were made consecutively for the first 24 hours for each sample and did not continue for the whole 14 day set-up. This experimental design was chosen because at least one of the gelatin samples would be gel slowly enough to allow the network to be probed for transient structures forming and give information about how the different parameters affect the diffusion in relation to the rheological changes.

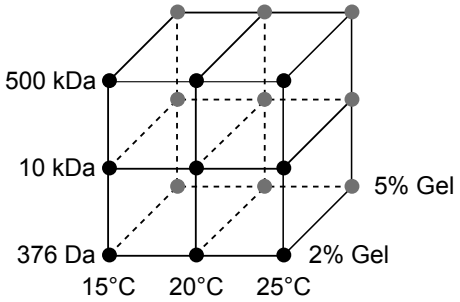

Figure 6.1: The experimental design of the study in gelatin. The molecular sizes refer to the size of the probes and the temperatures represents the different end temperatures to which the gelatin solution was quenched.

There are several FRAP studies how gel concentration affects the diffusion coefficient for different gels [17, 30, 68, 86] and a common result in the studies is that increasing gel concentration leads to an increase in the obstruction and therefore lower diffusion coefficients. The same was seen for all three probes in gelatin, which can be seen in Figure 6.2 in which the diffusion coefficient for all three probes is plotted for both gel concentrations at 20°C. The 2% gelatin gel allows slightly faster diffusion coefficients than the 5% gelatin gel, although the differences between the two gel concentrations depend heavily on the probe size. Comparing these diffusion coefficients with the rheological measurements for the same gel, as seen in Figure 6.3, it should be noted that there is a connection between gel stiffness and diffusion coefficient, but the correlation is not simple. For a solution of (bio) polymers, increasing the concentration will lead to

lower diffusion coefficients, partially due to an increase in viscosity which increases the resistance the probe experiences and partially due to the presence of more material that obstructs the probe as the probe diffuses around [1, 99]. With that in mind, it's easy to draw the conclusion that there is a purely rheological cause for the retardation of the probe diffusion in gels. That is, the higher the concentration in solution, the higher the retardation and in relation to gels, the higher the concentration, the stronger the gel. However, when combining the rheological measurements with the diffusion curves it became apparent that the true explanation is not as simple.

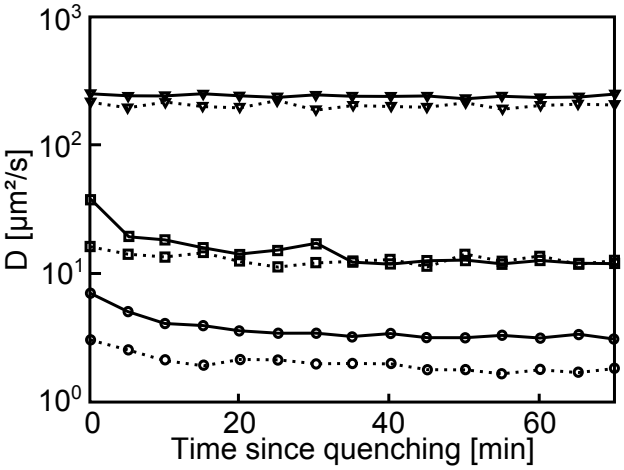

Figure 6.2: The absolute diffusion coefficient for the probes in gelatin as a function of time since quenching. The solid lines represent a 2% gelatin gel, the dotted lines represent 5% gelatin gel. The probes are fluorescein (▽), 10kDa FITC dextran (□) and 500kDa FITC dextran (○).

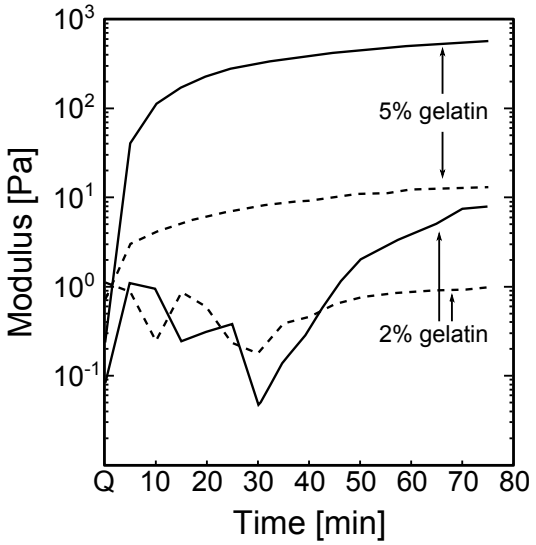

Figure 6.3: The modulus for a newly made sample with 2% respectively 5% gelatin concentration. The timescale is minutes since quenching the sample from 60°C to 20°C.

Figure 6.4 shows the results of the rheological measurements combined with the temperature normalized diffusion coefficients for the entire experimental space. What can be seen in the figure is that the time it takes for gelation differs between the samples. The gelatin with 5% concentration gels much faster than the 2% in all cases and, as Figure 6.4B, D and F shows, the samples with 5% concentration gels within 10 minutes. For the samples with 2% concentration, the time it takes to form a gel is significantly longer. The sample with 2% concentration quenched to 15°C (Figure 6.4A) gels almost instantly, while the higher end-temperatures took 40 minutes and 4 hours respectively to form a gel (Figure 6.4C and E). Note also the difference in modulus for all samples as there is a significant difference between how hard the gels become in the different samples. The diffusion coefficients show similar trends for all samples. The smallest fluorescein probe report the existence of the gelatin strands and cannot move as fast as in distilled water, but does not report any changes in the microstructure of the gelatin network. The two larger probes on the other hand show retardation in diffusion over time before reaching a minimum plateau. As this happens at approximately the same time in all samples, it must happen regardless of when the gelatin gels; this would indicate that there are transient networks forming in the gelatin prior to a full percolation of the network. When comparing the modulus for the different samples it can be seen that if there is any connection between the diffusion coefficients and the gel strength, then it is only a weak correlation as the diffusion coefficients are hardly influenced by the gel strength.

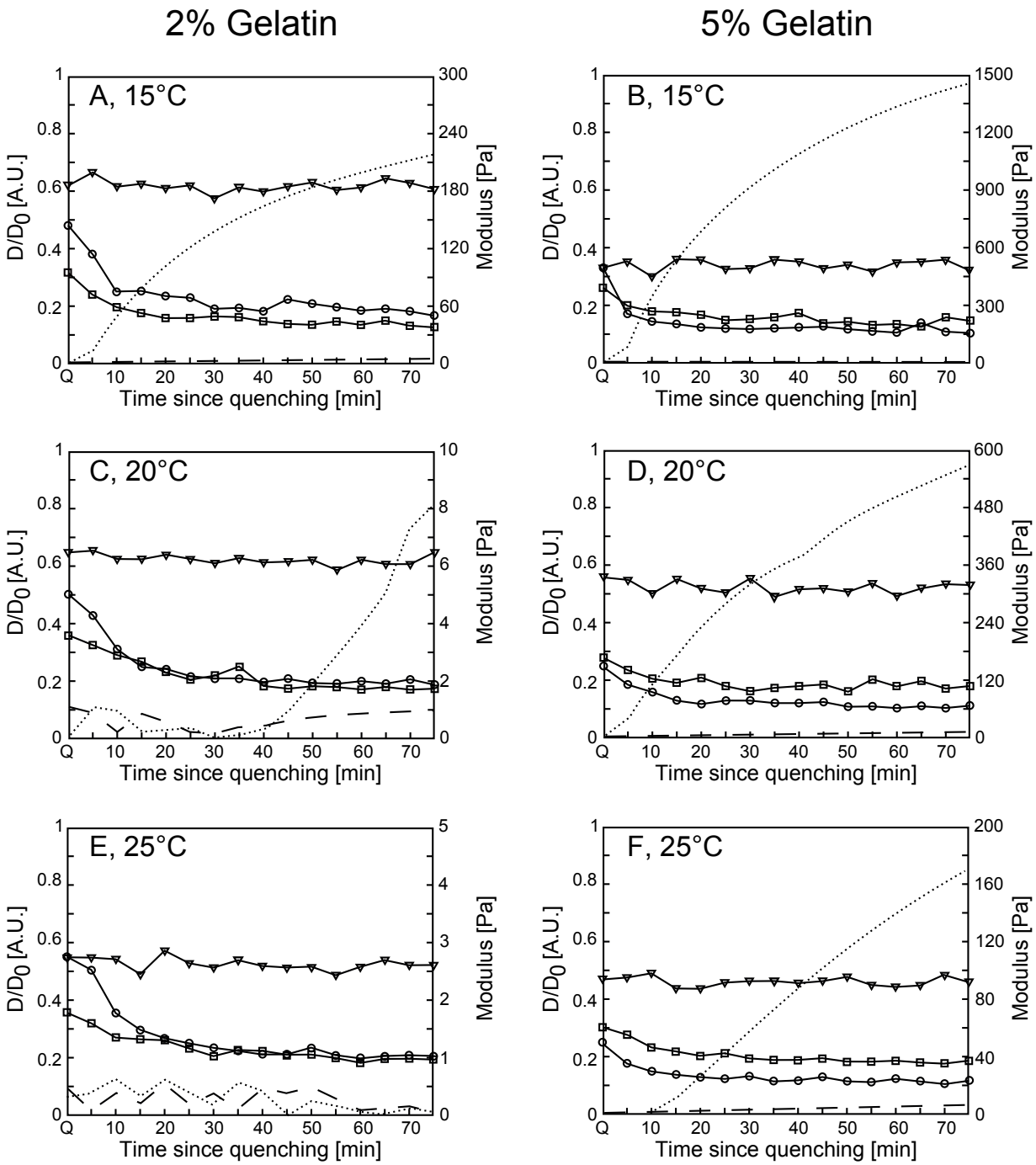

Figure 6.4: The normalized diffusion coefficient for probes in gelatin combined with rheological measurements. The probes are fluorescein (▽), 10kDa FITC dextran (□) and 500kDa FITC dextran (○). (A) and (B) are 2% and 5% gelatin at 15°C, (C) and (D) are 2% and 5% gelatin at 20°C, (E) and (F) are 2% and 5% gelatin at 25°C. The dotted lines represent the storage modulus (G') and the dashed lines represent the loss modulus (G''). Note the difference in modulus.

The effect of ageing on the gelatin gels showed an increase of the diffusion coefficients over the course of the two weeks during which the samples were kept. Gelatin rearranges and grows in strength with time and the reinforcement of the network might cause the mesh to open up more and more as there is a finite number of gelatin strands. The smallest probe (fluorescein) demonstrated this as it could diffuse around faster in the gelatin gels with time. The larger probes did show a similar, albeit very weak, trends towards diffusion faster with time. The result of the ageing on gelatin for the fluorescein probe can be seen in Figure 6.5 in which an increase in normalized diffusion coefficients can be seen from the first two points at 1 hour and 24 hours to the later points at 7 days and 14 days. The exact reason for why the effect was only clear for the small fluorescein probe was beyond the scope of Paper II, however it is reasonable to believe that the opening of the network is on a relatively small length scale. What probably happened is that the junction zones where the gel strands bind together grows slightly, which causes a stiffening of the gel, and while that happened the gel strands move enough to allow fluorscein to move more freely but not enough to allow the larger probes to diffuse faster.

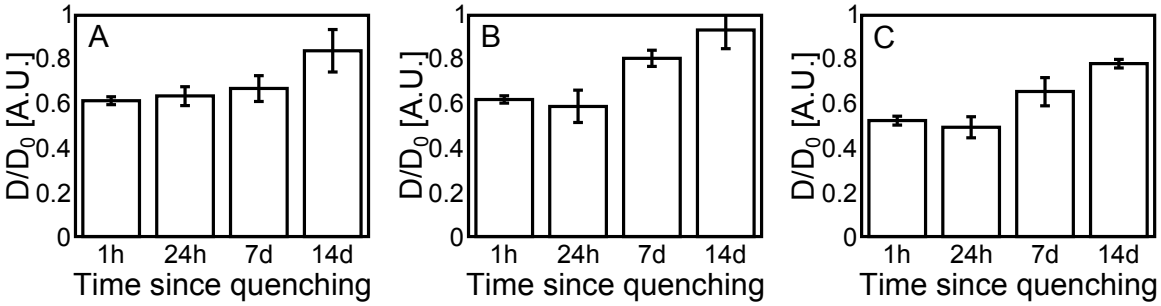

Figure 6.5: The ageing effect of a 2% gelatin gel on the temperature normalized diffusion coefficients for fluorescein. A is the effect at the end temperature 15°C, B is the effect at the end temperature 20°C and C is the effect at the end temperature 25°C.

6.1.2 Dynamics in carrageenan gels

(Paper IV)

κ-carrageenan has been proven to have transient structures that form after gelation [52] and the gel formations is through percolation [87], but it is controlled in a different manner than gelatin. It was therefore of our interest to see whether the aggregation after gelation would affect the probe diffusion coefficient and whether FRAP could be used for probing the structure dynamics. Carrageenan is highly salt sensitive and the gel formation can be controlled by controlling the salt type and ionic concentration [43, 50, 84, 89]. For example, potassium ions will bind strongly on specific sites and yield a gel network that can vary from a finer type with small voids to coarse strands with a larger void space in between, depending on the amount of potassium used [77, 129].

Walther et al. [129] and Lorén et al. [77] have studied probe diffusion in κ-carrageenan gels using NMR diffusometry to measure the diffusion in relation to TEM images of the gel. The experimental design was chosen to be of a similar design so that the result could be compared to their study. By changing the ionic concentration and the gel concentration the degree of heterogeneity and the void space in the microstructure could be controlled. The design was:

- To vary the gel concentration using 250 mM Na^+ as ion concentration. The κ-carrageenan concentrations were: 0.5%, 1%, 2%, 3% and 4%.
- To vary the ion concentraition in a 1% κ-carrageenan gel. The ion concentrations were: 20 mM K^+, 100 mM K^+, 20 mM K^++ 200 mM Na^+, 250 mM Na^+ and 1 mM K^++ 8 mM Na^+ (no additional salt added).
- To try to slow down the gelation a by chosing a temperature near the gel temperature. A 1% κ-carrageenan with ion concentration of 20 mM K^+ and 100 mM K^+ was kept near the respective gelation temperature.

The probes used were intended to be both a 10kDa and a 500kDa FITC dextran, however it turned out that the larger probe phase separated from the carrageenan gel and could therefore not be used.

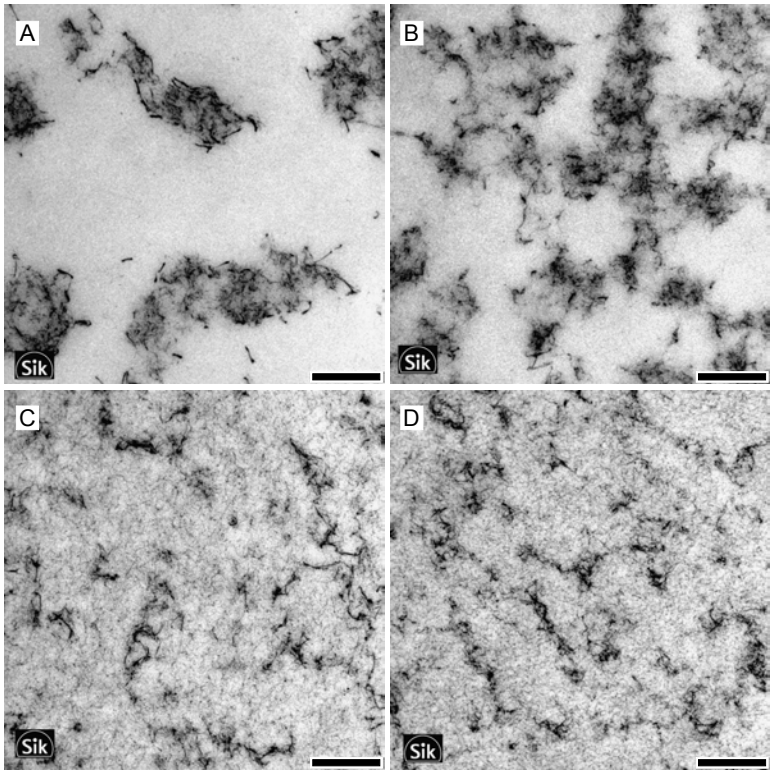

Figure 6.6: TEM images of a κ-carrageenan concentration series with 250 mM Na^+. The gel concentrations shown are 0.5% (A), 1% (B), 2% (C) and 4% (D). The scale bar represent 500nm.

Changing the gel concentration between 0.5% to 4% of a κ-carrageenan with 250mM Na^+ will create structures ranging from highly heterogeneous to relatively homogeneous. Figure 6.6 shows TEM images of the microstructure as a function of concentration for 0.5% (A), 1% (B), 2% (C) and 4% (D). In the images with 0.5% and 1% concentration (Figure 6.6A and B) the microstructure is mainly composed of large dense domains with a fairly open structure between the domains. This changes with increasing concentration in such a way that the dense domains

seem to take on a looser appearance and the open void space seems to shrink. At 2% concentration and above (Figure 6.6C and D), there are thin strands visible in the previous open areas and the dense clusters have diminished in size. These changes in microstructure seem to influence how the probe experiences the gel, which can be seen in the normalized diffusion coefficients in Figure 6.7. The normalized diffusion coefficients are organized logically so that higher gel concentrations retard the probe more, but what is also seen in Figure 6.7 are trends towards a change in diffusion over the course of the experiment. The samples with 0.5% and 1% concentration, which are more open and more heterogeneous, seem to allow a slight increase of the normalized diffusion coefficient whereas the samples with 2% to 4% concentration, which have a finer network and more homogeneous appearance, seem to retard the normalized diffusion slightly. The FRAP measurements start directly after the gelling has initiated, and could therefore capture a rearrangement over the 60 minutes of which the samples were analyzed, whereas the structures seen in TEM images would have been locked after such rearrangement.

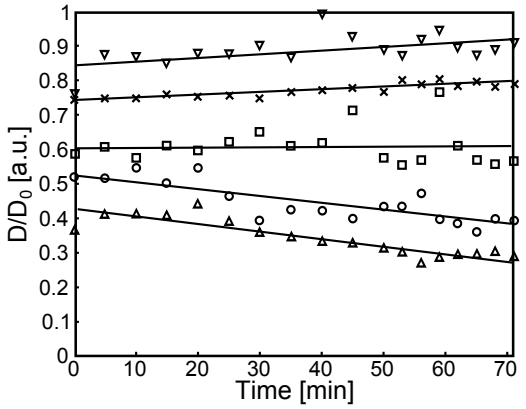

Figure 6.7: Effect of κ-carrageenan concentration on probe diffusion of 10 kDa FITC dextran probe. The gel concentrations are 0.5%($\triangledown$), 1% ($\times$), 2%($\square$), 3% ($\bigcirc$), 4% ($\triangle$) and the ionic concentration is kept constant at 250mM Na^+.

Figure 6.8 depicts TEM images that show how the ion concentration affects the microstructure of a 1% κ-carrageenan gel. The gel sample with 20 mM K^+ seen in Figure 6.8A has a dense network of fine carrageenan strands; this translates to the lowest diffusion coefficient among the samples which have gelled in Figure 6.9. The gels with 100 mM K^+, 20 mM K^+ + 200 mM Na^+ and 250 mM Na^+ are all significantly faster than the 20 mM K^+ gel and correspond to more open network structures, as seen in Figure 6.8 B, C & D. This is because the potassium ions have more specific binding sites which promote aggregation into a coarser network with increasing amount of ions, whereas the sodium ions bind less specifically and the strand aggregation therefore forms dense clusters [50, 129]. If the concentration of salts present in the dry carrageenan powder is high enough, κ-carrageenan can gel without the addition of salt. In this case, however, the 1% κ-carrageenan only contains 1mM K^+ and 8 mM Na^+ and thus only forms a viscous solution and not a fully percolated gel. As seen in Figure 6.9, the sample without additional salt has the lowest diffusion coefficient of all samples and thus the κ-carrageenan in solution leads to a far greater obstruction than if there was aggregation that resulted in the formation of a network structure.

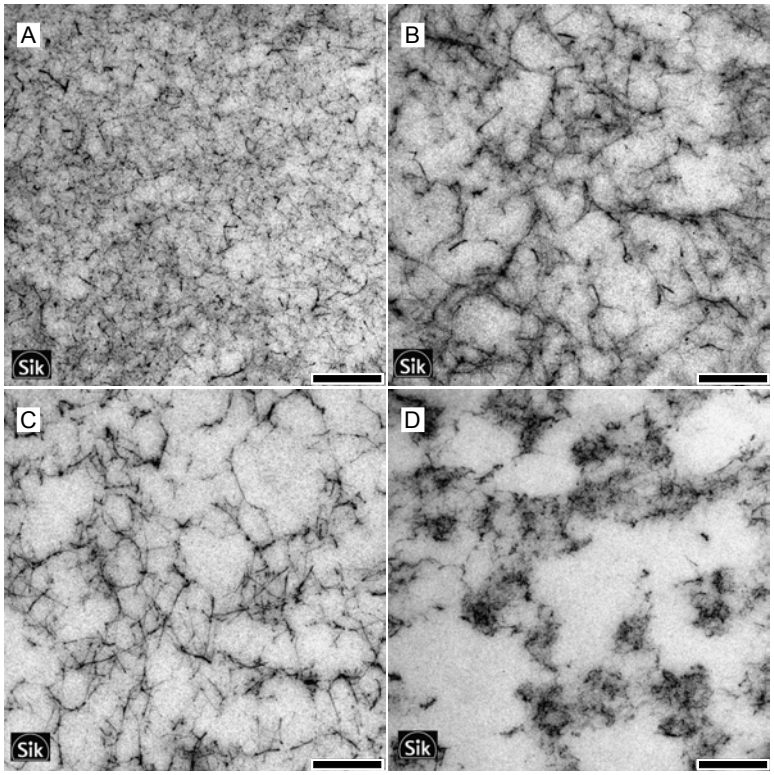

Figure 6.8: TEM images of 1% κ-carrageenan gels with different ion concentrations. A is 20 mM K^+, B is 20 mM K^+ + 200 mM Na^+, C 100 mM K^+, D is 250 mM Na^+. The scale bar is 500nm.

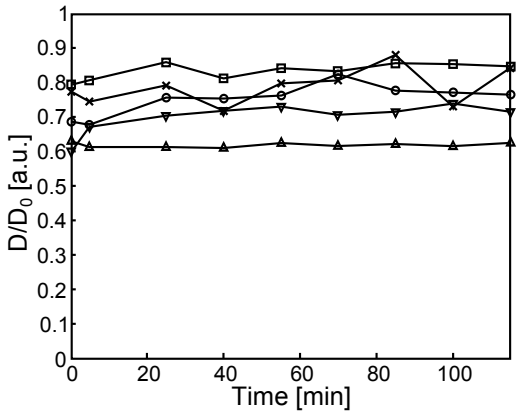

Figure 6.9: The normalized diffusion coefficients for a 1% κ-carrageenan gel. The ionic concentrations are 20 mM K^+($\triangledown$), 100 mM K^+ ($\times$), 20 mM K^+ + 200 mM Na^+ ($\square$), 250 mM Na^+ ($\bigcirc$) and no additional salt added ($\triangle$).

6.1.3 Comparison of transient phenomena in gelatin and carrageenan

(Papers II & IV)

Figure 6.10 shows how the normalized diffusion coefficient and the rheology of gelatin (A) and carrageenan (B) changes as a function of time during, and after quenching from 60°C to 25°C. Figure 6.10A show a 2% gelatin solution which is about to gel, the relatively high end temperature and the low concentration ensure a slow gelation process and it takes roughly 4 hours for gelation to occur. The probe used is a 10kDa FITC dextran probe. Figure 6.10B is a 1% κ-carrageenan gel with 20 mM K^+ and a 10kDa FITC dextran probe. In both figures the start (t=0) is counted from when the quenching of the samples started; this is slightly modified for the rheological curves as the rheometer could not quench as quickly as the cooling stage connected to the CLSM. However, since the rheometer showed that there were no change in the modulus during cooling, the start (t=0) is counted as when the end temperature is reached.

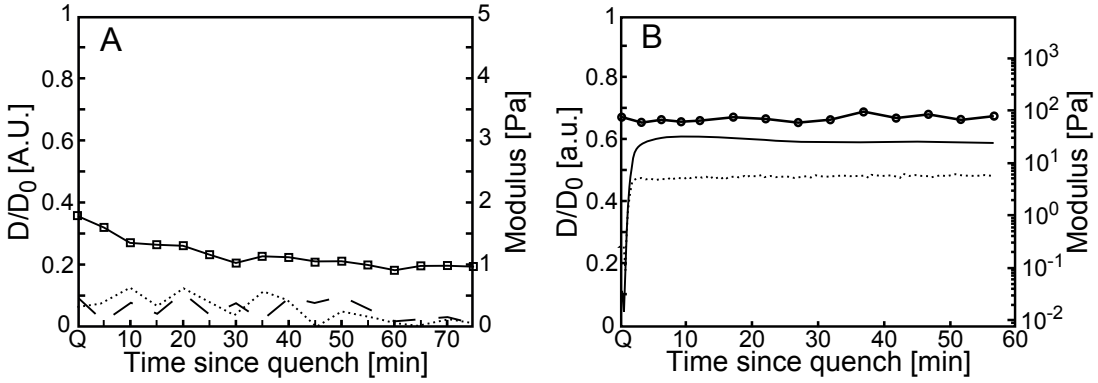

Figure 6.10: The normalized diffusion coefficients in relation to the rheological responses for a 2% gelatin gel (A) and a 1% κ-carrageenan gel with 20mM K^+ (B). The gels have been quenched from 60°C to 25°C and a 10kDa FITC dextran probe was used for the FRAP measurement. The solid lines represent G′ and the dotted lines represent G″. Note the difference in modulus.

What can be seen in Figure 6.10 is that the two materials behave quite differently. The carrageenan sample in Figure 6.10B gels almost instantly upon reaching the end temperature, whereas the gelatin in Figure 6.10A takes 4 hour in total before gelation occur. In relation to the gelation points of the samples, it can be seen that the normalized diffusion curves are different as well. The normalized diffusion coefficient of gelatin is much lower than that of carrageenan, indicating that the carrageenan network is more open than the gelatin network. However, there is more information in the diffusion curves as well; the normalized diffusion coefficient of gelatin decreases from 0.35 to 0.2, without any visible changes in the rheological response. This trend was not seen for carrageenan, which keeps roughly the same normalized diffusion coefficient of 0.68 throughout the experiment. The interpretation is that the gelatin network forms transient structures which retard the probe prior to percolation, while carrageenan does not. There are two reasons for why this is not seen in carrageenan: 1. despite that the temperature was chosen to be near the gelation temperature of carrageenan in order to slow down the gel formation, the carrageenan gels too quickly and any transient

changes would be locked before they could be captured with FRAP, 2. the probe could be too small to sense any changes in the carrageenan network. When using a smaller probe (fluorescein) in gelatin, a similar response was seen which, as the higher normalized diffusion coefficient in carrageenan suggests, could explain why there are no visible changes during the course of the experiment. Unfortunately, it turned out that the larger probe (500 kDa FITC dextran) was not compatible with the carrageenan gel, and it was therefore not possible to verify the theory that a larger probe might be able to sense changes in the network. The larger probe (500 kDa FITC dextran) phase separated and aggregated in the carrageenan sample.

The FRAP measurements during the gelation were performed once every third minute, in order to capture as much of the potential transient changes as possible. From a FRAP perspective, it can be concluded that as long as it was possible to sample the changes then FRAP was a useful tool to probe the material. Even though the effort was taken to slow down the gel formation in carrageenan, the process was over much faster than the microscope could handle. This result shows the importance of choosing the right tool for the right material unless it is possible to alter the process so that the time window is changed into a more feasible one. These experiments were carried out on a Lecia SP2 CLSM with a maximum scanning rate of 1000Hz. On a newer CLSM such as the Leica SP5, the maximum scanning rate is increased to 1400Hz and there is also the possibility to use a resonance scanner instead of a conventional scanner. The resonance scanner is an ultra fast mirror which scans at 8000Hz, at the price of reduced pixel dwell time, reduced signal-to-noise and disabled zoom-in during bleaching. With the set-up that was used on the SP2 (800Hz, 256x256 pixels and a total of 60 frames), the image acquisition was 2 frames per second. Using the same set-up on the SP5 with an active resonance scanner would mean increasing the acquisition rate to roughly 30 frames per seconds. As it is required that the sample be considered to have the same properties during the course of an entire bleach sequence, a change between the SP2 and a SP5 using these settings would mean that much faster transitions would be possible to capture. However, if it would be enough to actually capture the gelation of carrageenan is unknown. There are two factors that influence whether it would be possible to capture the gelation process with FRAP: whether it will be possible to perform enough FRAP measurements during the course of the gelation to show a trend and whether the frame rate matches the diffusion well enough so that the contrast between images are useful for calculations. Based on the rheological measurements made in Paper IV, an estimate would be that the gelation occurs over a few seconds. With 30 frames per second, it would be possible to acquire enough frames for a good calculation in 1–2 seconds. For minimal changes between bleach areas, it could be possible to capture three FRAP measurements for a 10 second long gelation process, which would be enough to give indications whether there is a linear change of the diffusion during gelation. The next problem that arises will be whether the frame rate matches the diffusion coefficient. The absolute diffusion coefficients for a 10 kDa FITC dextran probe in carrageenan was measured in Paper IV to range between 40 $\mu m^2/s$ to 60 $\mu m^2/s$ depending on the sample. For a frame rate of 30 fps, the average difference (root mean square distance) between two frames would be $\sqrt{8/3}\mu m$ to 2 µm.Using zoom 4, which was used on the SP2, the pixel size on the SP5 would be 0.7598 µm/pixel and a single probe molecule would travel less than 1.5 pixels per frame on average. For the entire ensemble, this would mean that there would be little difference in intensity between

images. It would, in theory, be possible to use data with little difference between frames while using a modern FRAP model, however it would verge on the limit of what is usable data. Using a different zoom to yield a higher pixel resolution could improve the calculations; another way would be to change to a smaller probe in order to yield higher diffusion coefficients, which instead would mean that there is a risk that the probe becomes too small to sense potential changes in the network during gelation. The conclusion is that it would be theoretically possible to capture the gelation process in carrageenan using FRAP, but it would pose as highly challenging.

6.1.4 FRAP as a tool for measuring the effect of swelling on diffusion

(Paper I)

The dynamic process of swelling of a gel offers a big challenge for FRAP and monitoring the swelling live in the CLSM is only possible at very low swelling rates. The reason for this is not due to the process being too fast, as was the case in carrageenan where gelation occurred faster than a typical FRAP measurement. Instead the changes in geometry pose a challenge. Figure 6.11 shows a concept image of a sample swelling in the CLSM. If the swelling of a gel happens quickly, the geometry will change during the FRAP experiment which will cause the bleach ROI to move and therefore disrupt the measurement. For a slow swelling, it will be difficult to control the sample in such way that the bleach ROI can be followed throughout the whole recovery, but it would be possible as long as the surface can be kept flat, which can be difficult if the swelling causes part of the sample to deviate from the cover glass and therefore creates cavities which creates refractive mismatch and bends the laser beam path. The problem with performign FRAP measurements during live swelling would be the fact that the probe will experience a flow or a directed diffusion caused by the absorption of liquid into the gel. As all current FRAP models assume free diffusion, the presence of a flow would render them invalid.

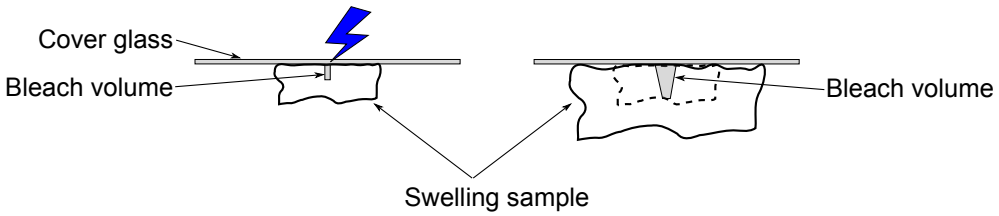

Figure 6.11: A concept image of a sample swelling in the CLSM. The bleach volume will only change if the swelling occurs on a timescale comparable to that of the FRAP measurement.

Swelling of super absorbing polymers (SAP) was performed as part of the model development of the Monotone MLE FRAP model in Paper I as SAP showed a significant variation in the diffusion coefficients depending on the degree of swelling. In order to address the problems which would occur during a live swelling, the SAP was kept at pseudo-steady states. That is, the gel was allowed to swell to a steady state condition, but with a limited amount of probe solution. This allowed the swelling to be controlled in such a manner that there were no gradients present as the gel was allowed to stabilize for 24 h before analysis and the exact degree of swelling

was known and constant throughout the entire FRAP analysis for each sample. The degree of swelling was defined as the amount of probe solution which the dry SAP was allowed to absorb, $m_{\mathrm{H_2O}}/m_{\mathrm{dry\ SAP}}$. For a low degree of swelling (<2), the bleach profile assumes an intensity profile best described as an "inverse hat function" (see Figure 6.12) and the diffusion coefficient cannot be estimated correctly by assuming a Gaussian shaped intensity profile, as stated in Jonasson et al. [62].

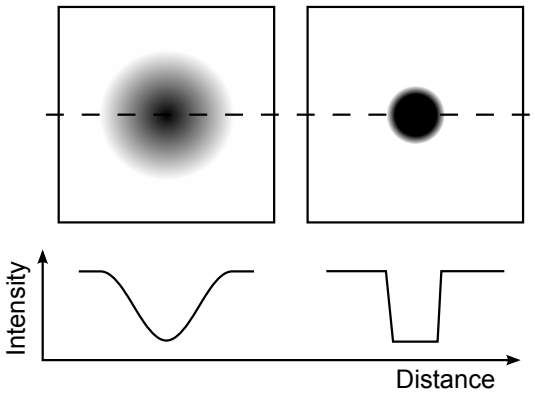

Figure 6.12: A typical bleach profile for a sample with a fast (A) and a slow (B) diffusion, images representing the first post bleach image. The faster diffusion will give a Gaussian like intensity distribution (measured along the dashed line), whereas the slower diffusion will give an intensity distribution which more closely resembles an inverse hat function.

In comparison to Figure 6.12, it can be seen in Figure 6.13 that SAP is capable of producing both types of initial distribution depending on the degree of swelling. Figure 6.13 shows a typical FRAP experiment in a 1× and a 20× swollen SAP gel and the difference in diffusion coefficients can be seen visually as the recovery of the bleached area takes roughly 5 seconds in the 20× swollen gel, whereas the recovery of the 1× swollen gel goes on for several minutes.

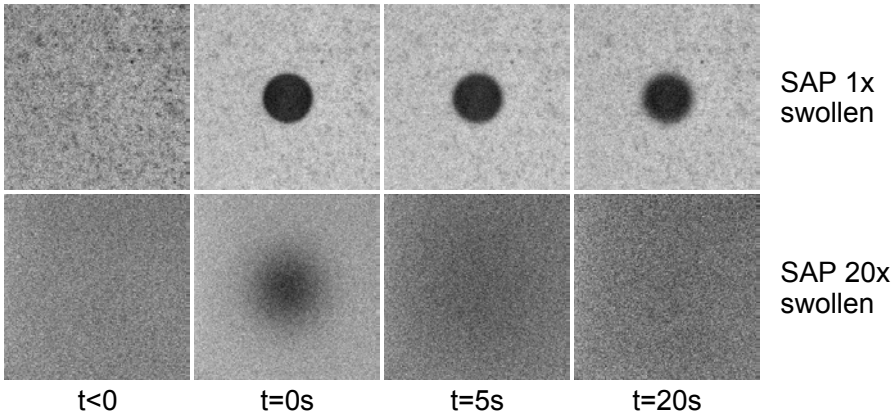

Figure 6.13: FRAP in a 1× and a 20× swollen SAP for different timesteps. The bleached disc is 30 µm in diameter.

Figure 6.14A shows the entire curve from 1.25× swollen up to 376× swollen, which was as much as the SAP could swell in the presence of the Na_2-fluorescein probe at 50 ppm. As the SAP swells, the fluorescein diffusion coefficient increases rapidly until 10× swollen and thereafter the increase in diffusion coefficient slows down. Upon reaching the maximum degree of swelling, the fluorescein probe barely notices the SAP network and moves almost as unhindered as it does in pure water. This means that to significantly retard a probe with a size of approximately 1 nm using solely an obstruction from the gel network, a high concentration is needed. Figure 6.14B shows a close-up of the fluorescein diffusion coefficient in SAP between 1.25× to 2× swelling estimated with both the Monoton MLE model and the Gaussian MLE model and it can be seen that the diffusion coefficient is underestimated for each sample when assuming a Gaussian initial profile.

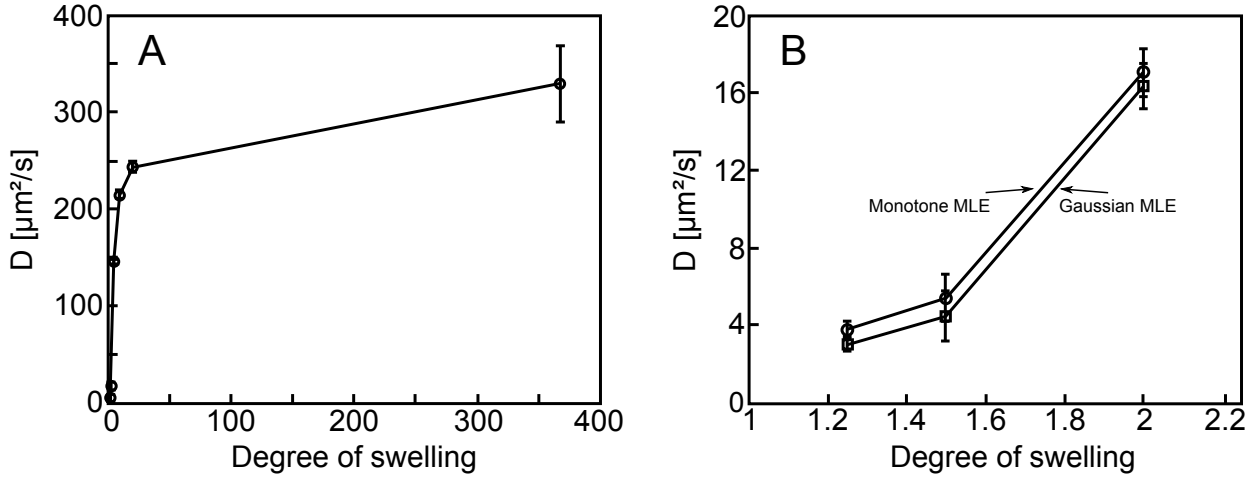

Figure 6.14: The diffusion coefficient in SAP as a function of the degree of swelling using a Na_2-fluorescein probe. (A) the full curve from 1.25× to 376× swelled SAP. (B) A close-up for 1.25× to 2× swelled SAP, showing the difference in estimation of D between the Gaussian MLE model [62] (□) and the Monotone MLE model [Paper I] (○). The solid lines are to guide the eye.

Monotone FRAP model

A comparison of the curve fit from Gaussian and Monotone MLE model can be seen in Figure 6.15. The gray dots represent the pixel values averaged over a thin torus with size increasing with the radial distance from the centre. This is solely for representation and is not used for the actual calculations. The black line represents the model fit and it can be seen that the model which assumes a Gaussian distribution cannot correctly fit the pixels in the centre of the bleached spot.

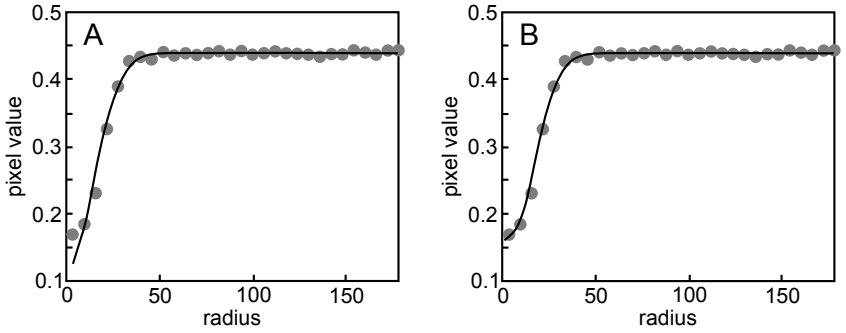

Figure 6.15: A comparison between the Gaussian MLE FRAP model fit (A) and the Monotone MLE FRAP model fit (B) for a 1.25× swelled SAP particle. The black lines are the model fits and the gray dots are averaged pixel values with respect to radius from the centre of the bleached disc.

When a non-parametric monotonically increasing function (the inversed hat like function) is used to describe the initial bleach profile instead of a Gaussian function, the time evolution of the fluorophore concentration after photobleaching will be described as

$$\lambda(x,t) = \sum_{y} C_0(|y|) f(|x-y|, t), \tag{6.1}$$

where x is the centre coordinates of a pixel ($x = [x(1), x(2)]$), C_0 is the initial concentration at time 0 at pixel y and the function f is the diffusion propagator, which describes the contribution to the intensity of pixel x due to diffusion from neighbouring pixels (at distance $|x-y|$). The size of the bleached disc will influence f in such way that if the bleached area is larger than the resolution of the detection PSF (ω) then f is described as

$$f(x,t) = \frac{1}{4\pi Dt} e^{-\frac{x^2}{4Dt}}. \tag{6.2}$$

If the size of the bleached disc is roughly equal to the size of ω, then f is instead described as

$$f(x,t) = I_{0d}\sqrt{\pi\omega_z^2/2} \cdot \frac{\omega_r^2}{8Dt+\omega_r^2} e^{-\frac{x^2}{4Dt+0.5\omega_r^2}}, \tag{6.3}$$

in which ω_r is the resolution in x-y plane, ω_z in depth and I_{0d} is a constant.

For this model, the noise in each pixel is assumed to be Poisson distributed, which is more accurate due to the nature of the CLSM detectors [95]. However, the Poisson distribution with

high expectation can be generalized as a normal distribution, which is the case for the pixel values from the images. The mean fluorescence intensity for a pixel at time t at coordinate x is described as $a\lambda(x,t)$, where a is a proportionality constant which is estimated by the variance in the pre bleach images divided by the average intensity in the same images. The fitting procedure is done in a similar manner as for the Gaussian MLE model (described in [62]), but the log-likelihood equation which is used is now described as

$$l(D,a) = -\frac{|T||S|}{2}\log(2\pi a^2) - \frac{1}{2}\sum_{t\in T}\sum_{x\in S}\log\lambda(x,t) \\ -\frac{1}{2a^2}\sum_{t\in T}\sum_{x\in S}\frac{(p(x,t)-a\lambda(x,t))^2}{\lambda(r,t)}, \tag{6.4}$$

in which T is the set of all times which corresponds to the recovery images, $|T|$ is the number of time points, S is the set of all pixels in an individual image, $|S|$ is the corresponding number of pixels and $p(x,t)$ is the pixel value at location x at time t. An added strength to the model is that it is possible to expand the functionality. This comes from the diffusion propagator ($f(x,t)$), as it take sums the contribution from each pixels in the set S; by dividing the pixels in the images into subsets, it can become possible to map different diffusion rates to different areas in the images.

Contrary to the Gaussian MLE model, this improved model is no longer described by a simple analytical solution. Instead It is instead a numercal solution, which is needed in order to handle arbitrary bleach profiles. The drawback with a change from an analytical expression into a numerical approach is the computational load; the calculations will become slightly slower but will, on the other hand, estimate the diffusion constant more accurately for slow diffusion. Another benefit is that any shape of the bleach ROI can be used, provided that the noise and inhomogeneities can be estimated in the first bleach image. There are also a few assumptions in the model that need to be taken into consideration:

- The probe molecules need to be homogeneously distributed initially.
- The diffusion process is isotropic and takes place in an infinite medium.
- There are no flows present in the sample.
- The objective used has a low NA.

6.2 Probes

(Papers II & IV)

It has become clear from this work that the choice of probe is of utmost importance. Not only does the probe have to fulfil all requirements that FRAP imposes, but it must also be compatible with the sample in such way that it reports useful information about the diffusion properties. There have been some earlier FRAP work which have taken the effect of the probe into account [21, 29, 30, 68, 85, 86, 92, 102, 112]. The most common approach has mainly been to test different probe sizes and compare how the probe are diffusing through solutions or gels. However,

a few of them have had some interesting results regarding the interaction between gel mesh size and the probe type and probe size. Cheng et al. [21] examined the mesoscopic domain in which the probe is roughly the same size as the mesh of Guar and PEO solutions. They also tested the effect of three different probe types: dendrimer, hard sphere and random coil. Their results included a master plot describing the different probe types in relation to their size relative to the mesh size. The random coil probes were seen to move most easily through dense areas whereas hard spheres were the most hindered probe. The result of the dendrimers varied depending on dendrimer generation: low (G0) and high generations (>G8) acted like a hard sphere whereas the intermediate generations acted more like a random coil. Pluen et al. [102] and Shen et al. [112] used the diffusion measurements to calculate the pore size of the gels in that the probes were to diffuse through. They used the Zimm model [35] and the De Genne's reptation model [28] to estimate the pore size of an agarose gel as well as bovine cervical mucus and their results were in agreement with previously published data.

The size of the probe compared to the mesh size of the network is of importance. Figure 6.16 shows a concept image of how a small and a large probe might experience a gel network. If only the obstruction is of importance and the interactions are neglible, then probes that are very small compared to the typical network mesh size will barely notice the presence of the network and the diffusion will only be slightly reduced. Larger probes, on the other hand, will be more obstructed by the network and if the probe size is comparable to the mesh size then there is the risk of the probe getting stuck if the network does not rearrange (self diffuse or "breathe") sufficiently to let the probe pass. Depending on which type of probe is used, they will get obstructed differently; a probe behaving like a hard sphere will be more dependant on self-diffusion of the gel network to pass through, whereas a random coil has the ability to deform slightly in order to bypass denser areas [21].

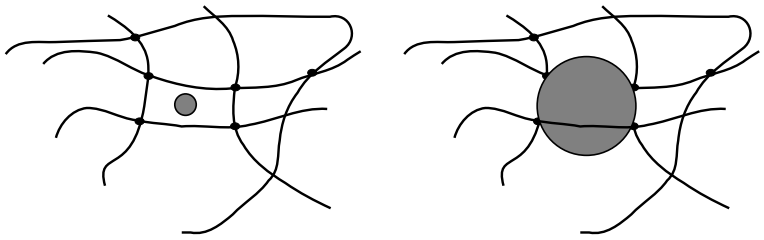

Figure 6.16: A concept image of a small and large probe interacting with a gel network. The smaller probe is freer, relatively speaking, than the larger probe, which might get stuck if the (bio) polymer strands are crosslinked.

Table 6.1 shows the probe size expressed as hydrodynamic radius (r_H) for three different FRAP probes. With the different probe sizes in mind, Figure 6.17 shows the network of a 3% gelatin gel (the scale bar represents 100nm) as a size comparison. The void between the gelatin strands is relatively dense; however, it should be noted that the TEM image is a 2D projection of a thin 3D slice of the gel sample and that therefore some strands will be tilted upwards and downwards. The mesh size of the gel will therefore be slightly larger than what is apparent in the image. Although it should be understood that the three different probes experience the sample differently.

Table 6.1: Hydrodynamic radius (r_H) for three different FRAP probes with regard to temperature. The r_H values have been calculated using the Stokes-Einstein equation based on FRAP measurement of free diffusion in deionised water.

Probe	Na_2-Fluorescein	10kDa FITC dextran	500kDa FITC dextran
15°C	0.5 nm	2.86 nm	12.05 nm
60°C	0.94 nm	5.12 nm	21.95 nm

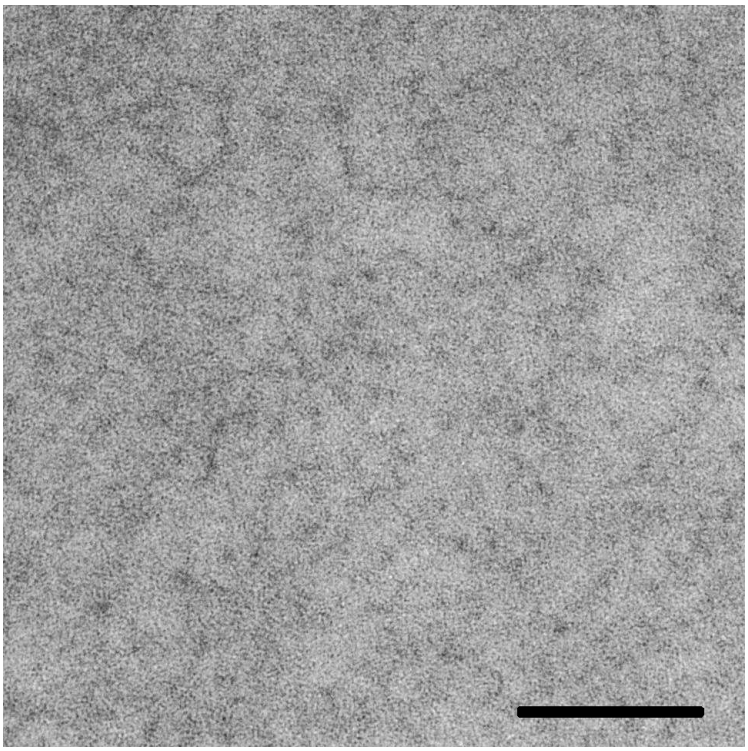

Figure 6.17: A TEM image of a 3% PS gelatin gel in 0.2 M NaCl, pH 7. Image courtesy of Altskär & Hermansson. The scale bar represents 100nm.

Figure 6.18 shows how the three probes will experience moving around in a newly formed 2% gelatin gel. The gel is formed by quenching a gelatin solution from 60°C to 15°C and the x-axis shows time since the quenching started. The smallest fluorescein probe ($\triangledown$) "barely notice" the gel and the only information obtained is that the presence of a biopolymer forces the probe to move at 60% of its free diffusion coefficient. The other two probes, however, are more retarded and they experience the structural changes in the gel conformation from a weak to a harder gel; the normalized diffusion coefficient decreases for both as a function of time. The conclusion drawn from this is that the probe size can give information about the apparent mesh size that is formed in the gelatin gel; even though the probes are smaller than the voids in the gel, they sense the changes in the gel structure. It should also be understood that the choice of diffusion probe is important.

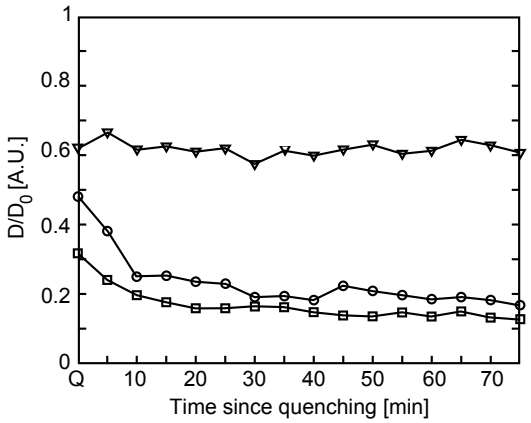

Figure 6.18: The normalized diffusion coefficient of three different probes in a newly formed 2% gelatin gel. The probes are fluorescein (▽), 10kDa FITC dextran (○) and 500 kDa FITC dextran (□). The gel is formed by quenching from 60°C to 15°C at the leftmost point of the graph.

6.2.1 Effect of temperature on the diffusion probes

The temperature of the medium strongly affects the diffusion coefficient of the probes as a higher temperature means more kinetic energy in the system. If the temperature is changed during an experiment, the diffusion coefficients obtained will need to be normalized with the free diffusion coefficient (D_0) to be comparable. Figure 6.19 show the D_0 values for three different FRAP probes in pure water. It can be seen that the diffusion coefficient for the small fluorescein probe (▽) increases linearly with temperature, which is expected from the Stokes-Einstein relation. There are, however, slight deviations from linearity for the larger FITC dextran probes (□ & ○). The weak tendencies to non linearity can be seen in at the lower temperatures and they are likely caused by conformational changes in the random coil of the dextran chain as a result of the probes being further away from θ temperature [24, 56]. This effect is barely influencing the results and a linear curve fit for each probe all gives an r^2 value of 0.96 or higher.

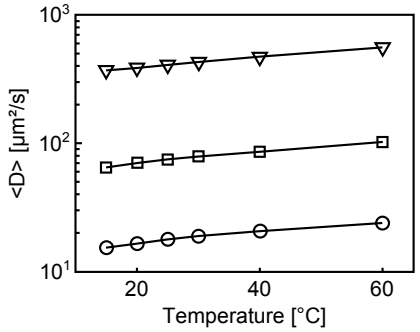

Figure 6.19: Diffusion coefficients in distilled water (D_0) as a function of temperature for three different probes: fluorescein (▽), 10 kDa FITC dextran (□) and 500 kDa FITC dextran (○). Each point is the average of at least 5 FRAP measurements.

6.2.2 Effect of ionic conditions on the diffusion probes

Another important aspect when it comes to how the probes experience the medium they are in is the presence of ions. If the probe is ionic, which is the case of Na_2-fluorescein and FITC dextrans, then the presence of other ions will affect the probe behaviour. To circumvent this influence, the result from the diffusion measurement needs to be normalized with the free diffusion coefficient of the probe in an ionic solution rather than in distilled water. An example of such system is κ-carrageenan, which requires the presence of salt ions to gel [43, 50, 89] and the dried carrageenan usually contains a small amount of counter ions itself which have to be taken into account when calculating the effective ion concentration. The κ-carrageenan used in Paper IV contained 1 mM Na^+ and 8 mM K^+ naturally in a 1% solution and while it wasn't sufficient in order to initiate gel formation, it was sufficient to alter the behaviour of the probe. Figure 6.20 show a solution of 1% κ-carrageenan without any additional salt added; the two first points are at 60°C and solution is thereafter quenched to 15°C. The two different curves show the diffusion coefficient normalized only for the temperature change (□) and normalized for both temperature change and ion concentration (○). The effect of the salt can clearly be seen on the probe; it will appear as if the diffusion coefficient which is only normalized for temperature changes over time for the first 20 minutes, whereas the true curve which is normalized for both ion concentration and temperature show that no significant changes occur.

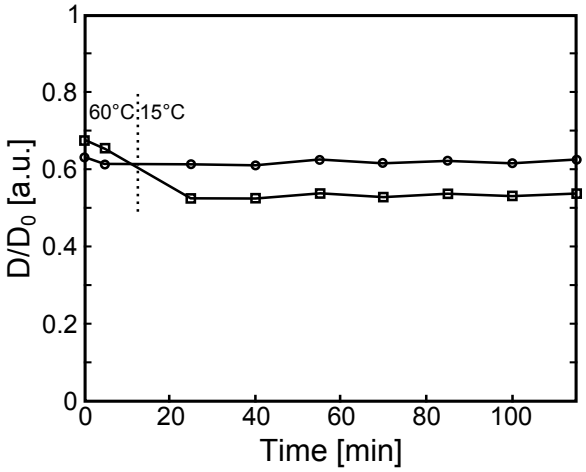

Figure 6.20: A 1% κ-carrageenan solution with 1mM Na^+ and 8mM K^+ which is quenched from 60°C to 15°C. The curves represent the normalized diffusion coefficient for a 10kDa FITC dextran probe and are normalized with regard to temperature (□) and with regard to temperature as well as ion concentration (○).

The reason for the erronious normalization curve can be seen in Figure 6.21, in which there is a difference in temperature dependence for the different ion concentrations. The different salt concentrations are significantly different from each other in how they affect the probe diffusion, and the largest difference occurs for a probe in deionised water. By adding salt to the solution, the viscosity will change slightly, which is part of the reason, but for a dextran conjugate it could also be a result of a change in how the probe experiences the solvent. Since the polymer-solvent

interactions will affect the shape of the probe coil, the quality of the solvent will determine the radius of gyration (r_G) of the probe depending on whether or not the polymer–polymer interactions are more favourable than polymer–solvent interactions [24, 28, 56]. If the polymer chain has favourable interactions with the solvent (i.e. being near or at the theta conditions), the random coil formation takes on a more loose arrangement; if the polymer–polymer interactions are more favourable, the random coil expels the solvent and takes on a denser arrangement.

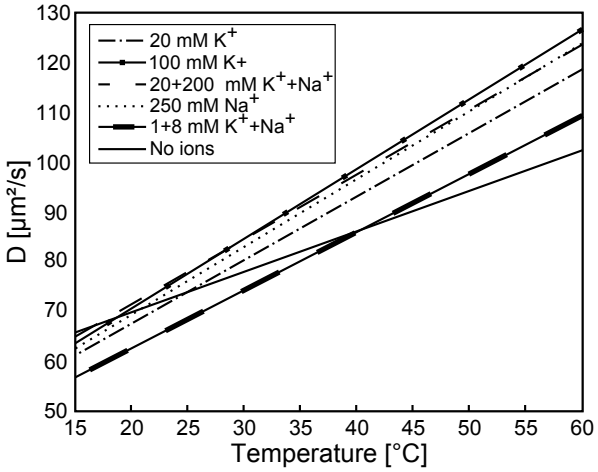

Figure 6.21: The free diffusion as a function of temperature of a 10kDa FITC dextran probe in deionised water with different amount of salt added. The interpolations were done with data at 15, 20, 25, 50, 55 and 60 °C with 5 measurements per temperature; all of the curve-fits have an r^2 value of 0.97 or higher

6.2.3 Probe compatibility

When introducing a probe to a system of interest, there is a risk that the probe is not compatible and therefore prefers to stay clustered rather than distributing itself throughout the sample. Figure 6.22 shows two almost identical samples, the only difference being the probe. Both samples are a solution of 1% κ-carrageenan without additional salt and the probes added are a 10kDa FITC dextran probe and a 500kDa FITC dextran probe. The 10kDa probe distributes itself homogeneously throughout the sample whereas the 500kDa probe phase separates and is seen mostly as bright dots. The reason for this is that the tendency for phase separation increases with increasing molecular weight due to a decrease in entrophy [91, 101]. As the larger probe is not compatible with the κ-carrageenan, it will not be able to report any relevant diffusion coefficients because the contrast between the bleach area and the background will be too low. Furthermore, as the current FRAP models require the probe to be distributed homogeneously, there is a risk that the measured diffusion is affected by the pools where the probe is gathered either because there might be gradients present or because the darker areas might have insufficient probe present to allow the bleached amount of probe to be negligible compared to the amount of fresh probe present. Should the aggregates not be kinetically trapped in the sample, they also risk diffusing around which would interfere with FRAP measurements.

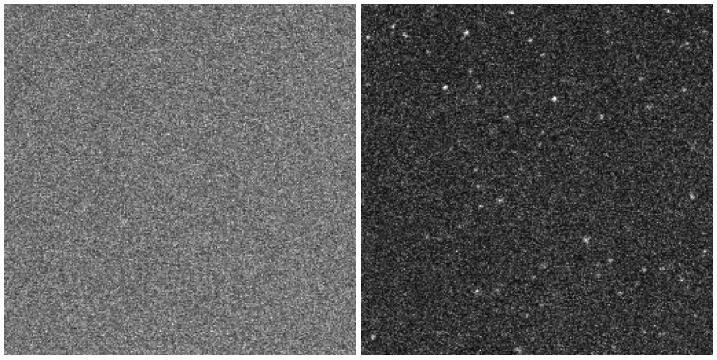

Figure 6.22: A κ-carrageenan sol with a 10kDa FITC dextran probe (left) and a 500kDa FITC dextran probe (right). Both samples have equal CLSM settings for gain and offset and are taken at equal depth. The bright dots in the right hand sample indicates phase separation between the sample and the probe.

Even if the probe does not phase separate from the system, it can become unevenly distributed when probing a multiphase system. Figure 6.23 show a phase separated gelatin–maltodextin sample in which a 10 kDa FITC dextran probe has been dissolved into the aqueous phase prior to phase separation. As the phases separates, the probe will redistribute itself in the system. This leads to different equilibrium concentrations of the probe and different intensities in the different phases. The redistribution of the probe can be influenced by a different affinity for the two phases or simply be a result of the water concentration shifting during the phase separation. Probing the darker phase of the resulting network can become difficult if it gets too dark due to an increased amount of noise, but it is fully possible to do so using a modern FRAP model (Paper III). Due to differences in material structure between the different phases, the probe may experience different diffusion coefficients in the two phases. To avoid boundary effects between the phases, it is important to bleach sufficiently far away from the interfaces.

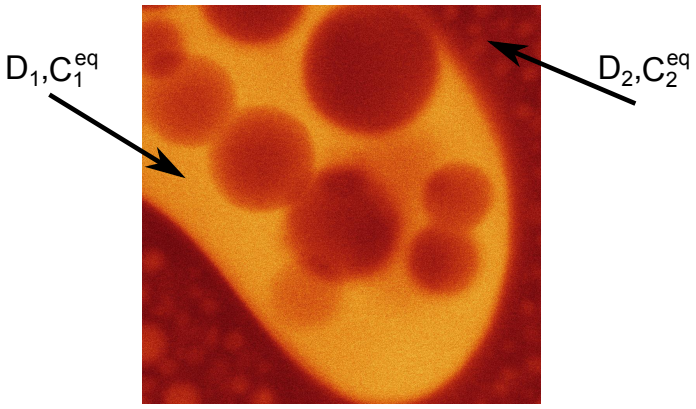

Figure 6.23: A multiphase gel stained with a 10 kDa FITC dextran probe, dissolved in the aqueous phase. The difference in colour is caused by a difference in probe affinity for the different phases.

6.3 FRAP and structural heterogeneity

Heterogeneity might be easiest to describe through its antonym 'homogeneity', which Merriam-Webster defines as "the state of having identical cumulative distribution function or values" [57]. That is, if something is homogeneous, it will have a uniform appearance regardless of where one looks; if something is heterogeneous then it will be the opposite, which means that the chosen spot to look will influence the values of what is measured. When determing whether a material is homogeneous or heterogeneous, the relative length scale between the "window" with which one is looking through and the typical length scales of the object under study will be factors to consider. That is, the visible area/volume of the sample needs to be large enough to be able to correctly tell whether the material structure appears uniform or not. A continuum approach to homogeneity in a material structure is seen is in Figure 6.24A, in which the black dots represent a material structure and the material is viewed through the squares of increasing size and magnification. When moving around the "windows" in a zoomed-in view, the placement will greatly affect the density of black dots that are observed, ranging from zero to 100%. If one were to plot the density as a function of the observable area, the graph would look like Figure 6.24B. As the size of the observable area goes up, there will be fewer differences between selected areas and the noise caused by placement will even out. Once the point is reached where there are no differences, a continuum is reached and the material will appear homogeneous instead of heterogeneous [131]. Should the "window" become larger than the size of the sample (the dashed square) then the apparent density will start to decrease (dashed line in the function). Since this is just a conceptual image, a real material might appear heterogeneous on different length scales and it is not always possible to image all of them, which therefore would render a continuum approach slightly difficult to use.

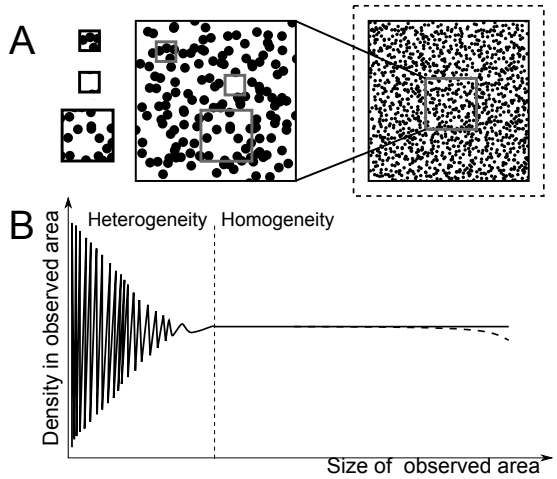

Figure 6.24: A continuum approach to heterogeneity/homogeneity using the density of black dots as definition. (A) The material structure on different length scale with the imaging windows drawn as squares. (B) The density of black dots as function of the size of the imaged area and placement.

Figure 6.25A shows a concept image of a material structure on many different lengthscales and it should be noted that the material appears homogeneous on at least two length scales: inside the second and fifth image from the left. This type of detail might, of course, be difficult to find in a real material and Figure 6.25B show three length scales of a 0.5% κ-carrageenan gel with 250mM Na^+. It should be mentioned that the three different images are imaged to scale but from different areas. The two first images are from a thin sectioned TEM sample while the third is from CLSM and it can be seen that the sample appears highly heterogeneous in the TEM but entirely homogeneous in the CLSM. For a sample with heterogeneity on the CLSM imaging scale, such as a multiphase sample, there would be a structure visible in the third image of Figure 6.25B, comparable to (although often stronger than) the faint structure seen in the rightmost image in Figure 6.25A.

This example has also only taken the material structure into consideration, as it is possible to determine a sample to be either homogeneous or heterogeneous based on structural information obtained by microscopy techniques. However, the same approach would be valid for any other properties which can be measured on different length scales or on different locations. An example would naturally be diffusion, where the correlation between local diffusion coefficients and the material structure is of high interest in this work.

Depending on what is of interest to study in the material, there might be limitations which causes challenges for FRAP. If the sub resolution heterogeneity is of interest, then one needs to be aware that the FRAP measurement might remove information through averaging; if a single phase is of interest in a multiphase sample, then a FRAP model capable of bleaching small enough areas is required.

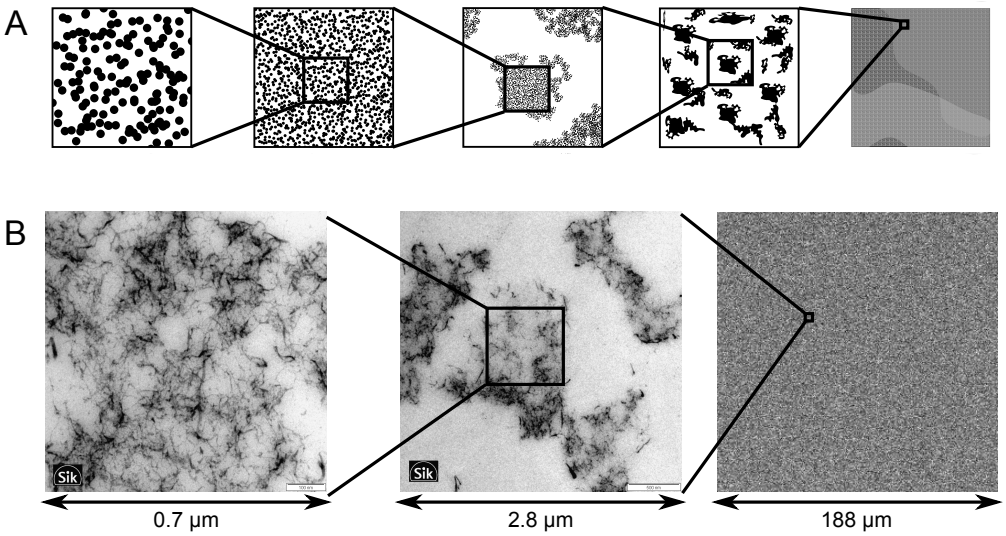

Figure 6.25: Heterogeneity on different length scales for a concept material (A) and a real material (B). The images on different length scales are composed of both TEM and CLSM images. The real material in (B) is 0.5% κ-carrageenan with 250mM K^+ added. The two TEM images are not from the same area in the sample.

6.3.1 FRAP in a multiphase system

(Paper III)
Many materials or products consist of different phases that have different properties. With regard to transport of molecules, the diffusion properties and the solubility can differ considerably between the phases. In addition, the interface between the phases can either promote or inhibit the transport. The overall transport is dependent on the morphology of the multiphase system i.e. the spatial distribution and volume fraction of the different phase. When probing diffusion in a single phase of a multiphase system using FRAP, the placement and size of the bleach ROI become extra important. Since one requirement for FRAP is that the diffusion can be considered free and unaffected by boundaries in the sample, it follows that the bleach ROI needs to be placed so that the diffusion front during recovery will not be influenced by the other phases surrounding the phase of interest. Whether this can be accomplished will in turn depend on the size of the bleach ROI in relation to the domain sizes in the sample, and to a certain degree the diffusion coefficient as well. The smaller the bleach ROI can be made, the easier it will be to place it in such way that the diffusion front will not reach the boundaries. Figure 6.26 shows an example of a phase separated gel consisting of 4% gelatin (dark areas) and 6% maltodextrin (bright areas). The multiphase structure is rather heterogeneous and consists of a bicontinuous structure at longer length scales (hundreds of micrometers) and a secondary phase separated structure with spherical inclusions at short length scales (tens of micrometers). In order to probe diffusion in the bright maltodextrin phase, the bleach ROI cannot be much larger than about 10 µm in order to fit. The position must also be carefully selected. For such small bleach areas, the influence from the radial resolution of the laser beam (imaging PSF) needs to be taken into account in order to retain accuracy in the estimation of the diffusion coefficient [11]. Furthermore, it is in general more demanding to estimate the local diffusion coefficient in small bleach areas because the influence of noise is larger and the intensity recovery is much faster. In Paper III we have addressed these issues by introducing a new pixelbased FRAP model called rectangle FRAP (rFRAP) that effectively uses all temporal and spatial information in the FRAP data series.

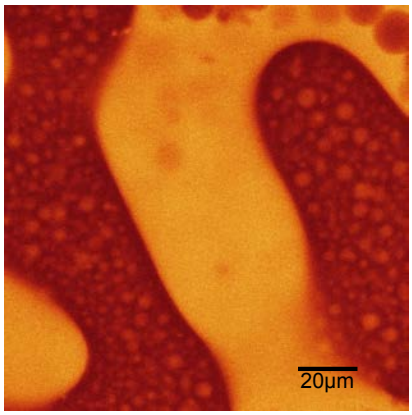

Figure 6.26: A phase separated sample with 4% gelatin (dark areas) and 6% maltodextrin (bright areas), stained with a 10kDa FITC dextran probe. The scale bar is 20 µm.

Rectangle FRAP model

As the name of the rectangle model suggests, the bleached area is changed from a circle to a rectangle. Even though it may sound like a trivial change, it makes it possible to create a pixel based model with an analytical solution which still can take the bleaching step and the imaging PSF of the microscope into account. This means that the model therefore can handle any size and aspect ratio of the bleached rectangle that the CLSM is capable of creating. Furthermore, the model has the advantage of not being limited by a Gaussian shaped distribution in the bleach profile and an analytical expression is not as demanding and time-consuming to calculate as a numerical solution.

The base assumption for the rFRAP model starts with the assumtion of a linear photobleaching process, described as

$$C_b = C_0 \left(1 - \frac{\alpha}{\nu \Delta y} K(x, y, z)\right) \tag{6.5}$$

where α is the bleach rate of the fluorophores, ν is the line scanning speed, Δy is the distance between two scanned lines and K is a bleaching parameter. Taking the PSF into account (intermediate steps are described in detail in Paper III) the observed fluorescence after recovery can then be described as

$$\begin{aligned} \frac{F(x,y,z,t)}{F_0} =& 1 - \frac{K_0}{4} \frac{Z_{b,n}}{\sqrt{2}} \frac{1}{\sqrt{Z_{m,n}^2 + 4Dt}} e^{-\frac{1}{Z_{m,n}^2 + 4Dt} z^2} \\ & \times \left[\operatorname{erf}\left(\frac{x + \frac{l_x}{2}}{\sqrt{r_{m,n}^2 + 4Dt}} \right) - \operatorname{erf}\left(\frac{x - \frac{l_x}{2}}{\sqrt{r_{m,n}^2 + 4Dt}} \right) \right] \\ & \times \left[\operatorname{erf}\left(\frac{y + \frac{l_y}{2}}{\sqrt{r_{m,n}^2 + 4Dt}} \right) - \operatorname{erf}\left(\frac{y - \frac{l_y}{2}}{\sqrt{r_{m,n}^2 + 4Dt}} \right) \right], \end{aligned} \tag{6.6}$$

for a general multi-photon case, where both the n-photon photobleaching intensity distribution and m-photon imaging PSF are assumed to be 3-D Gaussian functions with radial resolution $r_{m,n}$ and axial resolution $Z_{m,n}$. The radial and axial resolution parameters are a combination of the bleaching and imaging resolution and is defined as

$$r_{m,n}^2 = \frac{r_{b,n}^2 + r_{i,m}^2}{2} \tag{6.7}$$

$$Z_{m,n}^2 = \frac{Z_{b,n}^2 + Z_{i,m}^2}{2}. \tag{6.8}$$

The length of the sides in x- and y-direction of the bleached rectangle is denoted l_x and l_y; K_0 is a bleaching parameter and erf is the error function, which is defined as

$$\operatorname{erf}(z) = \frac{2}{sqrt\pi} \int_0^z e^{-x^2} dx. \tag{6.9}$$

Since the model is derived for a multi-photon case, the equation can be simplified for a single photon case by letting $n = m = 1$ (replacing $r_{1,1}$ with R) and neglecting diffusion along the

z-axis ($Z_{b,n} \to \infty$), which changes Equation 6.6 into

$$\begin{aligned}\frac{F(x,y,t)}{F_0} =& 1 - \frac{K_0}{4}\left[\operatorname{erf}\left(\frac{x+\frac{l_x}{2}}{\sqrt{R^2+4Dt}}\right) - \operatorname{erf}\left(\frac{x-\frac{l_x}{2}}{\sqrt{R^2+4Dt}}\right)\right] \\ &\times \left[\operatorname{erf}\left(\frac{y+\frac{l_y}{2}}{\sqrt{R^2+4Dt}}\right) - \operatorname{erf}\left(\frac{y-\frac{l_y}{2}}{\sqrt{R^2+4Dt}}\right)\right].\end{aligned} \tag{6.10}$$

The fitting procedure can be done both with least square fitting or with maximum likelihood estimation, similar to the Monoton MLE model. For the parameters $\Theta = [D, k, K_0, r_{m,n}^2]$ the log-likelihood is

$$\begin{aligned}l(\Theta \mid x,y,t) = &-\frac{|T||S|}{2}\log(2\pi\beta) - \frac{1}{2}\sum_{t\in T}\sum_{x,y\in S}\log\lambda(x,y,t \mid \Theta) \\ &-\frac{1}{2\beta}\sum_{t\in T}\sum_{x,y\in S}\frac{(p(x,y,t)-\lambda(x,y,t \mid \Theta))^2}{\lambda(x,y,t \mid \Theta)},\end{aligned} \tag{6.11}$$

in which T is the set of all times which corresponds to the recovery images, $|T|$ is the number of time points, S is the set of all pixels in an individual image, $|S|$ is the corresponding number of pixels and $p(x,y,t)$ is the pixel value for a pixel at position (x,y) with time t. Since the PSF resolution ($r_{m,n}$) is estimated, it does not need to be known in advance and the model is valid for any size of the bleached ROI.

The accuracy of the rFRAP model for different sizes of the bleach ROI can be seen in Figure 6.27, using a 150 kDa FITC dextran probe in 60% sucrose solution. In Figure 6.27A a square with a side length of 2.5 µm, 5 µm, 7.4 µm, 10 µm and 12.4 µm was bleached. In Figure 6.27B a rectangle with a width of 10 µm was bleached and the height varied as 2.5 µm, 5 µm and 10 µm. Each point is the average of 10 measurements and all use the same microscope settings. It can be seen that the model is independent of the bleach ROI down to 2×2 µm; the main reason that the error bars increase as the bleach ROI size is decreased is that fewer pixels are available in the bleach ROI.

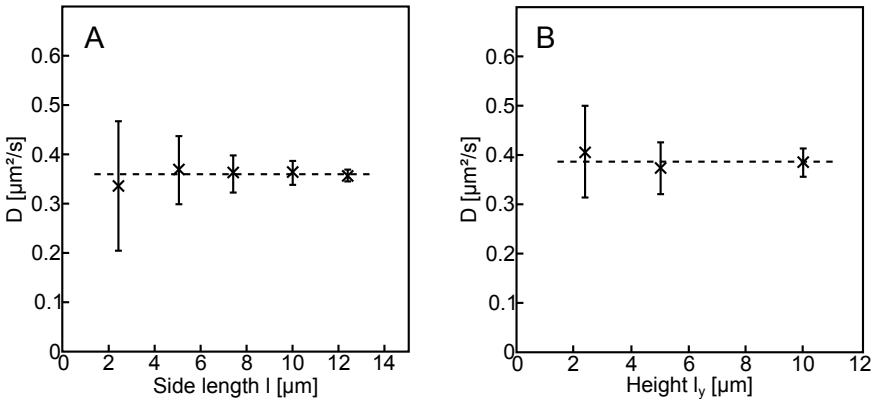

Figure 6.27: The diffusion coefficient of a 150kDa FITC dextran probe as a function of the size of the bleached ROI. (A) The effect of the side length of a square bleach ROI. (B) The effect of the height of a rectangle with $l_x = 10$ µm. The dashed lines indicate the averages of all measurements.

In Paper III, the rFRAP model was tested on the 4% gelatin/6% maltodextrin multiphase system shown in Figure 6.26 to show the applicability of the new FRAP model to heterogeneous materials. Not only was it possible to bleach the individual phases, it was also possible to differentiate between the diffusion coefficients in the two phases despite that $D_{gelatin}$ is close to $D_{maltodextrin}$. Figure 6.28 shows a typical bleach series in the maltodextrin phase of the multiphase sample in which a 7×7 µm large rectangle is bleached.

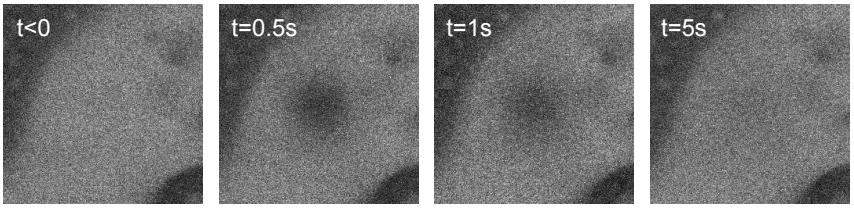

Figure 6.28: A typical bleach series in the maltodextrin phase of a 4% gelatin (dark areas)/6% maltodextrin (bright areas) sample. The probe used is a 10kDa FITC dextran probe. The bleach ROI is 7×7 µm and the image represents a 60×60 µm area of the sample

To create the multiphase sample, the two biopolymers were mixed and then allowed to phase separate and gel over night, using a furnace to slow down the cooling rate. The furnace was heated to 60°C, turned off and was then allowed to self cool to room temperature. This gave a cooling rate shaped like an exponential decay with an average of -0.14°C/min during the gel formation and allowed the phases to separate into a bicontinuous system with some minor spherical inclusions in each phase. Once mixed, the phases would never separate to 100% pure phases because of entropic reasons and the diffusion coefficients of the separated phases is therefore slightly higher respectively slightly lower than pure samples. Figure 6.29 show a bar plot with the results from the different phases. It can be seen that the two phases in the multiphase system have rather similar diffusion coefficients, although a 95% confidence t-test showed them to be significantly different (P=0.00042). This clearly shows that the new rFRAP model is capable of measuring diffusion rates in very heterogeneous materials. The rFRAP model has also been used in heterogeneous model chocolate systems to determine the effect of tempering and solid particle addition on the fat crystallisation and the diffusion rate of fluorescent fatty acid analogs. The results showed that tempering has a large impact on the diffusion coefficient of fatty acids in chocolate [125].

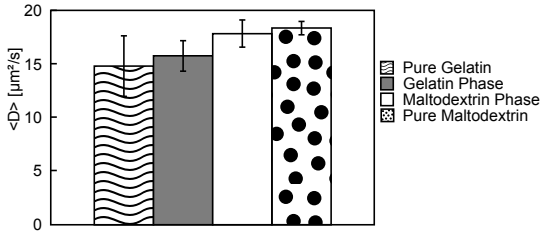

Figure 6.29: The diffusion coefficient for a 10 kDa FITC dextran probe in the separated phases of the 4% gelatin/6% maltodextrin sample compared to the pure phases with equal concentrations. Each bar show the average and SD error for at least 10 measurements.

Experimental considerations when bleaching in a multiphase system

When bleaching a multiphase sample, the 3D structure of the sample needs to be taken into account when selecting the bleach area regardless of CLSM. Even though it might appear to be possible to place the bleach ROI far enough from the boundaries in the focal plane, the boundaries above and below need to be taken into account as they otherwise might influence the diffusion front. What this means when using a multi photon CLSM is that not only does one need to place the bleach ROI at enough distance from the phase edges, the focal plane needs to be placed so that the upper and lower boundaries of the bleached volume will be far away from the phase edges. As mentioned, one strength of the rFRAP model is that it is usable on both a multi photon CLSM as well as a single-photon CLSM. On a multi-photon CLSM the bleaching will be limited to the focal volume and will not go through the sample along the z-axis as is the case of a single-photon CLSM. These two different CLSM characteristics are utilized when bleaching as they make it possible to bleach a 3D volume with a multi-photon CLSM [81] while the bleach cylinder is used to simplify the diffusion to a 2D case when using a single-photon CLSM. For a single-photon case, the bleach volume penetrates through the phases with no regard to the surroundings; although if there are mismatches in the refractive index between the phases, the bleach volume might be distorted due to scattering effects when the laser passes through interfaces. If the two phases allow different diffusion coefficients for the probe, there is a risk that the bleached phase above and below will disrupt the recovery in such way that the z-direction needs to be taken into account.

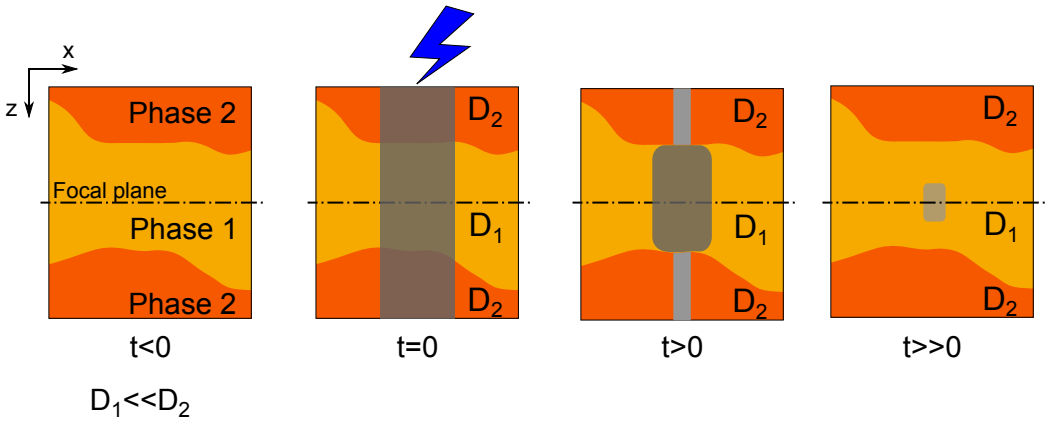

Figure 6.30: A concept image of a bleached volume in a multiphase sample. The picture illustrates what might happen if the diffusion coefficient is different in the two phases.

Figure 6.30 illustrates what might happen during an event where the diffusion in phase 1 (the phase in the focal plane) is much slower than that in the other phase. As there will be high contribution to the diffusion from phase 2, the effective height of the bleached volume will be reduced to the height of phase 1. If this distance is too short, there is a risk that the z-axis diffusion cannot be neglected. The bleached area therefore needs to be chosen with this in mind or a model which takes 3D diffusion into account needs to be used. The rFRAP model is developed to allow 3D diffusion, but if the bleach ROI is placed without regard to the 3D structure, the user might risk using the simplified version of the model, which assumes no effective diffusion along the z-axis.

When choosing an area to bleach, the easiest way to fit the bleach ROI is to only bleach squares, although if the phase of interest in the sample has an oblate shape, a small enough square which fits the area might recover too quickly if the diffusion coefficient is high. In such case a rectangle might be a good way to yield a good recovery and still allow a placement far enough from the edges. This leads to another important consideration, the practical CLSM limitations. Even though the model can handle any size and aspect ratios of the bleach ROI, it is important to realize that not every size and aspect ratio will be possible to actually use, depending on the CLSM used. What needs to be taken into account is the zoom-in function of the microscope. It is often a requirement to use the zoom-in function on the CLSM in order to obtain good bleaching using only one bleaching frame or else there is a risk that the interline distance between two laser lines will becomes too large and the bleached area will not become homogeneously bleached. For the Leica SP2 and SP5 CLSM, the zoom-in works best if the bleach ROI is chosen so that $l_y \leq l_x$.

6.3.2 Heterogeneity on a sub-resolution scale

(Paper I)

When the structure in a sample is heterogeneous on a smaller length scale than the resolution of the CLSM, the sample will naturally appear homogenous while imaged (cf. Figure 6.25). When bleaching different locations inside the sample, the estimated diffusion coefficients depend on the underlying averaged structure and can be noticable in the standard deviations. A sample with higher standard deviations can be interpreted as being more heterogeneous since the different areas will give rise to a wider variation in the estimated diffusion coefficients, provided that a modern FRAP model with high accuracy have been used.

The SAP used in Paper I was a cross linked polyacrylic acid gel created through radical polymerization. Since polymer networks synthesized by free radical polymerization are inherently inhomogeneous due to non ideal effects [72], the SAP network will have areas of varying density depending on physical location in the sample. The diffusion coefficient of a fluorescein probe in a SAP gel for different degrees of swelling can be seen in Table 6.2, in which the degree of swelling is expressed as $m_{\mathrm{H_2O}}/m_{\mathrm{dry\ SAP}}$ (cf. Section 6.1.4, for further details see Paper I). The most likelihood estimation (MLE) models which were used gives an error estimate for each parameter on a 95% confidence and no individual measurement had an error larger than $\pm 1.75\%$. What is notable is that despite the high accuracy of each individual measurement, the samples with a lower degree of swelling have a fairly large standard deviation and the standard deviation decreases with an increased degree of swelling. This is interpreted as the samples being heterogeneous on a lenght scale noticable to the probe while there are 30% SAP or less in the sample; thereafter the denser areas in the SAP will have swollen large enough to not influence the probe as much. Another noticable detail is that there seems to be a shift in how large the standard deviation will be at around $2\times$ swollen SAP, which was the same point where the Gaussian MLE model no longer could fit the FRAP data accurately. At a degree of swelling lower than $2\times$, the initial bleaching profile was not Gaussian shaped and instead resembled an inverse hat function which led to that the Monotone MLE Model was required in order to achieve a high accuracy in the calculations, where the Gaussain MLE model would have estimated D with a larger error. At higher degree of swelling, both models estimate the diffusion coefficient with roughly the same error. It should therefore be noted that the increase in standard deviation for the estimates of

Table 6.2: The diffusion coefficient of fluorescein as a function of the degree of swelling of SAP. Each point is an average of four measurements using a 30 µm bleached disc and no individual measurement has an error larger than ±1.75%.

Degree of swelling	1.25×	1.5×	2×	5×	10×	20×
<D> [µm^2/s]	3.79	5.42	17.13	145.59	215.00	243.02
SD error [%]	11.74	22.33	7.19	1.81	2.55	2.07

D is, in fact, not caused by a change in model.

The FRAP results in Paper I were compared to NMR diffusometry to verify the accuracy of the model, using a 400 Da PEG probe instead of the 376 Da fluorescein FRAP probe. There was a high degree of compatibility between the FRAP estimations and the NMRd measurements for the larger degrees of swelling (10× and 20×) and for those samples no heterogeneites were seen by NMRd. It should be noted that an observation time of 100 ms was used for NMRd, during which the PEG probe had a RMS displacement of 7 µm in the 10× swollen SAP. As the expected heterogeneites were on a sub resolution length scale for the CLSM (<1 µm), the probe would therefore experience the material as homogeneous in the NMRd measurements. In addition, the FRAP measurements on the 10× swollen SAP revealed more homogeneous results than for the SAP gels which were ≤2× swollen. There might had been indications from NMRd in the lower swollen samples, unfortunately it was not possible to properly prepare samples for NMRd measurements at those low degrees of swelling as the gels were highly adhesive and it was not possible to get them down into the test tubes without causing damage to the tubes. As a test, the SAP was added dry to the tubes with the water added afterwards; however, it turned out that the limited geometry prevented the SAP from swelling properly. Since ideal gels swell isotropically, a limitation in any direction needs to be overcome through an entropy cost [40]. The SAP used was cross-linked macro particels and the limited x-y geometry of the NMR tube therefore prevented the swelling to continue once the gel hit the tube walls. To continue swelling in z-direction, the gel would have to break the chains or the cross-linking sites.

Another material study have shown the degree of heterogeneity as being linked to a high standard deviation. Svanberg et al. [125] studied the growth of fat crystals in chocolate and tested two different methods, seeding and traditional tempering. While not really being on a sub resolution scale, the result from CLSM micrographs showed that the fat crystals in the seeded chocolate grew more homogeneously while the traditional tempering caused much more heterogeneous structures. The result from the FRAP measurements which Svanberg et al. [125] performed on the materials showed a higher standard deviation for the samples which were seen as heterogeneous, both immediately and after storage.

6.3.3 Probing structure heterogeneity using spatial correlation of FRAP data

The microstructure of a heterogeneous soft material can, in a simple manner, be seen as domains with different properties. These domains can either be well defined areas with abrupt changes in properties, or diffuse areas in which the properties vary gradually. An example of a material with well defined areas is a multiphase sample in which the properties of phase 1 differ from the

properties of phase 2. An example of a material with more diffuse areas is boiled pasta, where a large portion of the structure is swelled starch granules [16]. If the pasta structure is simplified to only consider the starch granules, then the structure can be thought of as a starch gel with denser and softer areas caused by the granule core and the diffuse borders. This is because the outmost parts of a granule have had more time to swell while the water is penetrating in and the outer parts of the granules fuses together as they swell.

A novel way to probe the structure heterogeneity is proposed here. The diffusion speed of the probe molecules is affected by the microstructure which the probe diffuses through and will vary spatially as the microstructure varies. By measuring the spatial variation of diffusion coefficients it will become possible to obtain a measurement of the spatial variation of the microstructure. This can be useful to characterise materials, especially if the microstructure is on a sub resolution scale of the microscope. It is expected that adjacent regions in a material will have similar diffusion properties whereas regions with longer distance in between only correlates if the underlying structure is similar or the structure is periodic. The distance where this transition occurs will most likely vary between different types of materials and it can be used as one type of measurement of the structure heterogeneity. This section is an ongoing work.

The experimental procedure involves bleaching at specific locations in the material, using a high precision x-y-table on the CLSM to ensure accuracy in the placement of the bleach ROIs. By assuming an isotropic material, the measurement is simplified to 1D and the bleach ROIs are only placed along a line. In order to achieve longer distances inside the material while keeping time efficiency, the bleach ROIs are placed in clusters of 5 ROIs which are repeated with a distance between each cluster. This pattern is shown in Figure 6.31, and the bleached ROIs are either 5 µm or 10 µm squares. The run order is chosen randomly with the restriction that no spots lying directly next to each other in space are bleached consecutively. This restriction is chosen to allow a recently bleached ROI to fully recover before the neighbours are bleached.

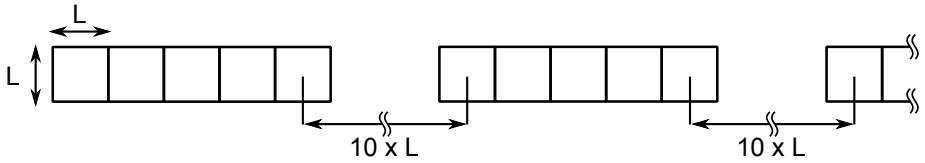

Figure 6.31: The pattern for the placement of bleach ROIs. L represent the side length of each ROI and is either 5 µm or 10 µm. The distance between each block of bleach ROIs is 10 times larger than the size of the bleach ROI. The pattern repeats so that up to 6 blocks are bleached.

The materials chosen to demonstrate the use of the FRAP and spatial correlation method are κ-carrageenan, β-lactoglobulin and cooked pasta made from durum wheat. The heterogeneity of κ-carrageenan is on a sub resolution length scale of the CLSM, which can be seen in the TEM images in Figure 6.6 and 6.8, and the FRAP data should therefore not yield any autocorrelation. β-lactoglobulin has longer typical length scales close to the isoelectric point and the structures formed show high degree of self-similarity [4, 70, 71, 93]. Since the bleach ROIs are >5 µm, any heterogeneity smaller than that will be averaged and depending on the domain size of the β-lactoglobulin, there should be possible autocorrelation in the FRAP data. The pasta contains type A and B granules and the type A granules are roughly 30 µm while the type B granules are

around 3 µm in diameter [16]. Autocorrelation in the FRAP data caused by the type A granules is expected. The type B granules are smaller than a bleached ROI and should therefore only be seen as noise in the data, provided that their presence influence at all. The probes used are 10 kDa and 500 kDa FITC dextran.

The autocorrelation calculations are done according to Equation 3.8. The step sizes (δ) are those which corresponds to the physical distances in the bleach pattern and the correlation coefficients are calculated for each individual δ. The results are then seen as a discrete function from which the correlation coefficients vary between -1 and 1. Normally, values of 0.8 or higher would indicate strong correlation, values around 0.5 would indicate weak correlation and values around 0.2 or less would be interpreted as having no correlation [20]. However, since the data comes from measurements in heterogeneous materials, it is not expected to reach as high values and lower intervals are used. The error in the estimated diffusion coefficients will come both from the heterogeneity of the material as well as noise in the images used for estimation. How large the error in the diffusion coefficients estimate is will directly influence how well the estimation of autocorrelation can be done. The amount of bleached ROIs will also influence the outcome as a low amount yields low statistical significance. Negative correlation coefficients indicate a negative correlation between data points. It could be interpreted as the underlying structure being highly different, such as a dense correlated to an open structure. However, a negative correlation needs a physical explanation and, unless the material has several types of structures with different properties, it is more reasonable to expect that there either is positive correlation or no correlation in real materials.

The results from the measurements can be seen in Figure 6.34. The data is presented as the diffusion coefficients for each bleach spot can be seen in the left column along with the corresponding correlogram for each distance in the right column. Figure 6.34 shows pasta, β-lactoglobulin at 0.1°and 10°C/min cooling rate and κ-carrageenan in rows A, B, C and D, respectively. It can be seen that the diffusion coefficients in pasta (Figure 6.34A) are ordered to a certain degree. Each individual cluster of bleached spots lies tight together but the clusters varies around the average D for the sample. The corresponding correlogram show a high degree of correlation for spots right next to each other and the correlation then decrease with distance. The correlation disappears at a distance somewhere around 30–50 µmwhich matches well with the average size of a type A starch granule. The notch in the correlogram at $\delta = 140$ µm corresponds to the distance between the mid cluster and the side clusters. The method appears to work well for pasta and the data is interpreted as showing strong indication of correlation within starch granules. The way the clusters of bleach ROIs vary around the average diffusion coefficient is interpreted such as reporting that the starch granules have swelled slightly differently relative each other.

The β-lactoglobulin was given different heating ramps during creation in an effort to create different sizes of the aggregates forming. The material structure can be seen in Figure 6.32 and it can be seen that the slower heating creates larger structures. When looking at the diffusion coefficients in Figure 6.34B and C, it can be seen that both materials appear relatively random. The corresponding correlograms shows that the correlation coefficients mostly varies within ± 0.2, which indicates that there are no correlations. There are, however, some correlation coefficients of interest. The correlation coefficient for $\delta = 5$ µm is roughly 0.45 respectively 0.2. Even though these values normally indicates none or possible weak correlation it does match the average size of individual globules in the domains, which are roughly 4 µm in diameter. Even though the

correlation coefficients in Figure 6.34B appears random, there are trends towards higher values at shorter δ and lower values at longer δ. This weak trend indicates potential correlation between domains on a length scale of up to 50 µm. It should be noted that since the values are low and the data set only contains 30 points the trends seen can also be due to chance. Figure 6.33 show a part of the region of the β-lactoglobulin with 0.1°C/min heat ramp with the bleach ROIs marked. Each square represent a 5×5 bleach ROI and it can be seen that the structure is heterogeneous. Even though the ROIs appear to be in a varying structure, there are potential for at least weak correlation between bleach ROIs.

The data for κ-carrageenan can be seen in Figure 6.34B. The data looks as if it reports no correlation since the correlation coefficients varies within ± 0.2. Unlike β-lactoglobulin, the microstructure of κ-carrageenan is completely homogeneous at the length scale of the CLSM and the potential weak trends that can be seen is instead interpreted as variations in the FRAP measurements. In theory, there could be heterogeneities in the gel structure at longer length scales, which would be caused by poor mixing of the sample. However, the sample preparation was made to ensure proper mixing of the gel and if such heterogeneities were present, they would be seen as shifting intensities in the fluorescence caused by shifts in the refractive index.

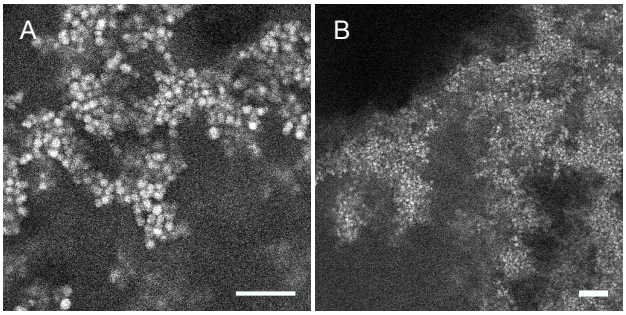

Figure 6.32: The microstructure of a β-lactoglobuline gel at pH 5.4 treated with a temperature ramp of 10°C/min (A) and 0.1°C/min (B). The scale bars is 25µm.

Figure 6.33: A close-up of the structure in β-lactoglobulin gel treated with a 0.1°C/min heat ramp. The squares represent the location of the bleach ROIs and each individual ROI is 5×5 µm.

All in all, the autocorrelation method looks promising. The high correlation in pasta matches

well with the size of the anticipated microstructure and there are trends indicating on possible correlation in β-lactoglobulin. It should be noted that the 3D structure of the β-lactoglobulin caused some troubles in the selection of where to bleach, as it was difficult to find longer areas which were suitable for FRAP. A potential way to verify the weak trends in β-lactoglobulin is to not divide the bleach ROIs into cluster but instead bleach a long consecutive line, which yields a higher statistical significance for the shorter δ. There is too little data to draw more conclusions at the time of writing, but the result is intended for publication when more data is acquired.

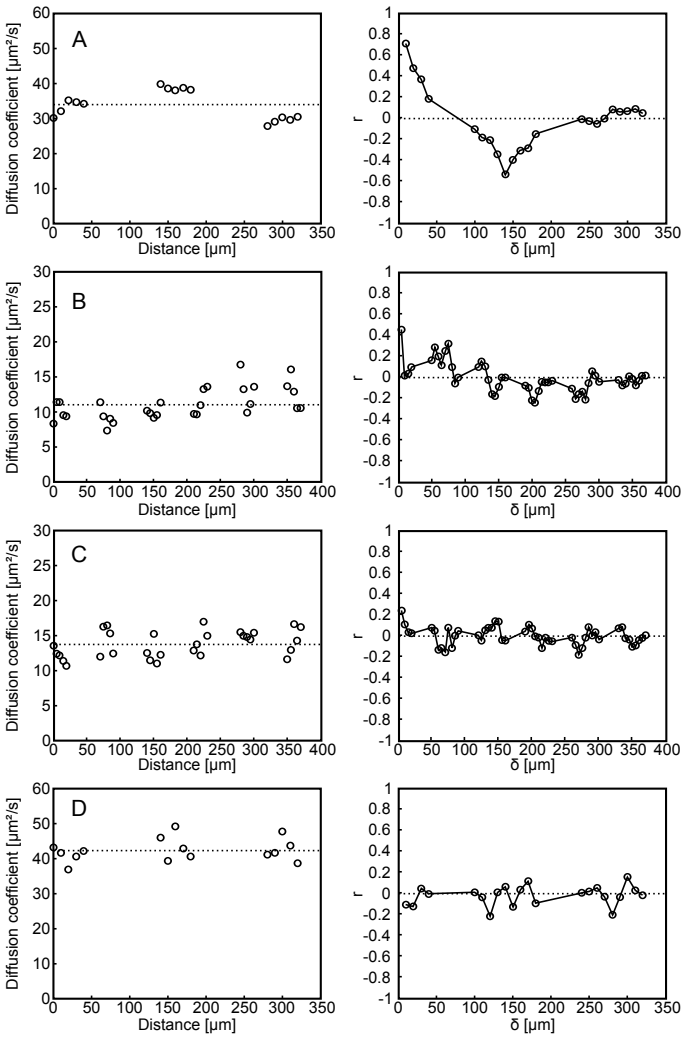

Figure 6.34: The data points and the corresponding correlograms for the different materials. (A) Pasta with a 10 kDa FITC dextran probe using 10µm bleach squares. (B) β-lactoglobulin created with a 0.1°C/min temperature ramp with a 500 kDa FITC dextran probe using 5µm bleach squares. (C) β-lactoglobulin created with a 10°C/min temperature ramp with a 500 kDa FITC dextran probe using 5µm bleach squares. (D) κ-carrageenan formed by 0.1mM KCl with a 500 kDa FITC dextran probe using 10µm bleach squares. The dashed line in the diffusion plots is the average D for all points; the dashed line in the correlograms is the zero line.

6.4 Experimental considerations for FRAP

(Papers I–IV)
In order to do a good FRAP measurement, there are some microscope settings which need to be taken into account. Even though many publications present the protocol that has been used, it is not always easy to start performing FRAP measurements from scratch. The FRAP measurements behind the publications in this thesis have largely been based on "hands-on" experience. Even though each individual CLSM will require unique fine adjustments to work well with FRAP, this section will present some of the basic settings and what is important to think of.

Scanning speed

The faster the scanning speed, the higher the image acquisition rate, which is desired in order to estimate the diffusion coefficient correctly. The most important information is in the beginning of the intensity recovery. However, there is a trade off with the image quality as higher scanning speeds will lead to more noise in each pixel. The optimal speed needs to be tested for each microscope and experiment.

Time between images

The image acquisition rate is not only dependent on the scanning speed but also other settings, such as the amount of pixels to scan. When taking the time between images into account for FRAP, the optimum settings will depend on the sample. For a sample with a high diffusion coefficient, there will be a need to record images as fast as possible in order to capture the recovery. For a sample with a low diffusion coefficient, it is recommended to try to optimize the acquisition rate. This recommendation is due to both hardware and software limitations. A CLSM can usually only acquire a limited amount of images during a FRAP experiment and the modern evaluation models requires enough contrast change between images in order to perform the calculations correctly. The easiest way is to continue to use the maximum acquisition rate and then remove superfluous images; although if the CLSM allows the user to set a time lag then another way is to try to adjust the waiting period to match the diffusion coefficient. The results In Paper III showed that a good acquisition rate should not be slower than the time it takes for a fluorophore to diffuse from the centre to the edge of the bleached region. That is, the time step should not be slower than

$$\Delta t = \frac{(L/2)^2}{4D}, \tag{6.12}$$

where L is the length of the shortest path from middle to the edge. Although, this means that an estimate of the diffusion coefficient is needed before the acquisition rate can be adjusted.

Zoom

Most CLSM have a zoom-in function, which should be adjusted so that the size of the bleach ROI will be somewhere between $1/9^{\text{th}}$ to $1/25^{\text{th}}$ of the scanned area. If the bleach ROI is too small, then there will not be enough pixels in the bleached region for appropriate calculations

of the diffusion coefficient. On the other hand, if the bleach ROI is too large compared to the image, then there will be too few background pixels available for the diffusion calculations.

Interline distance

Most FRAP models require the bleached ROI to be homogenously bleached. To ensure this, the interline distance should be less than or equal to half the width of the laser beam [11]. This can be achieved by setting the CLSM to zoom-in to the bleach ROI during the bleaching phase or by increasing the image format i.e. decreasing the scale factor (length per pixel).

Beam expander

Not all microscopes have the ability to adjust the beam expander, but if the possibility exists then it should be used. Lowering the beam expander means that the back aperture of the objective is not entirely filled. This leads to a lowering of the effective NA and a more cylindrical beam shape. It also means that the laser beam is more concentrated and gives a higher intensity. Figure 6.35 shows a concept image of how the laser beam is affected by the beam expander. It can be seen that a fully open beam expander will give a sharper laser beam, which is useful to resolve fine details for imaging. However, since it is not necessary to resolve fine details when performing FRAP, and since FRAP benefits from a more cylindrical shaped laser, the beam expander should be changed.

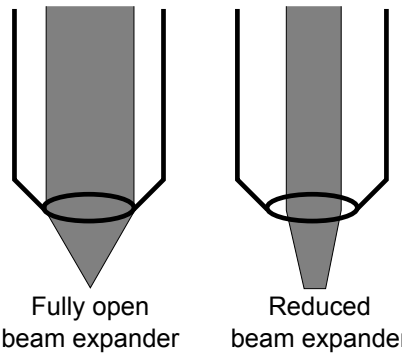

Figure 6.35: Lowering the beam expander leads to a lowered NA of the objective, and a more cylindrical laser beam.

Number of pixels and pixel bit depth

Each pixel in a CLSM image corresponds to a physical area in the sample and the more pixels, the higher the resolution of the sample and the better estimation of the diffusion coefficient. Nonetheless, there are two drawbacks with having too many pixels. One is that the more pixels there are, the fewer photons will be detected in each individual pixel. This will lead to slightly lower contrast between the bleached and non bleached probe molecules, but can often be compensated by increasing the gain of the detector. The raster scanning of the laser beam causes the other drawback, which is that the more pixels, the longer the time it will take between images in

the time series. The bit depth of each pixel should be as high as possible as it means more distinct gray levels and therefore a higher precision in determining the diffusion coefficient. Modern computers usually have no trouble handling the images but should it be necessary to change, then it is possible to reduce the bit depth after an image is taken. A subsequent increase in bit depth will, on the other hand, not lead to more information and therefore not lead to increase in precision of the diffusion coefficient estimate.

Amount of pre- and post bleach images

The pre bleach part of a FRAP experiment only needs to be a few images to make sure that there is no bleaching during the recovery phase later on. If there is any unwanted bleaching it can be seen as a decrease of the overall intensity in the collected pre bleach images and for a sensitive sample it is often seen already at $\sim$10–20 images. The post bleach images are the ones recording the recovery. There is no need to capture the entire recovery sequence as the recent models can estimate the diffusion coefficient with high precision regardless, as long as no anomalous diffusion is present. However, it was seen during the experimental work for Paper I that there should be at least 20 frames in total for the model to work well and there need to be sufficient change between each image. This means that if the diffusion is slow and the image acquisition rate is high, there should be at least 20 images left after removing the intermediate images.

Number of bleach images and the amount of bleaching

Most modern FRAP models [11, 62] (as well as Paper I and paper III) assume that there is no diffusion during the bleaching step and to accommodate this, the number of bleach images should be kept as low as possible. There are models which allow or can be extended to allow diffusion during the bleaching [64, 69, 126] (as well as Paper III) although most of them recommend to minimize the number of bleach images in order to minimize the amount of bleaching introduced. The amount of bleaching is a combination of all high intensity light that the sample is exposed to during the bleaching step and therefore naturally increases with the laser intensity and the amount of bleaching steps. For a sensitive sample, an amount of bleaching that is too high risks damaging the structure and therefore disrupting the diffusion measurement. The model in Paper III also assumes linear bleaching, which will only be valid for a low amount of bleaching. In order to yield enough contrast for the models to estimate the diffusion coefficient, it is recommended to bleach a "depth" roughly 30% [11]. The bleach "depth" is here defined as

$$1 - \frac{\text{average intensity in bleach ROI in first post bleach image}}{\text{average intensity in the pre bleach images}}. \tag{6.13}$$

7 Conclusions

The work presented in this thesis shows that FRAP is a highly versatile tool, with great potential for measuring local mass transport during dynamic changes inside highly heterogeneous materials. The new evaluation models developed have readily expanded the range where FRAP is usable; this is achieved by taking all pixel information into account, as well as allowing more accurate calculations for slow diffusion and decreasing the size of the bleached ROI with maintained accuracy. An additional bonus from the maximum likelihood statistics used in the models is the abillity to obtain error estimates for each parameter estimated.

The combination of FRAP and rheology measurements during gelation of gelatin showed strong indications of the formation of transient networks inside gelatin prior to gelation. The combination of techniques have also revealed a non trivial connection between rheology and the diffusion coefficient, where harder gels do not necessarily lead to slower diffusion.

By using the rectangle FRAP model, the possibility to measure inside highly heterogeneous multiphase samples was successfully achieved. FRAP was proven to be able to probe inside smaller areas with high accuracy and able to discern the difference in diffusion coefficients between the two phases despite $D_1 \sim D_2$.

Even though FRAP was not able to capture structural changes in in κ-carrageenan during the actual gelation process, it was a useful technique to evaluate the changes in the network post gelation. This was possible *despite* troubles finding a probe that worked well with the carrageenan.

The importance of the probe has been evaluated and it has been shown that the data obtained from FRAP strongly depend on correctly selecting which probe to use. In addition to this, the probe behaviour at different temperatures and ion concentration has been evaluated and the result have shown that there is a need to correct for these effects by means of normalization.

FRAP has also been successfully used to measure the degree of heterogeneity, both on the subresolution scale by means of analysing standard deviations and on larger length scales through spatial statistics and correlation analysis. The influence of sub resolution structural heterogeneity on the probe diffusion was compared to TEM data and a correlation between the TEM images and diffusion was seen.

Some of the FRAP data have been compared to NMRd measurements and the results match well. Even though there have been differences between the results from the two techniques, most of those differences can be explained by differences in the experimental set-up as it has not always been possible to use exactly the same probe and/or same concentrations.

All together, the work in this thesis has helped expand the usefulness of FRAP; it becomes an additional asset for those in need of expanding their toolbox when probing dynamic and heterogeneous materials.

8 Outlook

There are still challenges for FRAP to conquer, both in regards to dynamic processes and model development. The development of the latest models have ensured that the limit of how small a bleach ROI can be lies within the limitations of the CLSM; which means that the next advance in that area will not be possible before higher resolution is achieved. The stimulated emission depletion (STED) addition to CLSM has yielded optical nanoresolution and would be the next natural stage of development of FRAP. Being able to bleach locally on a scale of $\sim$10 nm would mean an incredible increase in the possibillity to correlate diffusion to material structure. The current problem, however, is that the probes used for STED are too stable and does not bleach easily, meaning that they are not useful for FRAP (yet).

Dynamic processes which would be an interesting challenge for FRAP would be e.g. phase separation, film formation through evaporation or even extremely fast gelation processes.

Capturing the gelation process of carrageenan (or other quick gelation processes) might be possible at the moment but will require even better hardware than currently available in order to make it an easy task.

Whether an evaporation process could be followed dynamically by FRAP is dependent on certain factors. Unless the evaporating phase is extremely volatile, there should not be any problem to match the timescales for FRAP and dynamic changes of the structure. Whether the evaporation can be followed live will therefore depend on how the probe concentration changes with time and it is likely that one will have to use samples at a pseudo steady-state.

A similar, but most likely easier, problem would be to follow a phase separation process. The benefit would be that the sample volume would remain the same and that the total concentration of probe would not change. However, if the phase separation influences the distribution of the probe molecules, then it might cause anomalous diffusion or apparant flows due to gradients induced. Another problem that could occur is that the initial phases during the separation might be too small to allow a good placement of the bleach ROI and a higher resolution of the CLSM would be needed.

All in all, there are still a lot of potential challenges for FRAP when it comes to dynamic measurements and further development. However, I am positive that there will be clever users who will think of a way to overcome them. FRAP is, after all, a great and versatile tool with a lot of potential.

Acknowledgements

There are many persons whom I would like to acknowledge here, many persons have helped me in some way during these years.

I would like to thank my supervisors *Anne-Marie Hermansson* and *Niklas Lorén* for all their time and guidance. I've learned a lot from your wisdom and you have made it possible for me to develop.

I give a big thank you to all of my co-authors (in addition to my supervisors), without you I would not have managed to build the foundation for this thesis: *Diana Bernin*, *Hendrik Deschout*, *Jenny Jonasson*, *Kevin Braeckmans*, *Magnus Nydén*, *Mats Rudemo* and *Sophia Wassén*.

My deepest gratitude goes to *Hans Lingnert* and *Lars Nordstierna* for reviewing this thesis

I also give my regards to the incredibly fun people at SIK, each day have been a fun adventure with you and your help have been invaluable. I would like to specifically acknowledge *Annika A* for always shining as brightly as the sun, my roommate *Emma* for the wonderful company and occasional poems, *Lotta* for having the biggest smile at SIK, *Magda* for letting me baby-sit her charming cat Smilla and *Sophia* for being my "PhD sister" (I'm sorry if I've been teasing you too much). I also thank everyone whom did *not* bash me with a mallet when I played music at maximum volume. And for the record, I claim to be innocent for any and all practical jokes that have occurred throughout the years.

This work has been a part of the VINN Excellence Centre SuMo Biomaterials (Supramolecular Biomaterials – Structure dynamics and properties) and the financial support from the centre is gratefully acknowledged. I would also like to thank all people involved in SuMo for fruitful and insightful discussions; it has been really great to work together with you all.

I thank all of my friends; you have given me great joy and relief when the workload has been high.

A great acknowledgement goes to my family; I wouldn't have made it this far without your support. I love all of you and I promise that I'll try to call more often now that my thesis is done.

And last but not least, *Marie*, thank you for your love and support. I love you ♡.

Bibliography

[1] Amsden, Brian. Solute diffusion within hydrogels. mechanisms and models. *Macromolecules*, 31:8382–8395, 1998.

[2] Amsden, Brian. An obstruction-scaling model for diffusion in homogeneous hydrogels. *Macromolecules*, 32:874–879, 1999.

[3] Axelrod, D.; Koppel, D. E.; Schlessinger, J.; Elson, E., and Webb, W. W. Mobility measurement by analysis of fluorescence photobleaching recovery kinetics. *Biophysical Journal*, 16:1055–1069, 1976.

[4] Aymard, Pierre; Nicolai, Taco, and Durand, Dominique. Static and dynamic scattering of β-lactoglobulin aggregates formed after heat-induced denaturation at pH 2. *Macromolecules*, 32:2542–2552, 1999.

[5] Barnes, H.A.; Hutton, J.F., and Walters, K. *An Introduction to Rheology*. Elsevier, 1989.

[6] Bausinger, Ralf; von Gersdorff, Katharina; Braeckmans, Kevin; Ogris, Manfred; Wagner, Ernst; Bräuchle, Christoph, and Zumbusch, Andreas. The transport of nanosized gene carriers unraveled by live-cell imaging. *Angewandte Chemie International Edition*, 45: 1568–1572, 2006.

[7] Berne, Bruce J and Pecora, Robert. *Dynamic light scattering: with applications to chemistry, biology, and physics*. Dover Publications, 2000.

[8] Blonk, J. C. G.; Don, A.; van Aalst, H., and Birmingham, J. J. Fluorescence photobleaching recovery in the confocal scanning light microscope. *Journal of Microscopy*, 169(3):363–374, 1993.

[9] Borchard, W. and Burg, B. Molecular mechanisms during the thermoreversible gelation of gelatin-water-systems. *Progress in colloid and polymer science*, 83:200–210, 1990.

[10] Bouchaud, Jean-Philippe and George, Antoine. Anomalous diffusion in disordered media: Statistical mechanisms, models and physical applications. *Physics Reports*, 195:127–293, 1990.

[11] Braeckmans, Kevin; Peeters, Liesbeth; Sanders, Niek N.; De Smedt, Stefaan C., and Demeester, Joseph. Three–dimensional fluorescence recovery after photobleaching with the confocal scanning laser microscope. *Biophysical Journal*, 85:2240–2252, 2003.

[12] Braeckmans, Kevin; Remaut, Katrien; Vandenbroucke, Roosmarijn E.; Lucas, Bart; De Smedt, Stefaan C., and Demeester, Joseph. Line FRAP with the confocal laser scanning microscope for diffusion measurements in small regions of 3-d samples. *Biophysical Journal*, 92:2172–2183, 2007.

[13] Brown, Edward B.; Wu, Shinn En; Zipfel, Warren, and Webb, Watt W. Measurement of molecular diffusion in solution by multiphoton fluorescence photobleaching recovery. *Biophysical Journal*, 77:2837–2849, 1999.

[14] Brown, Robert. Additional remarks on active molecules. *Philosophical Magazine and Annals of Philosophy*, 6:161–166, 1829. URL `http://archive.org/details/philosophicalmag06lond`.

[15] Buchholz, Fredric L. and Graham, Andrew T., editors. *Modern Superabsorbent Polymer Technology*. Wiley-VCH, 1998.

[16] Buléon, A.; Colonna, P.; Planchot, V., and Ball, S. Starch granules: structure and biosynthesis. *International Journal of Biological Macromolecules*, 23:85–112, 1998.

[17] Burke, Matthew D.; Park, Jung O.; Srinivasarao, Mohan, and Khan, Saad A. Diffusion of macromolecules in polymer solutions and gels: a laser scanning confocal microscopy study. *Macromolecules*, 33:7500–7507, 2000.

[18] Carr, H. and Purcell, E. Effects of diffusion on free precision in nuclear magnetic resonance experiments. *Physical Review*, 94:630–638, 1954.

[19] Carvajal-Rondanelli, Patricio A. and Lanier, Tyre C. Diffusion of active proteins into fish meat to minimize proteolytic degradation. *Journal of Agricultural and Food Chemistry*, 58:5300–5307, 2010.

[20] Chatfield, Christopher. *The analysis of time series : an introduction*. Chapman and Hall, 1989.

[21] Cheng, Yu; Prud'homme, Robert, and Thomas, James L. Diffusion if mesoscopic probes in aqueous polymer solutions measured by fluorescence recovery after photobleaching. *Macromolecules*, 35:8111–8121, 2002.

[22] Chronakis, Ioannis S. On the molecular characteristics, compositional properties, and structural-functional mechanisms of maltodextrins: A review. *Critical Reviews in Food Science and Nutrition*, 38(7):599–637, 1998.

[23] Clague, David S. and Phillips, Ronald J. Hindered diffusion of spherical macromolecules through dilute fibrous media. *Physics of Fluids*, 8:1720–1731, 1996.

[24] Cowie, J. M. G. *Polymers: Chemistry & Physics of modern materials (2nd edition)*. CRC Press, 1991.

[25] Cukier, R. I. Diffusion of brownian spheres in semidilute polymer solutions. *Macromolecules*, 17:252–255, 1984.

[26] Cunin, C.; Handschin, S.; Walther, P., and Escher, F. Structural changes of starch during cooking of durum wheat pasta. *LWT - Food Science and Technology*, 28:323–328, 1995.

[27] Davoust, Jean; Devaux, Philippe F., and Leger, Liliane. Fringe pattern photobleaching, a new method for the measurement of transport coefficients of biological macromolecules. *The EMBO Journal*, 1(10):1233–1238, 1982.

[28] de Gennes, Pierre G. *Scaling concepts in polymer physics*. Cornell University Press, 1979.

[29] De Smedt, S. C.; Lauwers, A.; Demeester, J.; Engelborghs, Y.; De Mey, G., and Du, M. Structural information on hyaluronic acid solutions as studied by probe diffusion experiments. *Macromolecules*, 27:141–148, 1994.

[30] De Smedt, S. C.; Meyvis, Tom K. L.; Demeester, Joseph; Van Oostveldt, P.; Blonk, J. C. G., and Hennink, Wim E. Diffusion of macromolecules in dextran methacrylate solutions and gels as studied by confocal scanning laser microscopy. *Macromolecules*, 30:4863–4870, 1997.

[31] Digman, Michelle A.; Brown, Claire M.; Sengupta, Parijat; Wiseman, Paul W.; Horwitz, Alan R., and Gratton, Enrico. Measuring fast dynamics in solutions and cells with a laser scanning microscope. *Biophysical Journal*, 89:1317–1327, 2005.

[32] Digman, Michelle A.; Sengupta, Parijat; Wiseman, Paul W.; Brown, Claire M.; Horwitz, Alan R., and Gratton, Enrico. Fluctuation correlation spectroscopy with a laser-scanning microscope: Exploiting the hidden time structure. *Biophysical Journal*, 88:L33–L36, 2005.

[33] Djabourov, Madeleine. Architecture of gelatin gels. *Contemporary Physics*, 29:273–297, 1988.

[34] Djabourov, Madeleine; Lechaire, Jean-Pierre, and Gaill, Françoise. Structure and rheology of gelatin and collagen gels. *Biorheology*, 30:191–205, 1993.

[35] Doi, M. and Edwards, S. F. *The Theory of Polymer Dynamics*. Clarendon Press, Oxford University Press, Oxford, New York, 1986.

[36] Egner, Alexander and Hell, Stefan W. Fluorescence microscopy with super-resolved optical sections. *Trends in Cell Biology*, 15(4):207–215, 2005.

[37] Einstein, Albert. Über die von der molekularkinetischen theorie der wärme geforderte bewegung von in ruhenden flüssigkeiten suspendierten teilchen. *Annalen der Physik*, 17: 549–560, 1905. doi: 10.1002/andp.19053220806.

[38] Elliot, J. Richard and Lira, Carl T. *Introductory Chemical Engineering Thermodynamics*. Prentics Hall PTR, 2001.

[39] Fick, Adolf. Ueber diffusion. *Annalen der Physik*, 170(1):59–86, 1855. ISSN 1521-3889. URL `http://dx.doi.org/10.1002/andp.18551700105`.

[40] Flory, Paul J. *Principles of polymer chemistry*. Cornell University Press, 1953.

[41] Ghosh, V.; Ziegler, G. R., and Anantheswaran, R. C. Fat, moisture and ethanol migration through chocolates and confectionary coatings. *Critical Reviews in Food Science and Nutrition*, 42(6):583–626, 2002.

[42] Gordon, Manfred and Torkington, John A. Scrutiny of the critical exponent paradigm, as exemplified by gelation. *Pure Appl Chem*, 53:1461, 1981.

[43] Grasdalen, Hans and Smidsrød, Olav. Cesium-133 NMR in the sol-gel states of aqueous carrageenan. selective site binding of cesium and potassium ions in κ-carrageenan gels. *Macromolecules*, 14:229–231, 1981.

[44] Gratton, Enrico and vande Ven, Martin J. *Handbook of Biological Confocal Microscpoy*, chapter 5 - Laser sources for confocal microscopy, pages 80–125. Springer Science+Business Media, 3rd edition, 2006.

[45] Guo, Jian-Hwa; Skinner, G.W.; Harcum, W.W., and Barnum, P.E. Pharmaceutical applications of naturally occurring water-soluble polymers. *Pharmaceutical science & technology today*, 1:254–261, 1998.

[46] Haining, Robert P. *Spatial Data Analysis: Theory and Practice*. Cambridge University Press, Cambridge, 2003.

[47] Hecht, Eugene. *Optics*. Addison-Wesley, 3rd edition, 1998.

[48] Hell, S.; Reiner, G.; Cremer, C., and Stelzer, E. H. K. Aberrations in confocal fluorescence microscopy induced by mismatches in refractive index. *Journal of Microscopy*, 169(3): 391–405, 1993. ISSN 1365-2818.

[49] Herman, B. *Fluorescence Microscopy*. BIOS Scientific Publishers, Royal Microscopical Society, UK, 2nd edition, 1998.

[50] Hermansson, A.-M.; Eriksson, E., and Jordansson, E. Effects of potassium, sodium and calcium on the microstructure and rheological behaviour of kappa-carrageenan gels. *Carbohydrate Polymers*, 16:297–230, 1991.

[51] Hermansson, Anne-Marie. *Functional Properties of food macromolecules*, chapter 6 - Water and fat holding, pages 273–314. Elsevier, 1986.

[52] Hermansson, Anne-Marie. Rheological and microstructural evidence for trancient state during gelation of kappa-carrageenan in the presence of potassium. *Carbohydrate Polymers*, 10:163–181, 1989.

[53] Hermansson, Anne-Marie and Svegmark, Karin. Developments in the understanding of starch functionality. *Trends in Food Science & Technology*, 7:345–353, 1996.

[54] Hermansson, Anne-Marie; Lorén, Niklas, and Nydén, Magnus. *Water properties of food, pharmaceutical, and biological materials*, chapter 5 - The importance of microstructure for solvent and solute diffusion on the micro and nano length scales, pages 79–100. CRC Taylor & Francis, 2006.

[55] Hollas, J. Michael. *Modern Spectroscopy*. John Wiley & Sons, Ltd, England, 4th edition, 2005.

[56] Holmberg, Krister; Jönsson, Bo; Kronberg, Bengt, and Lindman, Björn. *Surfactant and polymer in aqueous solution*. Wiley, 2nd edition, 2004.

[57] Homogeneity, . *Merriam-Webster.com*. http://www.merriam-webster.com/, 25 Mars 2012.

[58] Houtsmuller, Adriaan B. Fluorescence recovery after photobleaching: Application to nuclear proteins. *Advances in Biochemical Engineering/Biotechnology*, 95:1292–1296, 2005.

[59] Jensen, Søren; Rolin, Claus, and Ipsen, Richard. Stabilisation of acidified skimmed milk with hm pectin. *Food Hydrocolloids*, 24:291–299, 2010.

[60] Johansson, Lennart; Elvingson, Christer, and Löfroth, Jan-Erik. Diffusion and interaction in gels and solutions. 3. theoretical results on the obstuction effect. *Macromolecules*, 24: 6024–6029, 1991.

[61] Johnson, Erin M.; Berk, David A.; Jain, Rakesh K., and Deen, William M. Hindered diffusion in agarose gels: Test of effective medium model. *Biophysical Journal*, 70:1017–1026, 1996.

[62] Jonasson, Jenny; Lorén, Niklas; Olofsson, Paula; Nydén, Magnus, and Rudemo, Mats. A pixel-based likelihood methodology for analysis of FRAP data. *Journal of Microscopy*, 232: 260–269, 2008.

[63] Jonkman, James E. N. and Stelzer, Ernst H. K. *Confocal and Two-Photon Microscopy: Foundations, Applications and Advances*, chapter 5 - Resolution and contrast in confocal and two-photon microscopy, pages 101–125. Wiley, New York, 2002.

[64] Jönsson, Peter; Jonsson, Magnus P.; Tegenfeldt, Jonas O., and Höök, Fredrik. A method of improving the accuracy of fluorescence recovery after photobleaching analysis. *Biophysical Journal*, 95:5334–5348, 2008.

[65] Kang, Minchul and Kenworthy, Anne K. A closed-form analytic expression for FRAP formula for the binding diffusion model. *Biophysical Journal*, 95:L13–L15, 2008.

[66] Keller, H. Ernst. *Handbook of Biological Confocal Microscopy*, chapter 7 - Objective Lenses for Confocal Microscopy, pages 145–161. Springer Science+Business Media, 3rd edition, 2006.

[67] Keuren, E.V. and Schrof, W. Fluorescence recovery after two-photon bleaching for the study of dye diffusion in polymer systems. *Macromolecules*, 36:5002–5007, 2003.

[68] Kosto, Kimberly B. and Deen, William M. Diffusivities of macromolecules in composite hydrogels. *AIChE*, 50(11):2648–2658, 2004.

[69] Kubitscheck, Ulrich; Wedekind, Peter, and Peters, Reiner. Lateral diffusion measurement at high spatial resolution by scanning microphotolysis in a confocal microscope. *Biophysical Journal*, 67:948–956, 1994.

[70] Langton, Maud and Hermansson, Anne-Marie. Fine-stranded and particulate gels of β-lactoglobulin and whey protein at varying pH. *Food Hydrocolloids*, 5:523–539, 1992.

[71] Langton, Maud and Hermansson, Anne-Marie. Image analysis of particulate whey protein gels. *Food Hydrocolloids*, 10:179–191, 1996.

[72] Larsson, Mikael; Gustafsson, Stefan; Olsson, Eva, and Larsson, Anette. Effect of calcium neutralization on elastic and swelling properties of crosslinked poly(acrylic acid) - correlation to inhomogeneities and phase behaviour. *e-Polymers*, 141:1–14, 2009.

[73] Le Bon, Christel; Nicolai, Taco, and Durand, Dominique. Kinetics of aggregation and gelation of globular proteins after heat-induced denaturation. *Macromolecules*, 32:6120–6127, 1999.

[74] Levi, Valeria and Gratton, Enrico. Exploring dynamics in living cells by tracking single particles. *Cell Biochemistry and Biophysics*, 48:1–15, 2007.

[75] Lippincott-Schwartz, Jennifer; Altan-Bonnet, Nihal, and Patterson, George. H. Photobleaching and photoactivation: following protein dynamics in living cells. *Nature Cell Biology*, 5:S7–S14, 2003.

[76] Lorén, N.; Hermansson, A.-M.; Williams, M. A. K.; Lundin, L.; Foster, T. J.; Hubbard, C. D.; Clark, A. H.; Norton, I. T.; Bergström, E. T., and Goodall, D. M. Phase separation induced by conformational ordering of gelatin in gelatin/maltodextrin mixtures. *Macromolecules*, 34:289–297, 2001.

[77] Lorén, Niklas; Shtykova, Liubov; Kidman, Siw; Jarvoll, Patrik; Nydén, Magnus, and Hermansson, Anne-Marie. Dendrimer diffusion in κ-carrageenan gel structures. *Biomacromolecules*, 10:275–84, 2009.

[78] Lustig, Steven R. and Peppas, Nikolaos A. Solute diffusion in swollen membranes. ix. scaling laws for solute diffusion in gels. *Journal of Applied Polymer Science*, 36:735–747, 1988.

[79] Marchal, L. M.; Beeftink, H. H., and Tramper, J. Towards a rational design of commercial maltodextrins. *Trends in Food Science & Technology*, 10:345–355, 1999.

[80] Masaro, L. and Zhu, X. X. Physical models of diffusion for polymer solutions, gels and solids. *Progress in Polymer Science*, 24:731–775, 1999.

[81] Mazza, Davide; Braeckmans, Kevin; Cella, Francesca; Testa, Ilaria; Vercauteren, Dries; Demeester, Jo; De Smedt, Stefaan S., and Diaspro, Alberto. A new FRAP/FRAPa method for three-dimensional diffusion measurements based on multiphoton excitation microscopy. *Biophysical Journal*, 95:3457–3469, 2008.

[82] Meyvis, Tom K. L.; De Smedt, Stefaan C.; Van Oostveldt, Patrick, and Demeester, Joseph. Fluorecence recovery after photobleaching: A versatile tool for mobility and interaction measurements in pharmaceutical research. *Pharmaceutical Research*, 16(8):1153–1161, 1999.

[83] Moran, P. A. P. Notes on continuous stochastic phenomena. *Biometrika*, 37:17–23, 1950.

[84] Morris, Edwin R.; Rees, David A., and Robinson, Geoffrey. Cation-specific aggregation of carrageenan helices: Domain model of polymer gel structure. *Journal of Molecular Biology*, 138:349–362, 1980.

[85] Moussaoui, Mohsen; Benlyas, Mohamed, and Whal, Philippe. Diffusion of proteins in the chromatographic gel AcA-34. *Journal of Chromatography*, 558:71–80, 1991.

[86] Moussaoui, Mohsen; Benlyas, Mohammed, and Wahl, Philippe. Diffusion of proteins in sepharose Cl-B gels. *Journal of Chromatography*, 591:115–120, 1992.

[87] Nickerson, M. T. and Paulson, A. T. Rheological properties of gellan, κ-carrageenan and alginate polysaccharides: effect of potassium and calcium ions on macrostructure assemblages. *Carbohydrate Polymers*, 58:15–24, 2004.

[88] Norton, I. T. and Frith, W. J. Microstructure design in mixed biopolymer composites. *Food Hydrocolloids*, 15:543–553, 2001.

[89] Norton, Ian T.; Goodall, David M.; Morris, Edwin R., and Rees, David A. Role of cations in the conformation of iota and kappa carrageenan. *Journal of the Chemical Society, Faraday Transactions 1*, 79:2475–2488, 1983.

[90] Ogston, A. G. The spaces in a uniform random suspension of fibres. *Transactions of the Faraday Society*, 54:1954–1757, 1958.

[91] Olmsted, Peter D. and Milner, Scott T. Strain-induced nematic phase separation in polymer melts and gels. *Macromolecules*, 24:6648–6660, 1994.

[92] Olmstedt, Stuart S; Padgett, Janet L.; Yudin, Ashley I.; Whaley, Kevin J.; Moench, Thomas R., and Cone, Richard A. Diffusion of macromolecules and virus-like particles in human cervical mucus. *Biophysical Journal*, 81:1930–1937, 2001.

[93] Olsson, Camilla; Langton, Maud, and Hermansson, Anne-Marie. Microstructure of β-lactoglobulin/amylopectin gels on different length scales and their significance for rheological properties. *Food Hydrocolloids*, 16:111–126, 2002.

[94] Pawitan, Yudi. *In all likelihood: statistical modelling and inference using likelihood*. Clarendon Press, Oxford, 2001.

[95] Pawley, J. B., editor. *Handbook of Biological Confocal Microscopy*. Springer Science+Business Media, 3rd edition, 2006.

[96] Peters, Reiner; Peters, Jutta; Heinz Tews, Karl, and Bähr, Wolfgang. A microfluorimetric study of translational diffusion in erythrocyte membranes. *Biochimica et Biophysica Acta*, 367:282–294, 1974.

[97] Petersen, Nils O.; Höddelius, Pia L.; Wiseman, Paul W.; Seger, Olle, and Magnusson, Karl-Eric. Quantitation of membrane receptor distributions by image correlation spectroscopy: Concept and application. *Biophysical Journal*, 65:1135–1146, 1993.

[98] Petitot, Maud; Abecassis, Joël, and Micard, Valérie. Structuring of pasta components during processing: impact on starch and protein digestibility and allergenicity. *Trends in Food Science & Technology*, 20:521–532, 2009.

[99] Phillips, R. J.; Deen, W. M., and Brady, J. F. Hindered transport of spherical macromolecules in fibrous membranes and gels. *AIChE Journal*, 35:1761–1769, 1989.

[100] Piñeiro, Y.; López-Quintela, M. A.; Rivas, J., and Leisner, D. Percolation threshold and scattering power law of gelatin gels. *Phys. Rev. E*, 79(4):041409, Apr 2009.

[101] Piculell, Lennart and Lindman, Björn. Association and segregation in aqueous polymer/polymer, polymer/surfactant, and surfactant/surfactant mixtures: similarities and differences. *Advances in Colloid and Interface Science*, 41:149–178, 1992.

[102] Pluen, Alain; Netti, Paolo A.; Jain, Rakesh K., and Berk, David A. Diffusion of macromolecules in agarose gels: Comparison of linear and globular configurations. *Biophysical Journal*, 77:542–552, 1999.

[103] Pouzot, M.; Nicolai, T.; Visschers, R. W., and Weiljers, M. X-ray and light scattering study of the structure of large protein aggregates at neutral pH. *Food Hydrocolloids*, 19: 231–238, 2005.

[104] Price, William S. Pulsed-field gradient nuclear magnetic resonance as a tool for studying translational diffusion: part 1. basic theory. *Concepts in Magnetic Resonance*, 9(5):299–336, 1997.

[105] Qian, Hong; Sheetz, Michael P., and Elson, Elliot L. Single particle tracking. analysis of diffusion and flow in two-dimensional systems. *Biophysical Journal*, 60:910–921, 1991.

[106] Rayan, Gamal; Guet, Jean-Erik; Taulier, Nicolas; Pincet, Frederic, and Urbach, Wladimir. Recent applications of fluorescence recovery after photobleaching (FRAP) to membrane bio-macromolecules. *Sensors*, 10:5927–5948, 2010.

[107] Ross-Murphy, Simon B. Structure and rheology of gelatin gels: recent progress. *Polymer*, 33:2622–2627, 1992.

[108] Sawyer, Lindsay and Kontopidis, George. The core lipocalin, bovine β-lactoglobulin. *Biochimica et Biophysica Acta*, 482:136–148, 2000.

[109] Saxton, M. Single-particle tracking: the distribution of diffusion coefficients. *Biophysical Journal*, 72:1744–1753, 1997.

[110] Saxton, Michael J. Anomalous subdiffusion in fluorescence photobleaching recovery: A monte carlo study. *Biophysical Journal*, 81:2226–2240, 2001.

[111] Seiffert, Sebastian and Oppermann, Wilhelm. Systematic evaluation of FRAP experimants performed in a confocal laser scanning microscope. *Journal of Microscopy*, 220(1):20–30, 2005.

[112] Shen, Hong; Hu, Yueyue, and Saltzman, W. M. DNA diffusion in mucus: Effect of size, topology of DNAs, and transfection reagents. *Biophysical Journal*, 91:639–644, 2006.

[113] Singer, J. NMR diffusion and flow measurements and an introduction to spin phase graphing. *Journal of Physics E*, 11:281–291, 1978.

[114] Sinnecker, Daniel; Voigt, Philipp; Hellwig, Nicole, and Schaefer, Michael. Reversible photobleaching of enhanced green fluorescent proteins. *Biochemistry*, 44:7085–7094, 2005.

[115] Smith, Barton A. and McConnell, Harden M. Determination of molecular motion in membranes using periodic pattern photobleaching. *Proc. Natl. Acad. Sci. USA*, 75:2759–2763, 1978.

[116] Smoluchowski, Marian. Zur kinetischen theorie der brownsche molekularbewegung und der suspensionen. *Annalen der Physik*, 326:756–780, 1906. doi: 10.1002/andp.19063261405.

[117] Sniekers, Y. H. and van Donkelaar, C. C. Determining diffusion coefficients in inhomogeneous tissues using fluorescence recovery after photobleaching. *Biophysical Journal*, 89: 1302–1307, 2005.

[118] Song, Loling; Hennink, E. J.; Young, Ted, and Tanke, Hans J. Photobleaching kinetics of fluorescein in quantitative fluorescence microscopy. *Biophysical Journal*, 68:2588–2600, 1995.

[119] Soumpasis, D. M. Theoretical analysis of flourescence photobleaching recovery experiments. *Biophysical Journal*, 41:95–97, 1983.

[120] Sprague, Brian L.; Pego, Robert L.; Stavreva, Diana A., and McNally, James G. Analysis of binding reactions by fluorescence recovery after photobleaching. *Biophysical Journal*, 86:3473–3495, 2004.

[121] Srivastava, Mamta and Petersen, Nils O. Diffusion of transferrin receptor clusters. *Biophysical Chemistry*, 75:201–211, 1998.

[122] Stading, Mats and Hermansson, Anne-Marie. Viscoelastic behaviour of β-lactoglobulin gel structures. *Food Hydrocolloids*, 4:121–135, 1990.

[123] Stelzer, Ernst H. K. *Handbook of Biological Confocal Microscopy*, chapter 9 - The intermediate optical system of laser-scanning confocal microscopes, pages 207–220. Springer Science+Business Media, 3rd edition, 2006.

[124] Suh, Junghae; Dawson, Michelle, and Hanes, Justin. Real-time multiple-particle tracking: applications to drug and gene delivery. *Advanced Drug Delivery Reviews*, 57:63–78, 2005.

[125] Svanberg, Lina; Arhné, Lilia; Lorén, Niklas, and Windhab, Erich. Effect of pre-crystallization process and solid particle addition on cocoa butter crystallization and resulting microstructure in chocolate model systems. *Procedia Food Science*, 1:1910–1917, 2011.

[126] Tsay, Tsong-Tseh and Jacobson, Ken A. Spatial fourier analysis of video photobleaching measurements. principles and optimisation. *Biophysical Journal*, 60:360–368, 1991.

[127] Viebke, Christer; Piculell, Lennart, and Nilsson, Svante. On the mechanism of gelation of helix-forming biopolymers. *Macromolecules*, 27:4160–4166, 1994.

[128] Viridén, Anna; Wittgren, Bengt, and Larsson, Anette. Investigation of critical polymer properties for polymer release and swelling of HPMC matrix tablets. *European Journal of Pharmaceutical Sciences*, 36:297–309, 2009.

[129] Walther, Bernhard; Lorén, Niklas; Nydén, Magnus, and Hermansson, Anne-Marie. Influence of κ-carrageenan gel structures on the diffusion of probe molecules determined by transmission electron microscopy and NMR diffusometry. *Langmuir*, 22:8221–8228, 2006.

[130] Wedekind, Peter; Kubitscheck, Ulrich, and Peters, Reiner. Scanning microphotolysis: a new photobleaching technique based on fast intensity modulation of scanned laser beam and confocal imaging. *Journal of microscopy*, 176:23–33, 1994.

[131] Welty, James R.; Wicks, Charles E.; Wilson, Robert E., and Rorrer, Gregory. *Fundamentals of Momentum, Heat, and Mass Transfer*. John Wiley & Sons, Inc., 4th edition, 2001.

[132] Winter, H. H. Can the gel point of a cross-linking polymer be detected by the g' – g" crossover? *Polym. Eng. Sci.*, 27:1689–1702, 1987.